Characterization of Zika virus prevalence in Kenya and the innate antiviral type-I interferon response against infection

Theodore A. Gobillot

A dissertation

submitted in the partial fulfillment of the

requirements for the degree of

Doctor of Philosophy

University of Washington

2020

Reading Committee:

Julie Overbaugh, Chair

Adam Geballe

Trevor Bedford

Program Authorized to Offer Degree:

Molecular and Cellular Biology

University of Washington

Abstract

Characterization of Zika virus prevalence in Kenya and the innate antiviral type-I interferon response against infection

Theodore A. Gobillot

Chair of the Supervisory Committee:

Affiliate Professor Julie Overbaugh

Full Member, Divisions of Human Biology and Public Health Sciences, Fred Hutchinson Cancer Research Center

The recent unprecedented spread and severe pathogenic features of Zika virus (ZIKV) in the Americas have highlighted this emerging pathogen as a major threat to global public health. Substantial efforts have been devoted to examining novel aspects of ZIKV transmission and pathogenesis in the Americas. However, these studies are limited by the lack of ZIKV data from Africa, where the virus was discovered over 70 years ago and is believed to have been silently circulating for decades. The prevalence and importance of ZIKV infections and the properties of strains that circulate in East Africa, where the virus was first discovered, are unknown. In this thesis, we examined ZIKV circulation over two decades and its contribution to febrile illness in Kenya using two unique cohorts. Further, we interrogated the role of the innate antiviral type-I interferon (IFN-I) response in the restriction of ZIKV strains from Africa and the Americas, where there appears to be a difference in disease associated with ZIKV infections.

First, we screened plasma collected 2-12 months after febrile and/or exanthematic illness in densely populated, urban regions of Western and coastal Kenya between 1993-2016 for binding and neutralizing antibodies to distinguish ZIKV and Dengue virus (DENV) responses. We found DENV antibody responses were common in coastal Kenya. We identified two subjects with durable ZIKV-specific antibodies and two cases with evidence for both ZIKV and DENV infections. The cases span an ~20-year period (1994-2013), suggesting a very low, persistent burden of ZIKV in two major urban areas in East Africa, with no evidence for ZIKV outbreaks. Given that ZIKV is present at low levels in large population centers in Kenya, these findings highlight the need for continued arboviral surveillance and improved platforms for arboviral detection.

Next, we designed a phage-display based serological screening tool (PhIP-Seq) to specifically identify cases of prior ZIKV exposure by detection of ZIKV-specific IgG antibodies. Using PhIP-Seq, we identified preliminary ZIKV-specific peptides that are characteristic of ZIKV infection in non-human primate sera. Future studies are needed to validate this approach with a larger panel of human sera using bioinformatics tools that account for the high-dimensional PhIP-Seq data. We demonstrated that PhIP-Seq can also be used to map the epitopes of monoclonal antibodies directed against pathogens in the phage library. We successfully mapped the epitopes of twenty-two HIV-specific monoclonal antibodies isolated from three HIV-infected Kenyan subjects.

Finally, we compared the IFN-I-mediated restriction of ZIKV strains isolated in Africa and the Americas and examined the contribution of interferon-induced transmembrane protein-3 (IFITM3), the first interferon-stimulated gene (ISG) reported to inhibit ZIKV, to the overall IFN-I response against ZIKV. We identified a robust IFN-I-mediated antiviral effect on ZIKV infection in a commonly used cell line to study ZIKV replication, A549 cells. The effects of IFN-I on ZIKV replication varied by viral lineage in our panel of nine ZIKV strains. African-lineage strains, which have not been linked to pathogenesis, were less sensitive to IFNα ($p=0.049$) and IFNβ

(p=0.09) than Asian-lineage strains, which have seeded the American pathogenic outbreak. We did not identify a role for IFITM3 in the IFN-I-mediated restriction of ZIKV, suggesting that other ISGs are important mediators of the IFN-I response against ZIKV in A549 cells. Given the potent antiviral effect of IFN-I on ZIKV in these cells, they present an opportunity for the discovery of novel antiviral ISGs against ZIKV. To this end, we used A549 cells to develop a CRISPR screen that may be used to identify ISGs that inhibit ZIKV. Preliminary findings from three screens highlight the promise of this approach for identifying ISGs that inhibit ZIKV. Future work may identify as-yet undiscovered ISGs that restrict ZIKVs as well as those that have activity against other related flaviviruses and cytopathic viruses.

TABLE OF CONTENTS

LIST OF FIGURES

LIST OF TABLES

LIST OF ABBREVIATIONS

ADAR: adenosine deaminase acting on RNA

ADCC: antibody-dependent cellular cytotoxicity

A549-ISG-KO: A549 cell line transduced with ISG targeting sgRNA lentiviral library

BEI: Biodefense and emerging infectious research repository

CHIKV: Chikungunya virus

C5: constant region 5

DENV: Dengue virus

E-protein: envelope glycoprotein

ELISA: enzyme-linked immunosorbent assay

GBS: Guillain Barre syndrome

HIV-1 / HIV: human immunodeficiency virus-1

IAV: influenza A virus

IFITM3: interferon-inducible transmembrane protein 3

IFI6: interferon-alpha induced protein 6

IFNAR: Interferon alpha/beta receptor

IFNα: interferon-alpha

IFNβ: interferon-beta

IFN-I: type-1 interferon

IP: immunoprecipitation

IRF9: Interferon regulatory factor 9

ISGF3: Interferon stimulated gene factor 3

ISRE: Interferon stimulated response element

ISG: interferon stimulated gene

IgM: immunoglobulin M

JAK1: Janus kinase 1

JAK2: Janus kinase 2

JEV: Japanese encephalitis virus

KO: knockout

mAb: monoclonal antibody

MAC-ELISA: immunoglobulin M capture ELISA

MLV: murine leukemia virus

MOI: multiplicity of infection

nAb: neutralizing antibody

NAT: nucleic acid amplification test

NHP: non-human primate

NSB: non-specific background

NS1: non-structural protein 1

NTC: non-targeting controls

NT_{50}: plasma neutralization titer to achieve 50% neutralization

ONNV: O'nyong'nyong virius

prM: pre-membrane structural protein

PARP12: Poly(ADP-Ribose) Polymerase Family Member-12

Phage-DMS: phage-deep mutational scanning

PhIP-Seq: phage display immunoprecipitation sequencing

PRNT: plaque-reduction neutralization test

PRR: pattern recognition receptor

qRT-PCR: quantitative reverse transcription-polymerase chain reaction

RDT: rapid diagnostic test

RLU: relative luciferase unit

RVFV: Rift valley fever virus

RVP: reporter virus particle

sgRNA: single guide RNA

SPOV: Spondweni virus

STAT1: Signal transducer and activator of transcription 1

STAT2: Signal transducer and activator of transcription 2

S/W: supernatant & PBS wash sample

TBEV: Tick-borne encephalitis virus

TORCH: Toxoplasma gondii, Other, Rubella, cytomegalovirus, herpes simplex virus-1

$TCID_{50}$: median tissue culture infectious dose

TYK2: Tyrosine kinase 2

V3: variable loop 3

WNV: West nile virus

YFV: Yellow fever virus

ZCS: Zika congenital syndrome

ZIKV: Zika virus

ACKNOWLEDGEMENTS

Many thanks to:

Julie Overbaugh for your dedicated and impactful mentorship over the past four years. Your commitment to and style of mentorship has created a lasting impression and continues to inspire me. Through our many meetings about science and career trajectories, your thoughtful comments on drafts of manuscripts and grants, and guidance during lab meetings and practice talks, I have learned so much about not only the scientific process, but also how I want to mentor and lead in the future. Thank you for guiding me through this period of such rewarding intellectual growth.

Dara Lehman for always providing a listening ear, a calm presence, and important guidance to me throughout graduate school. I am so appreciative of all of our discussions about both science and things outside of the lab.

All of the members of the Overbaugh lab for creating a fun, collaborative, productive, and comfortable environment: Daryl Humes for serving as an important mentor and friend throughout my time in the lab. Caroline Kikawa for being a great colleague to work with on so many projects. Cassie Simonich for mentoring me during my rotation in the lab and providing guidance as a senior MD-PhD student. Amit Sharma for insights during experiment-planning and grant-writing and for being a great person to work with on our IFITM3 studies. Kate Williams for mentoring me during my rotation in the lab. Nicole Naiman and Mark Pankau for being great Kenya travel partners. Zak Yaffe for always being optimistic when I needed it and making the best coffee. Laura Doepker for being a great team-science partner on PhIP-Seq. Caitlin Stoddard for being enthusiastic and patient during my last few months in the lab during project transitions. Stephanie Rainwater for always being a helpful resource through graduate school and Vrasha Chonan for assisting with all of Kenyan cohort studies and samples. And the rest of past and present Overbaugh lab folks: Noah Sather, Meghan Garrett, Joshua Marceau, Mackenzie Shipley, Hannah Itell, Sonja Danon, Sara Drescher, Carolyn Fish, Bri Hennessey,

Dana Arenz, Haidyn Weight, Mark Pankau, John Nahabedian, Vera Okolo, Julie Weis, Adam Dingens, and Tucker Price.

Adam Geballe, Trevor Bedford, Jenny Hyde, Jesse Bloom, and Mike Gale for serving on my thesis committee. I would like to especially acknowledge Adam and Trevor for serving on my thesis reading committee.

The directors and administrators of the UW MSTP and MCB graduate programs for your continued commitment to providing outstanding graduate education: Marshall Horwitz, Mary-Claire King, Stephen Tapscott, Nina Salama, Richard Gardner, Maia Low, Marcie Buckner, and Sara Carlson.

Shama Samant and Jasmine Gonzalez for all of your administrative assistance throughout graduate school. Stephanie Hughes in UW Pathology for all of your help with submitting my F30 application.

All of the women who have participated in the studies utilized in this thesis and our collaborators both in Seattle and Kenya. Jillian Pintye for assistance with Mama Salama study samples. Our collaborators Bill Messer and the Messer lab at OHSU for being such a welcoming group when I came to do PhIP-Seq and Dan Streblow at OHSU. Collaborators at the Hutch: Leslie Goo, Sidney Bell, Kate Crawford, and Molly O'hainle for your help with various projects.

The Fred Hutch Flow Cytometry, Genomics, and Bioinformatics cores. Cassie Sather for assisting on PhIP-Seq deep sequencing. Ryan Basom for bioinformatics related to PhIP-Seq and Pritha Chanana for bioinformatics related to ISG CRISPR screening. Luna Yu and Pat Heath for your assistance with IT throughout my time in the lab.

Thursday Morning Virus meetings for an outstanding opportunity to present my work and get feedback. Michael Emerman for your commitment to organizing these meetings and your great virology graduate school course.

My sources of funding throughout graduate school: The Viral Pathogenesis and Evolution Training Grant, the ARCS Foundation, and the Ruth L. Kirschstein NRSA Predoctoral Fellowship (F30).

Drs. Jeff Houlton, Azeem Kaka, and Brittany Barber for being thoughtful mentors and engaging me in clinical medicine and research throughout graduate school. I am very thankful for your continued support and guidance as I make the transition back into medical school. Dr. Sean Houston who served as an important physician mentor to me during my senior year of high school.

Jeff Brodsky who provided close mentorship in the lab while I was an undergraduate at the University of Pittsburgh and, as a result, seeded my inspiration to pursue an MD-PhD career. Laurel Roberts who gave me with so many opportunities to teach and mentor in her freshman Biology course where I first discovered my passion for mentorship and teaching.

My mom and stepdad for being unwavering sources of support throughout my time in the lab. Thank you to my mom who brought me to “bring-your-kid-to-work day” in 7th grade where I first felt the excitement about pursuing a career in medicine. The entire Gobillot, Gittleman, and Gibson families for being a great support network.

My husband, Alec. None of this would be possible without you. There is no way to fully express how grateful I am for everything you do for me every single day. I am a better person, scientist, and student because of you.

DEDICATION

This thesis is dedicated to:

My mom, Chris Gobillot, who instilled in me the desire to always pursue my dreams, and

My husband, Alec Gibson, who makes life a dream that I am so thankful we get to explore together.

Chapter I

Introduction

Emergence of Zika virus as a significant threat to global public health

In December 2014, urban centers within Northeast Brazil began reporting an increasing number of cases of acute exanthematic febrile illness to the Brazilian Ministry of Health (1). This was shortly followed by reports from other Brazilian municipalities of an acute febrile illness accompanied by maculopapular rash, headache, conjunctivitis, arthralgia, and edema (timeline reviewed in (2)). At the end of February 2015, the Brazilian Ministry of Health began monitoring these cases, which at the time were self-limited and required no clinical intervention (2). Preliminary studies led by the Ministry of Health ruled out suspected pathogens, namely Dengue virus (DENV), Rubella, and Chikungunya virus, as causes of the reported cases (2). In late March 2015, Zika virus (ZIKV), a flavivirus transmitted by *Aedes* mosquitoes, was isolated from several patients with the aforementioned clinical history of acute exanthematic febrile illness, raising suspicions that ZIKV may be the causative agent underlying the outbreak of this illness (3-5). In May 2015, the Brazilian Ministry of Health reported autochthonous transmission of ZIKV in Brazil (2, 6).

In June 2015, reports of Guillain-Barre syndrome (GBS) following an acute febrile illness accompanied by rash in adults were reported to the Brazilian Ministry of Health (2). GBS is a group of immune-mediated polyneuropathatic illnesses characterized by paralysis (often ascending limb paralysis) following a recent infection by multiple types of pathogens (7). From January to July 2015, 121 cases of GBS were reported in Brazil with 62% of cases having symptoms consistent with ZIKV febrile illness preceding GBS (2, 6). In El Salvador, 22 cases of GBS were reported in December 2015 with 54% of cases having been preceded with ZIKV-like febrile illness (2, 6).

In October 2015, an increasing number of newborns with head circumferences 2 to 3 standard-deviations below the normal range were reported in Northeastern Brazil in regions impacted by the recognized ZIKV outbreak and a task force was established to examine the potential link between the observed spike in microcephaly cases and ZIKV infection of pregnant women (2, 6, 8). By the end of 2015, Brazil reported more than 4,000 total cases of microcephaly (Figure 1.1) (8). ZIKV was detected in the amniotic fluid of pregnant mothers who gave birth to newborns with microcephaly and the virus was isolated from tissues of a deceased newborn and from the placental tissue of a mother who experienced miscarriage at the 8th week of pregnancy (8). In February 2016, the World Health Organization declared a public health emergency of international concern, given the mounting evidence of an association between ZIKV and these neurological sequelae in both newborns and adults and its rapid spread to neighboring countries (9). The spectrum of neurologic abnormalities observed in ZIKV-infected newborns has since been formally defined as Zika virus Congenital Syndrome (ZCS; Figure 1.2) and ZIKV has been grouped with other teratogenic pathogens (TORCH pathogens – toxoplasmosis, other [syphilis, varicella-zoster, parvovirus B19], rubella, cytomegalovirus, and herpesvirus) that are known to cause neurological disease in infected newborns (10).

Altogether, from January 2015 to March 2017, 754,460 suspected and confirmed cases of ZIKV infection were reported to the Pan-American Health Organization, peaking in February 2016 (Figure 1.3) (11). Since January 2015, 69 countries have reported local active ZIKV transmission (12). In addition to the immediate neurological complications observed in ZIKV-infected newborns during the American ZIKV outbreak, longer-term studies have since identified medium- and long-term sequelae of ZIKV infection in newborns that do not show overt signs of ZCS at birth, including neurodevelopmental delay (Figure 1.2) (10, 13-16).

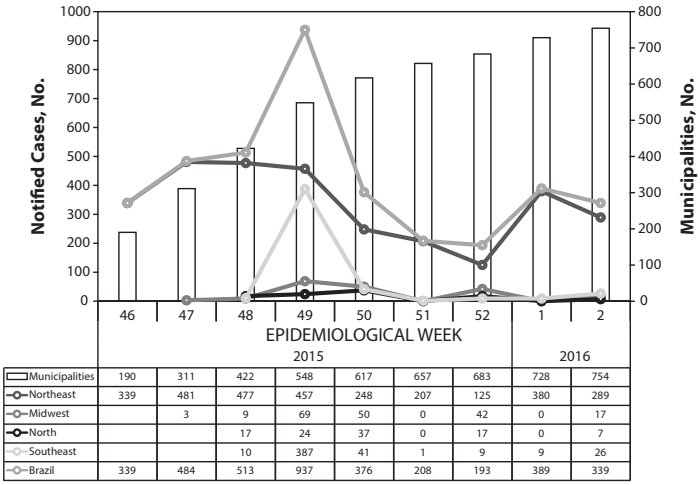

	46	47	48	49	50	51	52	1	2
Municipalities	190	311	422	548	617	657	683	728	754
Northeast	339	481	477	457	248	207	125	380	289
Midwest		3	9	69	50	0	42	0	17
North			17	24	37	0	17	0	7
Southeast			10	387	41	1	9	9	26
Brazil	339	484	513	937	376	208	193	389	339

Figure 1.1. Epidemiology of microcephaly cases in Brazil, 2015-2016. Figure from (8).The number of cases of microcephaly reported from municipalities in Brazil at the end of 2015 and beginning of 2016 is shown.

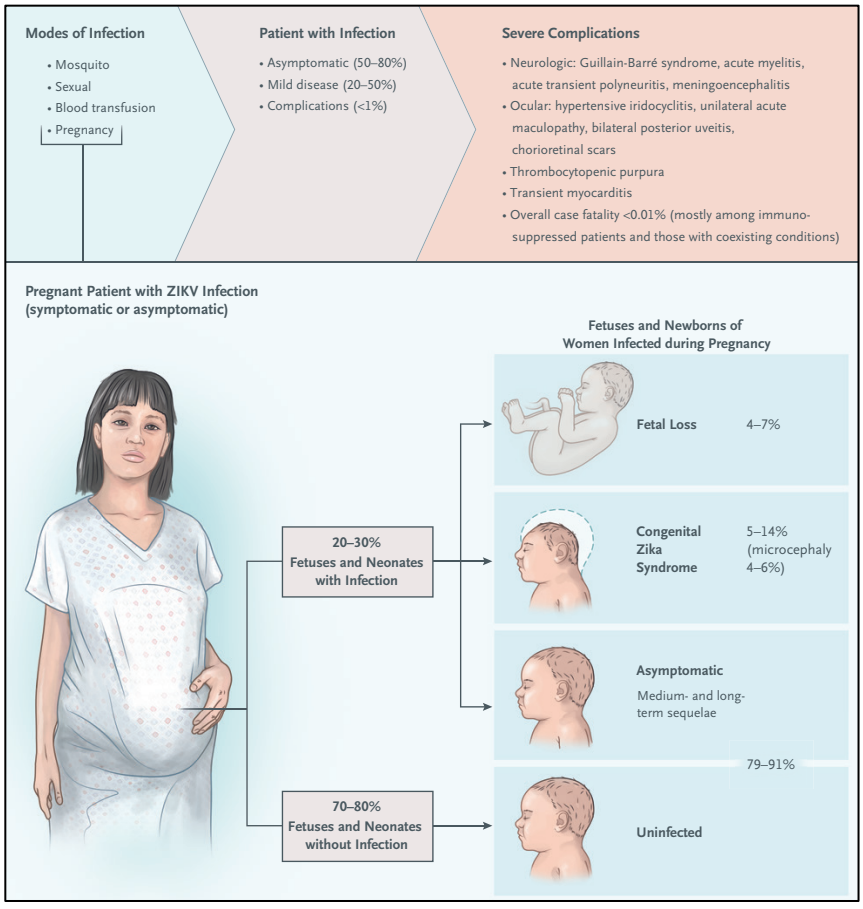

Figure 1.2. ZIKV transmission and pathogenesis in the American outbreak. Figure from (10). The modes of infection with an emphasis on complications following ZIKV vertical transmission is shown.

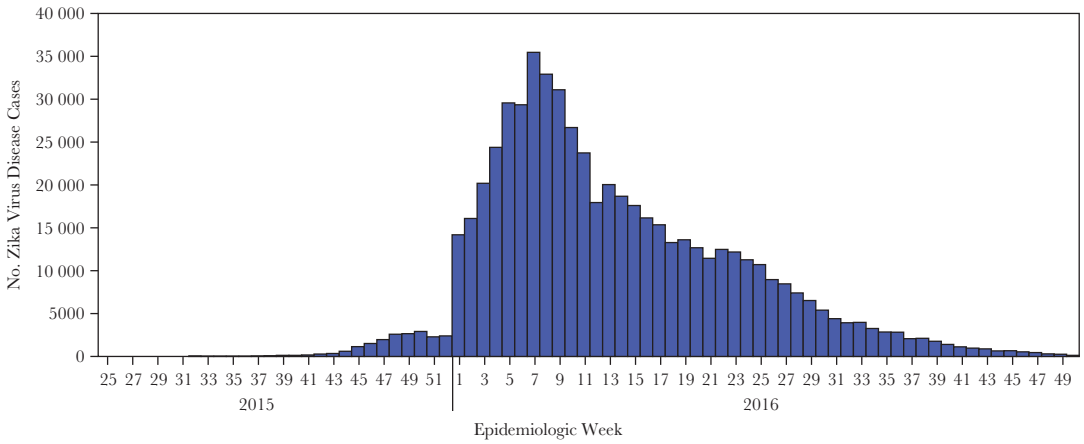

Figure 1.3. ZIKV epidemiology in the Americas, 2015-2016. Figure from (11). The number of suspected and confirmed ZIKV cases reported to the Pan-American Health Organization from the latter half of 2015 and 2016.

Outbreaks of ZIKV in the Pacific Islands, 2007-2014

Prior to the American epidemic, only two outbreaks of ZIKV had been reported, both of which were in the Pacific Islands (6). The first reported outbreak of ZIKV was in Yap State in 2007 (17). It was estimated that ~75% of the island's population (~5,000 individuals) was infected with ZIKV during the three-month outbreak. ZIKV infection throughout the Yap State outbreak was characterized by a mild, self-limiting febrile illness, which occurred in just a subset of infections (18.4%).

In 2013-2014, a larger outbreak of ZIKV occurred in French Polynesia (6, 18, 19). Approximately 30,000 individuals, or 11.5% of the population, was estimated to be infected with ZIKV. However, it is hard to quantify the exact number of ZIKV infections in this outbreak given the low percentage of people who exhibited symptoms and accessed care. Retrospective studies since the American ZIKV epidemic have identified GBS cases in adults during this ZIKV outbreak (6). Maternal-fetal transmission of ZIKV was also demonstrated, however no ZCS cases were identified (6). From French Polynesia, ZIKV quickly spread to other Pacific Islands before being introduced into Brazil in late 2013 – early 2014 (20), leading to the American ZIKV epidemic.

ZIKV in Africa

Discovery & conflicting evidence on ZIKV circulation

ZIKV was first isolated from a sentinel rhesus macaque in the Zika Forrest of Uganda in 1947 as part of Rockefeller Foundation-funded research programs on Yellow Fever (6, 21). The virus was isolated from “monkey no. 766” and, in fact, this strain (MR 766) is still highly utilized across laboratories studying ZIKV to this day. The first human ZIKV isolate came from a 10-year old female in Nigeria in 1954 (22).

Despite it being discovered on the African continent more than 70 years ago, the level of ZIKV prevalence on the African continent and the properties of viruses that circulate there are unclear. Between the discovery of ZIKV and its first reported outbreak on Yap Island in 2007 (an ~60-year period), there were less than 10 confirmed cases of ZIKV infection reported on the African continent (23-27). Serological surveys conducted during this same time period to examine the seroprevalence of many arthropod-borne viruses throughout Africa, on the other hand, have largely suggested that ZIKV is endemic on the African continent (reviewed in (6)). However, it is challenging to interpret and make comparisons from this collection of serosurvey data for several reasons. Different methods were used across the many studies to assay for the presence of ZIKV antibodies (hemagglutination inhibition, complement fixation, neutralizing antibody tests, mouse protection, hemagglutination, ELISA), and there were often discrepant results when comparing between methods or even when repeating the same method (6). Probably the largest issue in the interpretation of these early findings is the fact that most methods used at the time did not account for cross-reactivity in the antibody response between ZIKV and other closely related flaviviruses, such as Dengue virus (DENV). This is now a well-described aspect of the humoral response to flavivirus infections and is discussed in detail below.

Need for ZIKV data from Africa

Since the emergence of ZIKV in the Americas and its associated severe morbidity and mortality, significant efforts have been focused on elucidating novel aspects of the ZIKV epidemic in the Americas. The lack of ZIKV data from Africa described above, where ZIKV was first discovered and mosquito vectors capable of transmitting multiple arthropod-borne viruses are endemic, complicates these efforts (28-30). There is an urgent need to examine ZIKV population-level exposure, ZIKV pathogenesis, and the basic virology of ZIKV strains that circulate in Africa and the Americas, as these findings can provide insights into the importance of these factors in current and future outbreaks of ZIKV, improve our understanding of the future trajectory of this emerging pathogen, and guide the design of appropriate interventions in Africa. This is the focus of this thesis and an introduction to each of these aspects is discussed in the following sections.

Population-level exposure to ZIKV on the African continent

Methods of ZIKV detection and associated challenges

Clinically identifying individuals who have been infected with ZIKV is challenging, as the acute febrile presentation of ZIKV-infected patients is hard to reliably distinguish from infections with other many pathogens (31). In addition, methods to specifically detect ZIKV infection are limited. Existing tools to detect ZIKV infection can be divided into those that detect the virus itself and those that detect prior exposure to the virus (Figure 1.4) (32).

Direct detection of ZIKV typically involves amplification of ZIKV RNA by methods such as quantitative reverse transcription-PCR (qRT-PCR), although other methods have been used such as isolation of virus from plasma of infected individuals (18, 33). Detection of viral antigens such as non-structural protein 1 (NS1), which is produced from infected cells in the acute phase of infection, has been used to detect acute cases of DENV infection but this has not yet been clinically used in the case of ZIKV infection (32). Although ZIKV RNA detection is the gold-

standard for identifying cases of ZIKV infection due to its high specificity, its use is limited by the short period of detectable ZIKV viremia in infected individuals (~10-14 days) and low sensitivity in some assay formats (34) (Figure 1.4, “Challenges”).

Methods to detect prior exposure to ZIKV rely on the detection of binding or neutralizing antibodies to ZIKV that are produced several days following infection, some of which persist for months to years. The main antigenic determinant of flaviviruses, including ZIKV, is the Envelope glycoprotein (E-protein) present on the surface of the viral particle (35, 36). Thus, following ZIKV infection, antibodies targeting the E-protein are produced (Figure 1.5). The main clinically-approved serological test for ZIKV infection is an immunoglobulin M (IgM) antibody capture ELISA (MAC-ELISA), which detects IgM antibodies that bind the ZIKV E-protein. IgM antibodies develop in the first few days following infection and wanes over time and is typically undetectable in sera 90-120 days post-infection (37). Thus, MAC-ELISAs are not useful when testing samples that have been collected after ~3 months post-infection (38-40). Immunoglobulin G (IgG) antibodies, on the other hand, are long-lived in the serum (41, 42). Several assay formats, most commonly ELISA, exist to detect ZIKV IgG antibodies, although none are approved for use in the clinical laboratory setting (drawbacks discussed below). Methods to detect ZIKV neutralizing IgG antibodies (nAbs), such as the plaque-reduction neutralization test (PRNT), are long-standing in the field. In a PRNT, dilutions of serum are made to determine the reciprocal dilution that reduces the number of ZIKV plaques by typically 50% or 90% (6). PRNTs are used clinically when MAC-ELISAs are equivocal or negative in patients with a high pre-test probability of infection, although PRNTs are laborious and must be performed in highly-specialized reference laboratories for clinical use (38). More recently, studies have begun using GFP or luciferase reporter virus particles (RVPs) to examine antibody-mediated neutralization of ZIKV in an analogous manner to PRNTs, except the read-out is reduction of GFP or luciferase instead of plaques (43-45). ZIKV RVPs are made by complementation of a self-replicating flavivirus RNA encoding ZIKV non-structural proteins and

a reporter with structural genes provided *in trans* (46). RVP neutralization assays are used in this thesis to examine ZIKV neutralizing antibody responses.

A significant drawback of methods to detect ZIKV antibodies (IgM and IgG) is the cross-reactive nature of the antibody response elicited in flavivirus infections (6, 35, 38, 47). Historically, flaviviruses have been organized into distinct “serocomplexes” based on the cross-neutralizing properties of polyclonal flavivirus-infected sera (reviewed in (48)). Flavivirus serocomplex organization correlates with E-protein sequence identity. Antibodies elicited against ZIKV have been shown to be cross-reactive with DENV, which is not surprising given that their E-proteins have a high level of sequence identity (54-58% at the nucleotide level) and antigenic similarity (49). During an acute flavivirus infection, a highly cross-reactive antibody response is elicited that is comprised of antibodies that can neutralize and bind many flaviviruses (47, 50-53). Studies of the neutralizing antibody responses in DENV-infected individuals have demonstrated that cross-neutralization of ZIKV and all four serotypes of DENV is present in the acute and early-convalescent phases of infection (50-52). In individuals who have experienced a single DENV infection (“primary DENV infection”), it is known that the neutralizing antibody response is at first cross-reactive against all four DENV serotypes but gradually becomes focused towards, or narrows against, the infecting DENV serotype over a period of months following infection (47). Recent studies examining neutralizing antibody responses in DENV-infected and ZIKV-infected late-convalescent plasma (≥ 6 months post-infection) have extended these findings to ZIKV infection, as well. That is, the neutralizing antibody response in ZIKV-infected or DENV-infected individuals becomes type-specific to the infecting virus in late-convalescent serum. In fact, even ZIKV-naïve individuals who experience > 1 DENV infection (“secondary DENV infection”), in most cases, do not develop potent cross-neutralizing responses against ZIKV in late-convalescence but do have durable cross-neutralization of multiple DENV serotypes (53-55). The binding antibody response against all flavivirus infections, on the other hand, is notoriously cross-reactive, in large part due to binding

antibodies directed against the highly-conserved fusion loop on the E-protein (48). Nonetheless, promising methods that detect binding antibodies to ZIKV viral proteins, such as NS1, are in development (56).

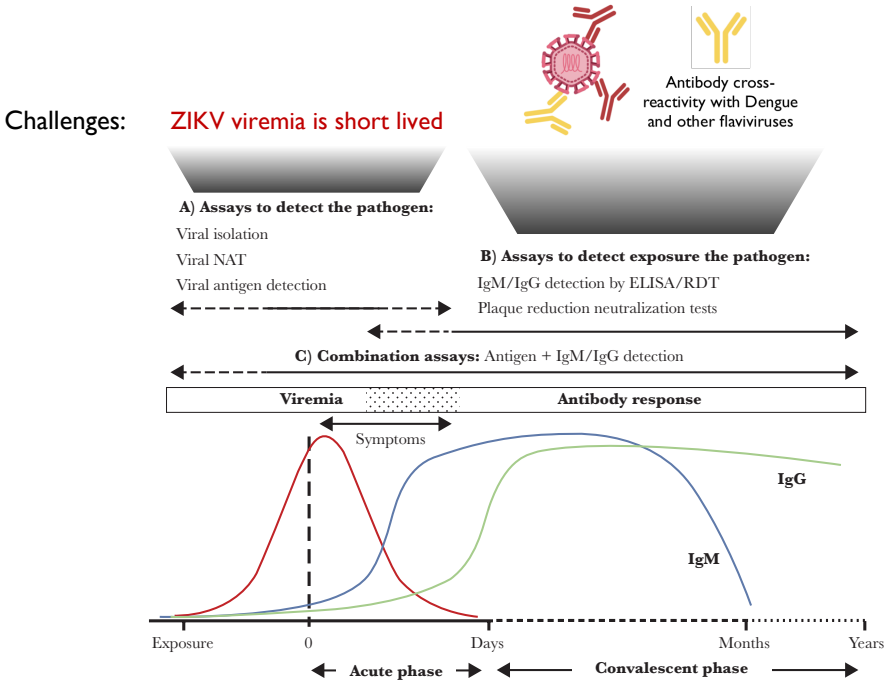

Figure 1.4. Temporal dynamics of ZIKV/DENV infection and tools available to detect infection. Figure modified from (32). The temporal dynamics of ZIKV/DENV viremia and the antibody response to infection are shown. Available tools to detect various aspects of infection are listed above the corresponding temporal phase (NAT, nucleic acid amplification test; RDT, rapid diagnostic test).

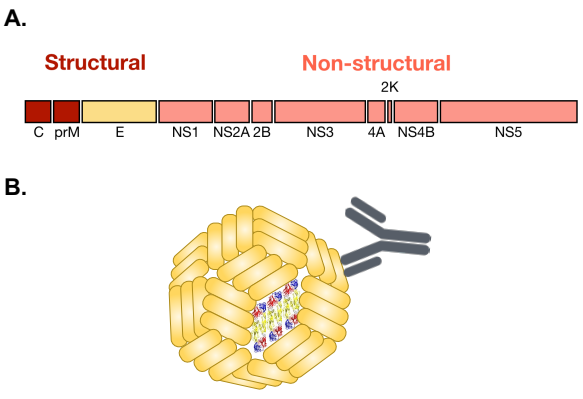

Figure 1.5. ZIKV genomic and antigenic structure. (A) The organization of the ~11-kilobase ZIKV genome is shown. Structural protein coding are in dark red, with the exception of the E-protein which is shown in yellow. Non-structural proteins ("NS") are shown in light red. (B) Figure modified from (57). A representative flavivirus particle. E-protein head-to-tail dimers are shown in yellow. Three representative ribbon head-to-tail E-protein dimers are shown on the structure of the viral particle.

Recent ZIKV seroprevalence studies in Africa

Several recent ZIKV seroprevalence studies on the African continent have been published (Table 1.1). Collectively, these studies largely report low levels of ZIKV circulation (0.1-0.8%) (58-63). However, the data also suggests that certain regions in Africa may experience higher levels of ZIKV circulation and related febrile illness. One study in West Pokot county, Kenya, and another in West Africa (Nigeria and Senegal) found higher levels of ZIKV seroprevalence (6.3-7.7%), although it is unclear how cross-neutralizing responses were accounted for in West Pokot county and nAb responses were not examined in West Africa (25, 58).

Table 1.1. Recent studies of ZIKV seroprevalence data on the African continent.
[a] It is unclear how antibody cross-reactivity was accounted for in these studies
[b] Only samples that were YFV ELISA+ were included for further ZIKV testing

Study	*Location*	*Years*	*Study design*	*Findings*	*Methods*
Chepkorir et al (58)[a]	Northern Kenya (West Pokot and Turkana counties)	2016-2017	Cross-sectional (age 13+)	• 33/464 (7.11%) - West Pokot • 1/413 (0.24%) - Turkana	PRNT
Tsegaye et al (61)[b]	Ethiopia	2014	Cross-sectional (age 5+)	7/1643 (0.4%) ZIKV PRNT+	IgG ELISA followed by PRNT
Kisuya et al (60)	Kenya (Nairobi, Eldoret, Kisumu)	2009-2014	Cross-sectional (healthy adults)	1/577 (0.2%) ZIKV PRNT+	NS1 ELISA followed by PRNT
Kayiwa et al (59)	Uganda (Nkokonjeru)	2014-2017	Prospective acute febrile illness surveillance	3/384 (0.78%) ZIKV PRNT+	IgM ELISA followed by PRNT
Herrera et al (25)	Nigeria & Senegal	1992-2016	Samples collected within 7 days of fever	24/387 (6.2%) ZIKV IgM ELISA+ / DENV IgM-	ZIKV and DENV IgM ELISA
Willcox et al (63)	Democratic Republic of Congo	2013-2014	Cross-sectional (children aged 6 months-5 years)	1/978 (0.1%) ZIKV neut+	ZIKV IgG ELISA followed by FRNT
Soghaier et al (62)[a,b]	Sudan	2012	Cross-sectional	1/845 (0.12%) ZIKV PRNT+	ZIKV ELISA followed by PRNT

Only a subset of these studies has focused on populations in East Africa, where ZIKV was first discovered (58-61). Further studies are particularly warranted in Kenya, where findings vary considerable by region even in recent studies. Chepkorir et al (58) reported 7.7% ZIKV seroprevalence in one county of Kenya while Kisuya et al (60) reported 0.2% ZIKV seroprevalence from multiple urban areas in Kenya. Past studies that used non-specific methods (discussed above) have found as a high as 52% ZIKV seroprevalence (reviewed in (6)). The level of continuous ZIKV circulation in East Africa is unclear, as samples from only a relatively limited time range (2009-2017) have been included (58-61) as compared to a study in West Africa (1992-2016) (25). Only a single study has examined ZIKV as a cause of febrile illness in East Africa (59). Perhaps most importantly, there is no existing ZIKV seroprevalence data from the coastal city of Mombasa, Kenya, a densely population region where there have been several large arboviral outbreaks in the past (64, 65).

ZIKV in East Africa and cohorts utilized in this thesis

In this thesis, we characterized ZIKV seroprevalence in Kenya by utilizing plasma samples collected from two unique cohorts in Mombasa and Kisumu, Kenya, where mosquitoes capable of transmitting ZIKV are endemic (66). The Mombasa cohort is an ongoing cohort study established in 1993 to study women at high-risk for acquiring HIV-1 (67) and the Kisumu cohort is a closed prospective cohort study (2011-2013) established to examine factors involved in HIV-1 acquisition during pregnancy and post-partum periods (68). Fever and rash are commonly reported symptoms of ZIKV infection (17). Thus, to examine ZIKV seroprevalence and its contribution to febrile illness, included visits were those from the Mombasa cohort (1993-2016) and Kisumu cohort (2011-2013) that were collected from individuals who had fever and/or rash that was either documented on exam (temperature ≥ 37.5℃) or self-reported. Overall, these cohorts are unique in at least two aspects that are relevant to studies of ZIKV presence in East Africa: 1) there are serum samples that span a 25-year time period, allowing us to examine

ZIKV prevalence over several decades and 2) extensive regular follow-up of study participants is well-suited for examining the serological response over extended time period in participants of interest.

Viral genetics of ZIKV

ZIKV phylogenetics and evolution

ZIKV belongs to the mosquito-borne *Flavivirus* cluster within the *Flaviviridae* virus family (6). ZIKV is most closely related to Spondweni virus (SPOV), another understudied virus that is also believed to be endemic on the African continent (Figure 1.6) (48). Phylogenetic analysis of sequenced ZIKV strains has revealed that they are broadly clustered into two lineages (Figure 1.7) (6, 69). Strains isolated from the African continent make up the African lineage, which can be further divided into West African ("Nigerian") and East African ("MR 766") sub-lineages (24, 25). Overall, African-lineage ZIKV genetic data from human infections is sparse, as only five partial-genome sequences and one complete-genome lab-passaged isolate (GenBank: KU963574.2) have been documented (24, 25). ZIKV sequences from human infections in East Africa have never been isolated. The East African sub-lineage is entirely comprised of sequences isolated from mosquitoes and a non-human primate. It is believed that ZIKV spread from Africa to Asia in the late 1940s, giving rise to the Asian ZIKV lineage (24). ZIKV strains isolated in Southeast Asia cluster within the Asian lineage as do isolates from the American outbreak and even form their own sub-lineage (6). More recent phylogenetic analyses including the large number of ZIKV isolated from the Americas have further organized the American ZIKV outbreak clade into even more sub-lineages (70).

Intriguingly, there is limited evidence that African-lineage ZIKV infections are associated with the severe pathogenic profile (Figure 1.2) that has been fueled by the American clade. This

raises the possibility that African- and Asian-lineage ZIKV strains may have distinct pathogenic properties (Figure 1.7).

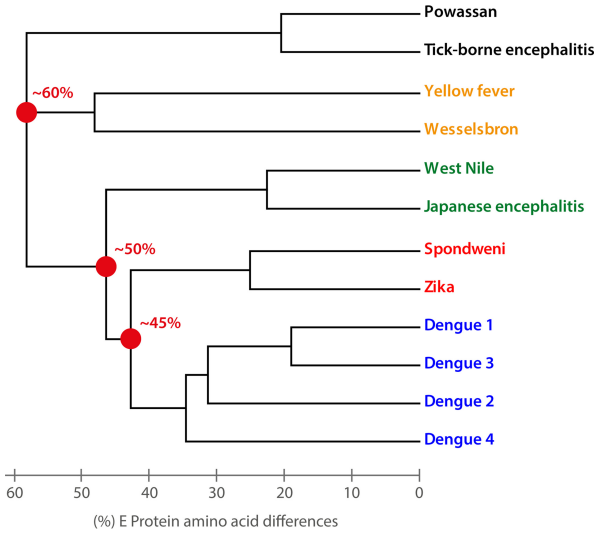

Figure 1.6. Phylogenetic relationships of main human pathogenic flaviviruses. Figure from (48). A phylogenetic tree of main human-pathogenic flaviviruses is shown. Spondweni and Wesselsbron virus are included because they are described as members of the same serocomplex as other viruses on the phylogeny. The tree is based on sequences of E-protein.

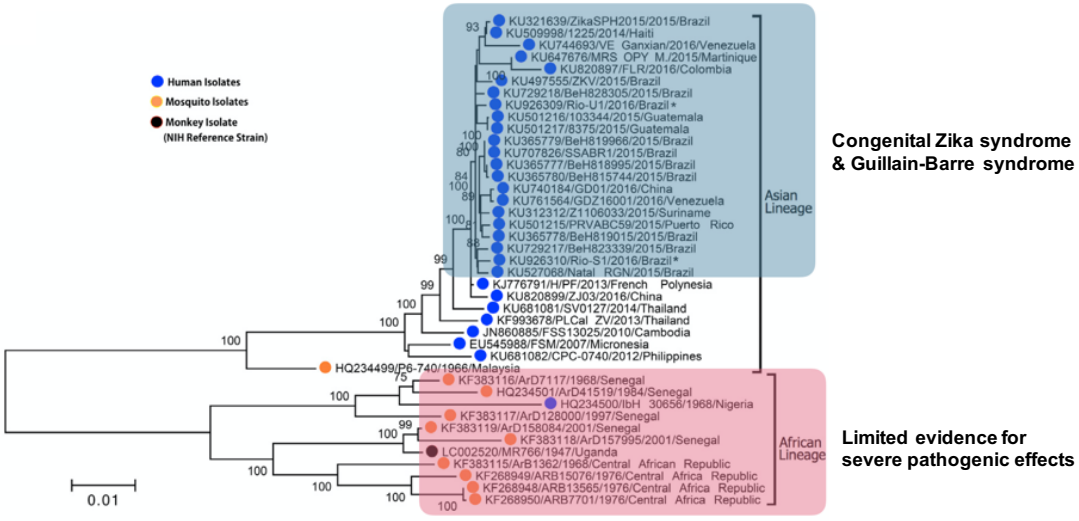

Figure 1.7 Phylogenetic relationships of African- and Asian-lineage ZIKV strains. Figure modified from (69). A phylogenetic tree of African- and Asian-lineage ZIKV strains is shown. The tree is based on full-length open reading framed of ZIKV strains. American outbreak strains are highlighted in red and African-lineage strains are highlighted in blue.

Comparative studies of ancestral vs. contemporary ZIKV strains

The apparent pathogenic differences in ZIKV transmission and pathogenesis between African- and to Asian-lineage ZIKV strains has motivated many groups to examine specific mutations as well as broader virologic characteristics of diverse ZIKV strains *in vitro* and *in vivo*. Specific mutations have been identified in the coding sequence of contemporary ZIKV strains as potential drivers of changes in ZIKV pathogenic properties (71-73). One group reported that the S139N mutation in the pre-membrane structural protein (prM) of ZIKV (Figure 1.5A), which arose before the 2013 French Polynesian ZIKV outbreak and has been maintained in American outbreak strains, was associated with an increase in microcephaly in mice (73). However, this study performed intracerebral viral injections which raises questions about the relevance of their findings to the setting of ZIKV vertical transmission which ultimately gives rise to ZCS. A single mutation in ZIKV NS1 (A188V), which was one of only two differences in NS1 sequence between a 2010 Cambodian Asian-lineage and American Asian-lineage ZIKV isolates, both enhances ZIKV infectivity in *Aedes* mosquitoes and reduces innate antiviral host defenses (71, 72). However, many other studies have used strains that differ in this NS1 residue and have not detected infectivity differences in *Aedes* mosquitoes, suggesting that further studies are needed to determine if this mutation plays a role in the emergence of ZIKV in the Americas (74).

A growing collection of studies have compared virologic characteristics between African and Asian/American ZIKV strains. Collectively, the results from many of these studies demonstrate that infection with African-lineage strains results in enhanced replication kinetics, virus production, cytopathicity, and disease progression in murine models (75-88). This seems counterintuitive given that African-lineage strains have not been historically associated with severe pathogenesis. However, it has been hypothesized that these attributes may enable Asian-lineage strains to better establish chronic infection of neural progenitor cells, undergo more efficient vertical transmission, and establish viral reservoirs in the central nervous system, lymph nodes, and gastrointestinal and genitourinary tracts (84, 89-92). In this thesis, I examine

the role of a critical innate anti-viral response mediated by type-I interferon in restricting diverse African- and Asian-lineage ZIKV strains.

The role of the type-I interferon response in ZIKV infection

The type-I interferon response

Type-I interferon (IFN-I) is a critical component of the host innate immune response to viral infection (93). Upon recognition of viral infection by pattern recognition receptors (PRRs), cells enter a transcriptional program that increases the production of IFN-I (IFNα and IFNβ) (Figure 1.8). When IFN-I engages its heterodimeric receptor (IFNAR) on the cell surface, IFNAR-bound Janus kinases (JAK1, JAK2, TYK2) are activated and phosphorylate highly-conserved IFNAR tyrosine residues. This results in conformational rearrangements that allow for the binding and phosphorylation of Signal Transducers and Activators of Transcription (STAT) proteins which, when phosphorylated, dimerize and interact with IFN regulatory factor 9 (IRF9) forming Interferon Stimulated Gene Factor 3 (ISGF3). ISGF3 then moves into the nucleus, where it engages Interferon-Stimulated Response Elements (ISREs) in the genome to induce the expression of hundreds of interferon-stimulated genes (ISGs) (Figure 1.9) (94). ISGs have a wide range of anti-viral functions and, together, establish an anti-viral state in bystander cells and restrict viral replication in infected target cells (94, 95).

Several studies have highlighted the importance of the IFN-I response in controlling flavivirus replication and tropism (96-100). More recently, IFN-I has been shown to restrict ZIKV in cell culture (101, 102). Further, most murine models of ZIKV pathogenesis require ablation of the IFN-I signaling pathway, underscoring the important role of ISGs in restricting ZIKV replication (81). However, the specific downstream ISGs remain poorly characterized in the context of ZIKV and other flavivirus infections.

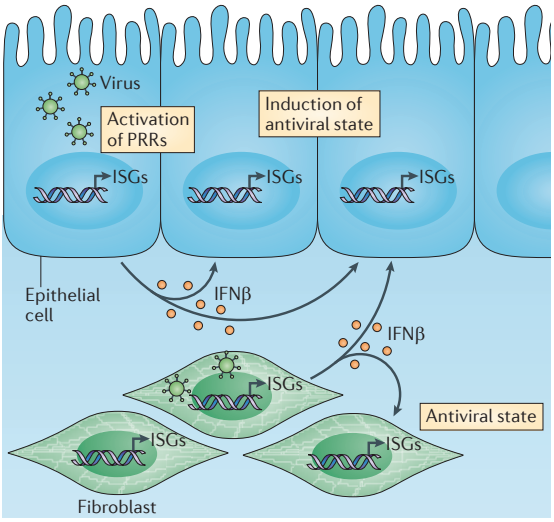

Figure 1.8. The IFN-I response in response to viral infection. Figure from (93). Upon recognition of viral infection, infected cells enter a transcription program ultimately resulting in the production of IFN. IFN then signals to other infected and bystander cells in an autocrine and paracrine fashion to enter an antiviral state through the induction of hundreds of IGS.

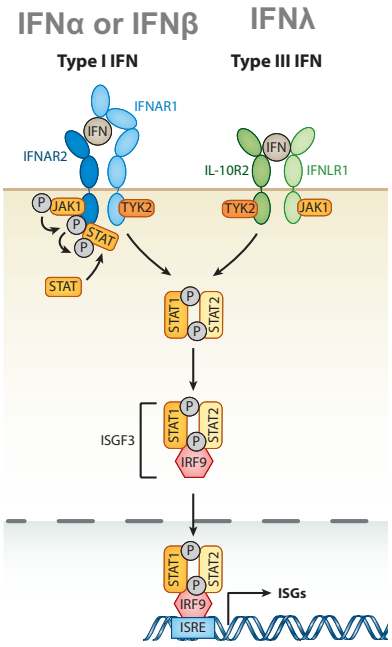

Figure 1.9. The IFN-I signaling cascade. Figure modified from (94). IFN-I first binds to its receptor (IFNAR) on the cell surface, which initiates a signaling cascade through the JAK-STAT pathway to ultimately induce the expression of hundreds of ISGs that act to protect the IFN-stimulated cell against viral infection. Type-III interferon is also shown in the figure, which converges on many of the same downstream signaling cascades as IFN-I.

ZIKV-restricting interferon stimulated genes

Since the renewed interest in the study of ZIKV over the past few years, several individual ISGs have been reported to have activity against ZIKV (Table 1.2). Most studies have focused on a single or small collection of ISGs (see below). Large-scale ectopic expression and gene silencing/knockout studies have identified anti-viral ISGs in the context of other flaviviruses, and provide support for broad approaches to understand the complexities of virus-host interactions and IFN-I signaling (103-110).

The first reported ISG to inhibit ZIKV was Interferon-induced transmembrane protein 3 (IFITM3) (111, 112). IFITM3 is a small transmembrane protein that restricts a broad array of viruses and is potently induced by IFN-I (113). A targeted gene knockout approach of 23 genes in A549 lung adenocarcinoma cells revealed that Poly(ADP-Ribose) Polymerase Family Member-12 (PARP12) inhibits ZIKV replication by promoting the degradation of viral non-structural proteins (NS1 and NS3) that are required for ZIKV replication (114). Viperin (RSAD2) was identified as a ZIKV restriction factor in the Huh7 hepatocyte cell line and mouse embryonic fibroblasts (MEFs) (115). When overexpressed in Huh7 and fetal neural progenitor cells, IFN-α-inducible protein 6 (IFI6) was shown to modestly restrict ZIKV (116).

CRISPR-Cas9 technology, which allows for precise editing of genomic loci based on sequence complementarity to a single-guide RNA (sgRNA) and endonuclease Cas9 activity, has been widely adapted in various forms to probe virus-host interactions on a large scale (reviewed in (117); more background provided in Chapter V, Introduction). To date, there has only been one published screen to designed specifically to identify ZIKV-restricting ISGs in a comprehensive manner (107). The screen, which employed a genome-wide CRISPR-activation strategy where all targeted genes in the library were overexpressed, also identified IFI6 as their consistently top-scoring hit. Interferon-stimulated gene 20 (ISG20) and IFN-lamba-2 (IFNλ2) were also identified as other potential ZIKV restriction factors. No other studies have surveyed ISGs for their restrictive capacity against ZIKV in a comprehensive manner.

A unifying feature of all of the aforementioned studies is that, despite interrogating the inhibitory capacity and, in some cases, the mechanism of these ISGs, none examine the contribution of the ISGs to the overall IFN-I response against ZIKV. In this thesis, I will perform more detailed mechanistic studies of IFITM3 to understand its contribution to the overall IFN-I response against ZIKV. In addition, I will develop a new CRISPR-knockout-based screening strategy for comprehensive identification of ZIKV-restricting ISGs.

Table 1.2. Interferon-stimulated genes reported to restrict ZIKV.
[a] This study is the only CRISPR screen designed to identify ZIKV-restricting ISGs.

Study	*ISG*	*Cell type(s)*	*Approach(es)*
Savidis et al (112)	IFITM3	HeLa, A549, MEF	Overexpression; knockout in MEFs
Monel et al (111)		HeLa, 293T, HFF, HDFa	Overexpression; shRNA-knockdown
Spence et al (118)		HeLa	Knockout
Li et al (114)	PARP12	A549, MEF, 293T, BHK-21, HeLa, Vero	Overexpression; knockout
Van der Hoek et al (115)	Viperin	Huh7, MEF	Overexpression; knockout in MEFs
Richardson et al (116)	IFI6	Huh7, Fetal human neural progenitor	Overexpression
Dukhovny et al [a] (107)		Huh7	Overexpression; siRNA-knockdown

Goals for this thesis

The overall goals for this thesis are to define population-level immunity to ZIKV in Kenya and to interrogate the role of the type-I interferon response in restriction of ZIKV strains from Africa and the Americas. In Chapter II, I report on the screening of convalescent plasma from febrile subjects in densely populated, urban regions of Kenya to define the level of ZIKV exposure and its contribution to febrile illness. In Chapter III, I describe the design of a phage-display based serological screening tool that shows promise in detecting signatures of ZIKV-specific antibodies in plasma to more specifically identify individuals with a history of ZIKV exposure. In the future, this tool can be applied to detect other pathogens that cause febrile illness in sub-Saharan Africa where there is a tremendous burden of undiagnosed acute febrile illness (31). I also extend the utility of this method in Chapter III by demonstrating its ability to epitope-map monoclonal antibodies isolated from Kenyan subjects. In Chapter IV, I compare the IFN-I-mediated restriction of diverse ZIKV strains and provide a detailed mechanistic understanding of IFITM3, the first ISG reported to be active against ZIKV. In Chapter V, I describe the development of a CRISPR-Cas9-based screening platform that can be used to identify ISGs that inhibit ZIKV as well as other cytopathic viruses.

Chapter II

Zika virus circulates at low levels in Western and Coastal Kenya

Sections of text in this chapter have been modified slightly from the following manuscript:

> **Gobillot TA**, Kikawa C, Lehman D, Kinuthia J, Drake A, Jaoko W, Mandaliya K, John-Stewart G, McClelland RS, Overbaugh J. (2020) Zika virus circulates at low levels in Western and Coastal Kenya. *In review. Journal of Infectious Diseases*.

Introduction

The recent unprecedented spread and severe pathogenic features of Zika virus (ZIKV) in the Americas have led to its recognition as a global threat to public health and the need to understand the global prevalence of ZIKV, which was first discovered in Uganda in 1947. Seroepidemiological surveys conducted in the decades following its discovery suggested that ZIKV is endemic on the African continent (6); yet, there is little evidence for the sequalae associated with the American ZIKV outbreak. Prior reports of ZIKV seroprevalence in Africa are hampered by methodological challenges that do not account for the extensive antibody cross-reactivity between ZIKV and other closely related flaviviruses, particularly Dengue virus (DENV), which is common in Africa. As a result of these challenges and little concern about ZIKV prior to the American outbreak, its prevalence in Africa remains poorly defined, particularly in East Africa where ZIKV was first discovered. More recent studies of ZIKV seroprevalence in East Africa have collectively reported low ZIKV exposure (0.2-0.8%) (58-61) and little evidence for ZIKV as a cause of febrile illness in East Africa (59). However, a study in northwestern Kenya found that 7.7% of samples contained ZIKV neutralizing antibodies (58), suggesting there may be regions of higher ZIKV prevalence in Kenya.

To better define the prevalence of ZIKV infections in East Africa, we focused on two of the most densely-populated regions of Kenya where the mosquito vector for ZIKV circulates, including Mombasa, where there have been several arboviral outbreaks (64, 65). We screened convalescent plasma from individuals who experienced ZIKV-like illness (fever and/or rash) in

cohorts in Kisumu (2011-2013) and Mombasa (1993-2016), Kenya for evidence of ZIKV exposure and identified cases of prior ZIKV infection.

Methods

Study Design and Plasma Samples

This study utilized samples from two cohorts of women in Mombasa and Kisumu, Kenya. (Table 2.1). The Mombasa cohort is an ongoing cohort study established in 1993 to study women at high-risk for acquiring HIV-1 (67) and the Kisumu cohort is a closed prospective cohort study (2011-2013) established to examine factors involved in HIV-1 acquisition during pregnancy and post-partum periods (68). Individuals with ZIKV-like symptoms were identified in each cohort. In the Mombasa cohort, individuals with fever (temperature ≥37.5˚C) on exam were included, as were individuals who had self-reported fever and rash either by self-report or on exam. In the Kisumu cohort, individuals with fever and/or rash on exam were included. For serological testing in this study, we utilized the first available plasma sample 2-12 months post-onset for each visit with ZIKV-like symptoms ("convalescent sample"), when ZIKV IgG should be high (37), as well as longitudinal samples in a subset of cases with evidence for ZIKV antibodies in the convalescent sample. For 32 women who had ZIKV-like illness during pregnancy in the Kisumu cohort, a sample 6-week post-partum was also included for serological testing if available. Plasma from subjects who had detectable HIV-1 RNA but undetectable HIV-1 antibodies were excluded, since febrile symptoms were likely due to acute HIV infection. Plasma of known infection status were kindly provided by NIAID's Biodefense and Emerging Infectious Disease Resource Repository (BEI Resources) and William Messer (Table 2.2).

Anti-ZIKV NS1 IgG ELISA

The anti-ZIKV NS1 IgG ELISA (R&D Systems) was performed on control samples and Kenyan convalescent plasma samples according to the manufacturer's protocol. Each sample was

diluted 100-fold (300 µL total) in R&D sample dilution buffer and treated with a proprietary reagent for 1 hour at room temperature to remove cross-reactive antibody responses. Treated samples were then each added to a ZIKV NS1-coated plate and background plate (100 µL / well) and incubated for 1 hour at room temperature. The plates were subsequently washed three times with R&D wash buffer (400 µL / well) and 100 µL of R&D human ZIKV IgG conjugate was added to each well and incubated at room temperature for 1 hour. The plates were washed again with R&D substrate solution (100 µL / well) was added to each plate and incubated for 20 mins in the dark. R&D stop solution (50 µL / well) was added to each well and the binding OD_{450} was measured on the ZIKV NS1-coated plate and the background plate. ELISA kit treatment-control, positive-control, and negative-control samples were also included in each assay. Dilution buffer alone served as a non-specific binding control (NSB). A background-adjusted Net OD_{450} value was obtained for each sample using the following calculation: Net OD450 = (OD_{450} plasma sample $_{\text{ZIKV NS1 plate}}$ – OD_{450} NSB $_{\text{ZIKV-NS1 plate}}$) – (OD_{450} plasma sample $_{\text{background plate}}$ – OD_{450} NSB $_{\text{background plate}}$). Net OD_{450} values were averaged between at least two replicate wells. As suggested by the manufacturer, Net OD_{450} values > 0.2 were considered positive, 0.1-0.2 were considered equivocal, and < 0.1 negative.

ZIKV & DENV neutralization studies

Neutralization studies using luciferase ZIKV (SPH2015), DENV-1 (WestPac), DENV-2 (S16803), DENV-3 (CH53489), and DENV-4 (TVP360) RVPs (Integral Molecular) were carried out as described previously (46). Plasma (100 µL final volume) and RVPs (100µL final volume) diluted in RVP infection media (DMEM [Invitrogen] supplemented with 10% FBS, 2mM L-glutamine, 10mM HEPES, 1X Anti-anti, pH 8.0) were added to each well of a white 96-well plate (Breiner Bio-One) and were incubated at room temperature for 1 hour. Following this incubation, 30,000 BHK-DCSIGN cells (100 µL final volume; Integral Molecular) were added to each well and the plates were incubated at 37˚C for 72 hours. Wells on outside rows and columns were

not used and instead filled with 300 µL media. Neutralization assays were harvested using a Renilla Assay Detection Kit (Promega) according to the manufacturer's protocol and read on a Thermo-Fischer Fluoroskan Ascent FL. To calculate a "% infection" value for each sample, relative luciferase unit values (RLUs) from each sample were background-adjusted by subtracting RLUs in wells that only contained cells and normalized to RLUs from wells where no plasma was added. A "% neutralization" value was then calculated by: % neutralization = 100 – [% infection]. All negative % neutralization values were considered 0% neutralization. Plasma samples were either tested at a single 75-fold dilution or, in the case of NT_{50} assays, were first diluted 75-fold and then serially diluted 3-fold across a row of a 96-well plate. Data from NT_{50} assays were plotted in GraphPad Prism 8 (% infection vs. log10 fold plasma dilution) and a non-linear regression curve was fit to the data to identify the fold dilution at which the plasma reached 50% infection (NT_{50}).

Results

In total, 327 plasma samples (235 from Mombasa and 95 from Kisumu) from 245 individuals, including 71 individuals with more than one plasma sample, were examined for ZIKV-specific antibodies (Table 2.1), starting with an ELISA that detects the presence of antibodies targeting ZIKV NS1. The ELISA was first validated with plasma samples from ZIKV-infected, ZIKV-naïve/DENV-infected, and flavivirus-naïve individuals (Table 2.2). All ZIKV-infected samples were positive by ELISA except one early-convalescent sample (50835) which was negative (Figure 2.1). Seventeen of 18 flavivirus-naïve and ZIKV-naïve/DENV-infected samples were negative by ELISA; 1 sample (Negative 4) was equivocal. Seven (2.1%) Kenyan convalescent plasmas were positive by the ELISA, of which 4 were from Mombasa and 3 were from Kisumu (Figure 2.3A). Forty-three (13.1%) samples were equivocal and 277 samples (84.8%) were negative.

Table 2.1. Characteristics of Mombasa and Kisumu cohorts utilized in this study.

Characteristic	Mombasa cohort	Kisumu cohort
No. of samples	232	95
Sample year range	1993-2016	2011-2013
Convalescent sample collection, mean months post Zika-like illness (range)	4.2 (1-42)[1]	7.1 (0.6-21)[2]

[1] 33 samples with unknown timing (2-12 months)
[2] 4 samples with unknown timing

Table 2.2. Control samples used to validate the anti-ZIKV NS1 IgG ELISA and RVP neutralization assays.

Sample ID	Infection history [1]	Timing of sample collection post-symptoms
50462	ZIKV	1 month
50615	ZIKV	7.5 months
50662	ZIKV	~10 months
50657	ZIKV	~3 months
50867	ZIKV	late convalescence
50848	ZIKV	early convalescence
50464	ZIKV with prior DENV infection	1 month
50459	ZIKV with prior DENV infection	1.5 months
50854	ZIKV with prior DENV infection	late convalescence
50835	ZIKV with prior DENV infection	early convalescence (ZIKV)
50852	ZIKV with prior DENV infection	late convalescence
50224	DENV-1	~9 months
50225	DENV-1	~48 months
50226	DENV-2	~120 months
50227	DENV-2	~180 months
50229	DENV-3	~60 months
50228	DENV-3	unknown
50232	Secondary DENV	~96 months
50230	Secondary DENV	unknown
50231	Secondary DENV	~408 months
50233	Secondary DENV	~96 months
Negative -1,3,4,5,6,7,8,9	Flavivirus-naive	N/A

[1] Infection history was defined by the source (BEI for positive samples, William Messer for flavivirus-naive samples) based on serology

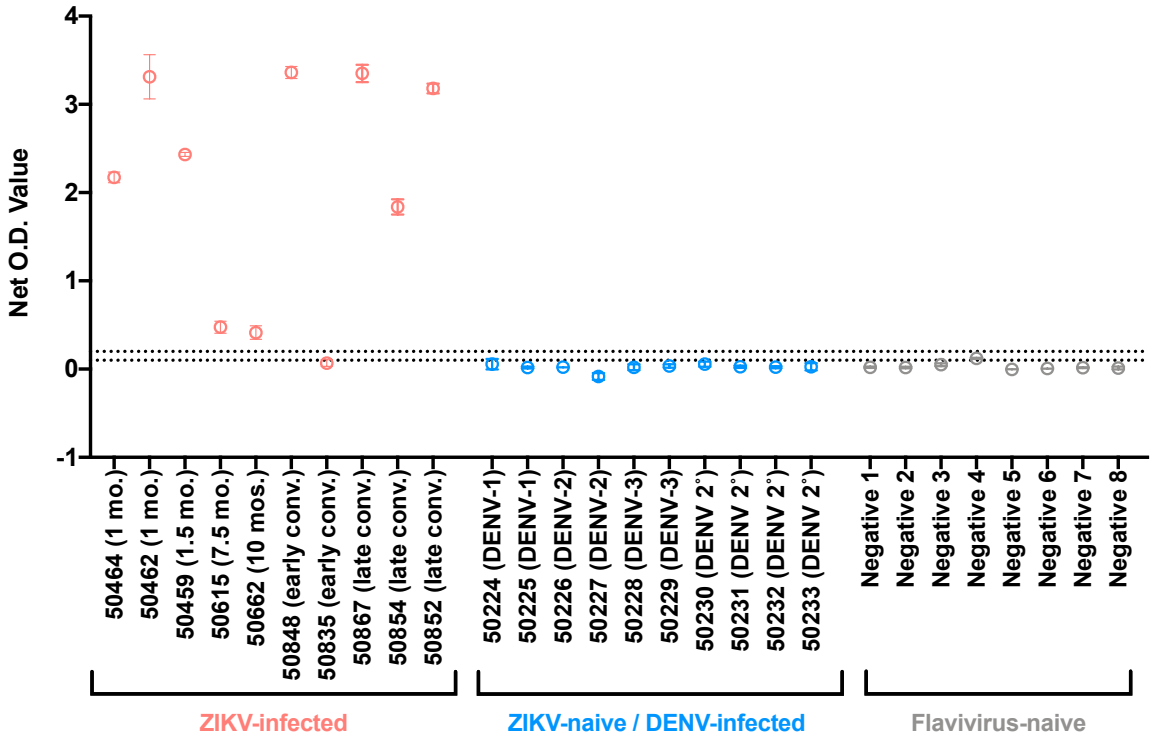

Figure 2.1. Control plasma binding in the anti-ZIKV NS1 IgG ELISA. The Net O.D. value obtained in the anti-ZIKV NS1 IgG ELISA is shown for well-characterized control plasma (see Table 2.2 for sample information). The dotted lines correspond to the positive and negative thresholds of the assay, as recommended by the manufacturer.

Neutralizing antibody (nAb) activity was then defined using a luciferase RVP assay. Control samples with established ZIKV infection potently neutralized ZIKV, with 100% neutralization at a 1:75 dilution for all cases except 50835, which showed lower neutralization that was dose-dependent (Figure 2.2). The ZIKV-naïve/DENV-infected control plasma had a significantly lower level of neutralization against ZIKV at 1:75 dilution ($p<0.0001$; range 3-59%). Only 1 of the 8 flavivirus-naïve samples showed detectable ZIKV neutralization (25%).

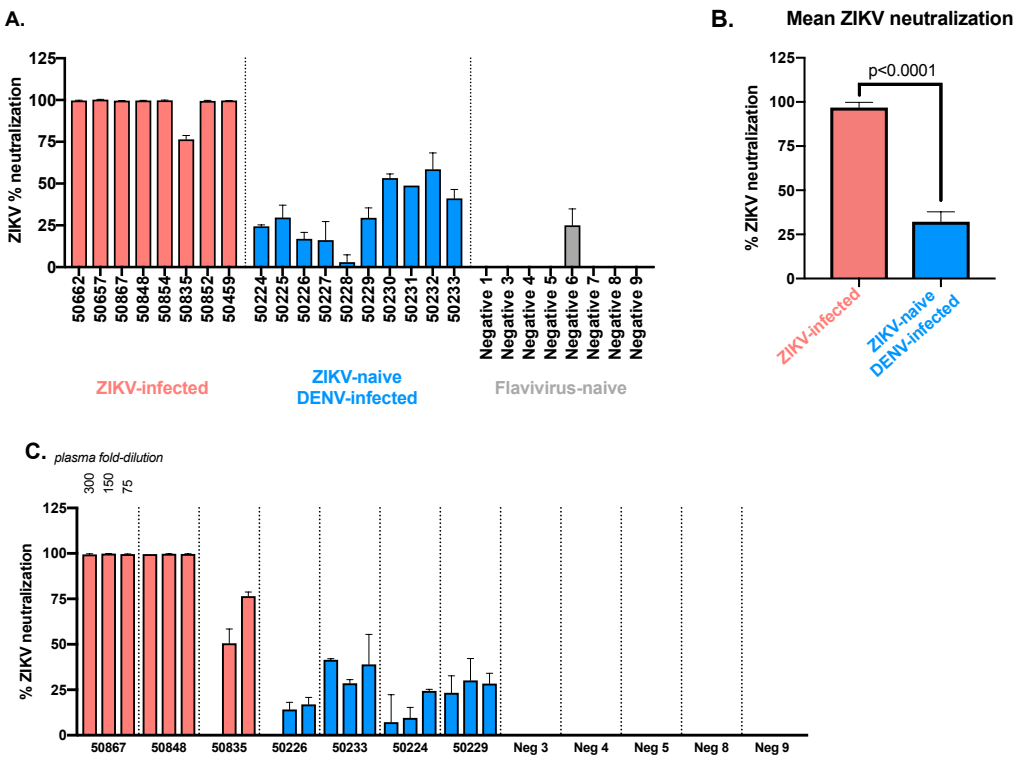

Figure 2.2. Control plasma neutralizing responses against ZIKV. (A) The percent ZIKV neutralization is shown for ZIKV-infected (orange), ZIKV-naïve/DENV-infected (blue), and flavivirus-naïve (gray) control plasma tested at 1:75 dilution. (B) The mean percent ZIKV neutralization is shown for ZIKV-infected and ZIKV-naïve/DENV-infected samples. A two-tailed student's t-test was used to compare the mean percent ZIKV neutralization of control ZIKV-infected plasma vs. ZIKV-naïve/DENV-infected plasma. (C) The percent ZIKV neutralization is shown for a subset of ZIKV-infected, ZIKV-naïve/DENV-infected, and flavivirus-naïve controls tested at 1:300 (left bar), 1:150 (middle bar), and 1:75 (right bar) dilutions.

Twenty-one (6.4%) Kenyan convalescent samples neutralized ZIKV above the highest level detected in the ZIKV-naïve/DENV-infected plasma (59%), of which 4 were ELISA-positive and 2 were equivocal by ELISA (Figure 2.3B). To better assess the specificity of the nAb responses of these 21 samples, ZIKV neutralization was compared to the highest level of DENV neutralization (Figure 2.3C). In each cohort, there was 1 sample (M-1, K-1) that had high levels of ZIKV neutralization (>90%) and low levels of DENV neutralization (<21%). The 19 remaining plasma samples, all of which were from Mombasa, had high DENV neutralization (>95%).

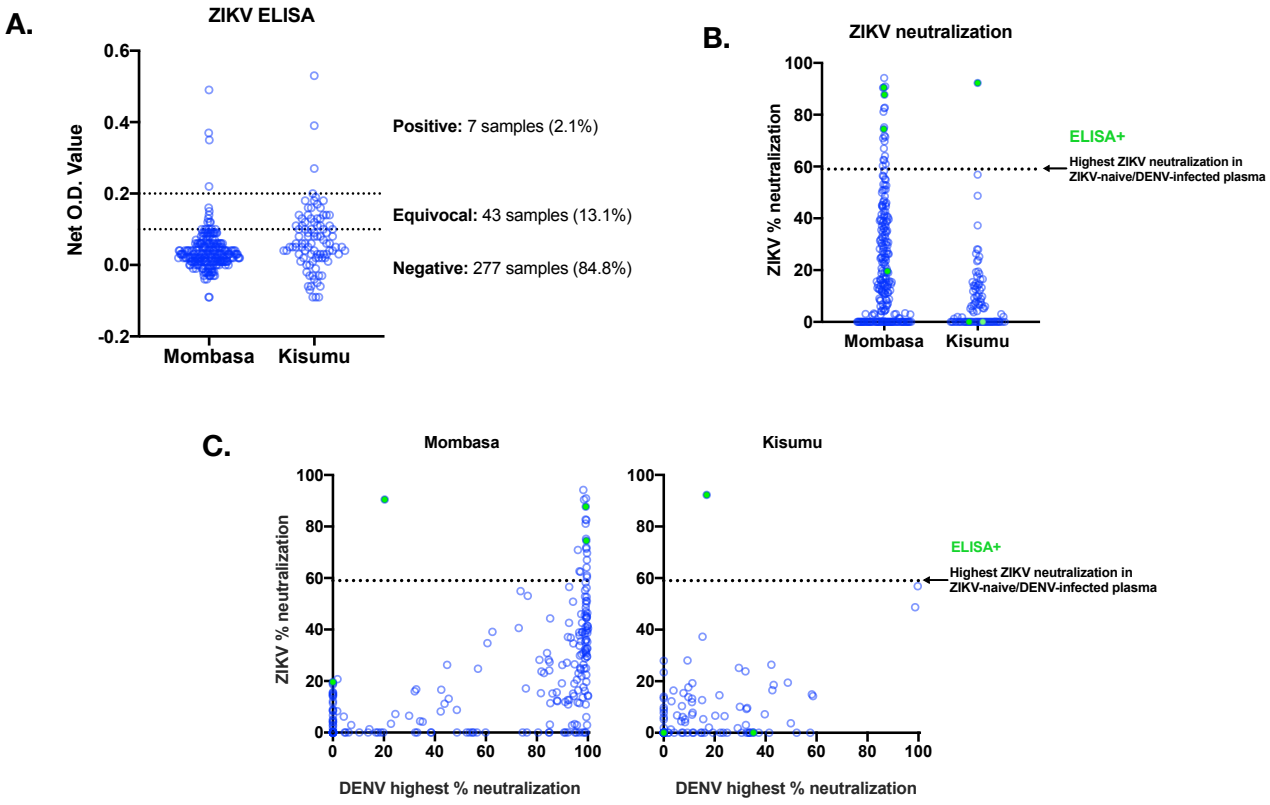

Figure 2.3. ZIKV and DENV antibody levels in convalescent plasma. (A) The Net O.D. value obtained in the anti-ZIKV NS1 IgG ELISA is shown for samples, grouped by whether they are from the Mombasa and Kisumu cohorts. The dotted lines correspond to the positive and negative thresholds of the assay, as recommended by the manufacturer. (B) The percent neutralization of ZIKV at 1:75 dilution of plasma is shown for all convalescent samples, grouped by the Mombasa and Kisumu cohorts. The dotted line corresponds to the highest level of ZIKV neutralization observed in the DENV-infected/ZIKV-naïve control plasma (Figure 2.2A). Samples that were positive in the anti-ZIKV NS1 ELISA are labeled with green dots. (C) The percent ZIKV neutralization in the Mombasa and Kisumu cohorts is shown compared to the highest level of percent DENV neutralization amongst the 4 serotypes. The dotted line corresponds to the highest level of ZIKV neutralization observed in the DENV-infected/ZIKV-naïve plasma (Figure 2.2A). Samples that were positive in the anti-ZIKV NS1 ELISA are labeled with green dots.

To attempt to distinguish if the responses in these 21 samples were due to ZIKV and/or DENV exposure, the IC_{50} of neutralization (NT_{50}) against ZIKV and each DENV serotype was determined for each sample (Table 2.3). ZIKV-only infection was assumed for two cases (M-1 and K-1) where there was a ≥4-fold higher NT_{50} against ZIKV than all DENV serotypes, a difference that was used to differentiate ZIKV and DENV infections in previous studies (17). For 2 cases (M-2, M-4), we could not predict which infection led to the responses because the NT_{50}

for DENV and ZIKV were within 4-fold of each other, but one (M-4) also had evidence of ZIKV NS1 antibodies by ELISA. Seventeen samples had >4-fold activity against DENV versus ZIKV and thus were defined as only DENV-infected (17), although 3 (M-5, M-10, M-15) did have evidence of ZIKV NS1 antibodies.

Table 2.3. NT_{50} results with the 21 Kenyan plasma samples that neutralized ZIKV above levels observed in ZIKV-naïve/DENV-infected plasma.

				NT_{50} [1]					
Cohort	**Sample ID**	**Year**	**Zika NS1 ELISA result[2]**	**ZIKV**	**DENV-1**	**DENV-2**	**DENV-3**	**DENV-4**	**Interpreted infection history**
Mombasa	M-1	1996	+	823	< 75	112	< 75	< 75	ZIKV
Kisumu	K-1	2013	+	1,158	< 75	< 75	< 75	< 75	
Mombasa	M-2	1997	-	562	1,036	187	601	892	DENV & possible ZIKV infection
	M-4	1994	+/-	1,538	2,410	2,160	1,253	3,819	
	M-6	1994	-	< 75	78	4,392	216	592	DENV-2
	M-18	1997	-	< 75	567	87	78	< 75	DENV-1
	M-19	1995	-	< 75	284	671	2,707	524	DENV-3
	M-5	2006	+	570	6,515	15,281	4,502	6,690	Secondary DENV[4]
	M-10	2013	+	380	3,015	4,875	3,425	3,488	
	M-15	2016	+/-	129	1,584	2,659	4,682	1,172	
	M-8[3]	1993	-	156	1,050	417	3,285	1,817	
	M-17	1996	-	145	804	141	590	245	
	M-3	1994	-	3,859	6,332	14,827	56,482	78,027	
	M-7	2006	-	326	2,015	131	1,232	236	
	M-9	2006	-	336	12,774	659	8,119	6,178	
	M-11	2012	-	112	2,062	558	2,172	1,075	
	M-12	2008	-	156	3,499	2,506	873	2,845	
	M-13	1994	-	< 75	< 75	149	672	875	
	M-14	2008	-	82	449	651	408	530	
	M-16[3]	1996	-	157	1,043	202	1,793	1,233	
	M-20	2006	-	< 75	213	2,018	4,817	3,856	

[1] The highest NT_{50} for each plasma sample is highlighted in red (ZIKV) or blue (DENV). NT_{50} values within 4-fold of the highest NT_{50} for each plasma sample are highlighted in light red (ZIKV) and/or light blue (DENV).
[2] Samples with positive (+) or equivocal (+/-) ELISA results are highlighted in green and light green, respectively.
[3] M-8 and M-16 samples are from the same subject who experienced two separate events of fever/rash ~2 years apart.
[4] Secondary DENV was defined as NT_{50} values within four-fold of each other for at least 2 DENV serotypes [9].

In order to examine the ZIKV nAb response over time in cases with evidence of either ZIKV binding or neutralizing responses, we tested available longitudinal plasma samples (Figure 2.4). In the 2 cases defined as ZIKV-only infections, potent ZIKV neutralizing activity was observed over time, including as far as 35.8 months before the reported time of a febrile illness (M-1) and at the reported time of febrile illness (K-1). Remarkably, the nAb titers against ZIKV in subject M-1 were durable over a period of ~10 years, with a spike of nAb titers against ZIKV

coincident with a lower spike of neutralizing activity against all serotypes of DENV at 67.8 months post-febrile illness.

For the 2 cases with similar levels of ZIKV and DENV nAbs (M-2, M-4), the levels of DENV nAbs were, in most cases, higher than ZIKV nAb levels in the subsequent longitudinal plasma. For M-2, there was an increase in DENV-1 and DENV-4 responses in plasma from 4 months after the convalescent sample. For M-4, there was a spike in neutralizing activity after febrile illness against 4 of 5 viruses tested that declined in subsequent samples for all viruses except DENV-1. For the 3 cases that were only positive or equivocal in the ELISA (M-5, M-10, M-15), there were potent responses to DENV and little evidence for ZIKV nAb activity at all time points tested.

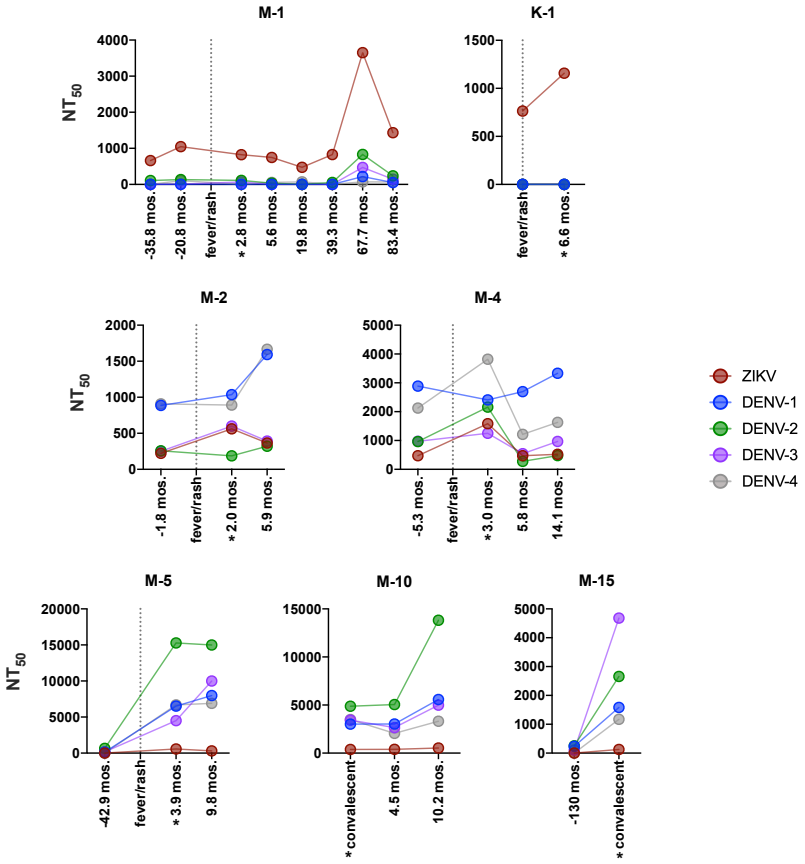

Figure 2.4. NT_{50} results with longitudinal plasma from ZIKV-only (M-1, K-1), ZIKV and DENV neutralizing (M-2, M-4), and ELISA-positive/equivocal (M-5, M-10, M-15) samples. NT_{50} values for each sample are plotted across the indicated time points relative to the time of fever/rash. For M-10 and M-15, where the time of fever/rash was not defined, sample timing is relative to the convalescent sample. Asterisks indicate the original convalescent sample tested in Figure 2.3 and Table 2.3.

Discussion

In this study, we screened convalescent plasma from subjects with reported febrile illness in Mombasa and Kisumu, Kenya for antibody responses to ZIKV and DENV in order to define ZIKV prevalence in these regions. We identified 2 subjects with ZIKV-only infections, and 2 cases with evidence for both ZIKV and DENV infections. The 4 cases span an ~20-year period (1994, 1996, 1997, 2013), suggesting a very low, persistent burden of ZIKV in two major urban areas in East Africa.

There was one ZIKV-only infection in each cohort (K-1, M-1). Both subjects had concordant binding and neutralizing responses against ZIKV without evidence for DENV antibodies. In Kisumu, there was little evidence for DENV infection overall, making it more straightforward to detect ZIKV infection. In the Mombasa cohort, where DENV antibodies were common, we detected 2 cases that suggested the individual had been infected with both ZIKV and DENV. In both cases (M-2, M-4), there were durable neutralizing responses to both ZIKV and DENV in longitudinal plasma samples. M-4 also had an equivocal ELISA result for ZIKV NS1 antibodies. This supports infection by both ZIKV and DENV in this case, although there was some evidence for a shift to a more dominant DENV-1 response at later time points as the other responses waned and thus we were not able to rule out a single DENV serotype infection with strong cross-reactive antibodies to ZIKV (55). Case M-2, was ELISA-negative and did show some evidence for more potent DENV responses over time, making it possible but less clear if infection with both viruses occurred. Including these 2 possible cases of ZIKV infection with the 2 clear cases indicate a prevalence of 1.2% among samples tested.

We found a durable ZIKV neutralizing response lasting over 10 years in ZIKV-positive subject M-1. To our knowledge, this is the first report of durable neutralizing responses against ZIKV over such a long time period. Intriguingly, ~6 years after ZIKV-specific nAbs were detected, there was spike in ZIKV nAb titers along with a coincident low-level spike in those

against DENV. This could represent an infection with a flavivirus other than ZIKV or DENV that triggered a cross-neutralizing response, as has been described previously (47).

The 3 subjects who had a positive or equivocal result for ZIKV NS1 binding antibodies with detectable but low-level ZIKV nAbs at multiple time points nonetheless had much higher levels of neutralizing responses against DENV. We defined these as cases of DENV infection with cross-reactive responses, although we cannot rule out that detection of an actual ZIKV nAb response is confounded by high DENV nAbs due to co-infection in these cases. We also identified three other samples that were ELISA-positive but did not have potent nAb titers against ZIKV or DENV (Figure 2.3B, green points). None of these cases present a strong case of ZIKV infection and suggest that the ZIKV ELISA has lower specificity than expected, at least for ZIKV strains in East Africa. This could reflect the development of this assay for the American ZIKV outbreak, which was fueled by the strains closely related to the Asian ZIKV lineage.
Our study has several limitations, including reliance on self-report of ZIKV-like symptoms in the Mombasa cohort, inclusion of only female individuals in both regions of Kenya, and differential follow-up of study participants. Further, this study is retrospective and utilizes samples from cohort studies that were not designed to define ZIKV seroprevalence and its contribution to febrile illness.

Our findings concur with other recent studies in East and Central Africa, and together, demonstrate low population-level exposure to ZIKV in many regions on the African continent (58-61, 63). They highlight that ZIKV does not have a large contribution to febrile illness in large urban areas of Kenya, which is in agreement with a recent prospective, hospital-based study in Uganda (59). However, a higher prevalence of ZIKV (6.3-7.7%) was reported in northwestern Kenya and West Africa, although it is unclear how cross-neutralizing responses were accounted for in northwestern Kenya and nAb responses were not examined in West Africa (25, 58). In any case, the prevalence of ZIKV is not nearly as high in Kenya as suggested by early studies (as high as 52% reported in coastal Kenya) that used assays that were poorly discriminating against

other flavivirus infections (6). Given that ZIKV is likely to continue its geographic expansion, with reported outbreaks of Asian-lineage ZIKV and related pathogenesis in Cape Verde and Angola (119, 120), our findings set an important baseline for future ZIKV surveillance in the major urban regions of Kenya where arbovirus infections are common.

Our findings demonstrate continued low-level ZIKV exposure in coastal and Western Kenya, with no evidence for ZIKV outbreaks. Given that ZIKV is present at low levels in large population centers in Kenya, our study highlights the need for continued arboviral surveillance and improved platforms for arboviral detection.

Chapter III

Phage-display immunoprecipitation sequencing for enhanced serological detection of Zika virus infection and epitope mapping of HIV-specific monoclonal antibodies

Sections of text in this chapter have been modified slightly from the following manuscripts:

William KL, Stumpf M, Naiman N, Ding S, Garrett M, **Gobillot T**, Vezina D, Dusenbury K, Ramadoss NS, Basom R, Kim PS, Finzi A, and Overbaugh J (2019) Identification of HIV gp41-specific antibodies that mediate killing of infected cells. PLoS Pathogens. 15(2):e1007572; (121)

Doepker LE, Simonich CA, Ralph D, Shipley M, Garrett M, **Gobillot TA**, Oliver B, Vigdorovich V, Sather DN, Nduati R, Matsen FA, and Overbaugh J (2020) Diversity and function of maternal HIV-1 specific antibodies at time of vertical transmission. *In press. Journal of Virology*; (122)

Simonich C, Doepker L, **Gobillot TA**, Garrett M, Shipley M, Hennessy B, Itell H, Chohan V, Nduati R, and Overbaugh J (2020) A large collection of B cells responded to HIV infection in infant BG505. *In preparation.*

Introduction

Identifying individuals who have been infected with ZIKV is difficult (38). The acute febrile clinical presentation of ZIKV infection is hard to reliably distinguish from infections with other pathogens, especially in regions such as sub-Saharan Africa where many febrile pathogens circulate (31). Further, existing diagnostic tools have significant limitations (see Chapter I for a more extensive discussion) (38). Molecular detection of ZIKV RNA is limited by a short period of detectable ZIKV RNA in blood. The extensive antibody cross-reactivity that exists among flaviviruses is a major obstacle to specifically differentiating flaviviral infections using binding or neutralizing antibody-based assays, which is particularly evident from our studies in Chapter II. Thus, to improve upon current tools, an immunodiagnostic tool that can detect ZIKV antibody responses with high specificity is needed.

Despite the cross-reactive nature of the antibody response to flaviviruses, several recent studies have described antibodies that target epitopes specific to ZIKV. Monoclonal antibodies directed against ZIKV NS1 have been isolated from ZIKV-infected donors and found to be highly

ZIKV-specific (123). In line with these findings, several new immunodiagnostics aimed at detecting ZIKV-specific anti-NS1 antibodies have been developed that have higher levels of specificity, although some have less sensitivity than traditional MAC-ELISAs (56, 124-126). A multiplex microsphere immunoassay comprised of ZIKV E- protein, NS1, and NS5 has revealed the potential of combining these antigens in detecting ZIKV-specific antibody responses (127). Further, immunization of mice with linear NS1 peptides elicit ZIKV-specific antibodies that can be used to detect infection in a rapid antigen test format, and a linear non-structural protein-2B (NS2B) peptide is a highly sensitive and specific target of ZIKV antibodies in human sera collected 2-3 weeks post-symptom onset in an ELISA format (128, 129). These studies highlight the potential of using ZIKV-specific antibody responses to discriminate ZIKV infections from infections with antigenically related viruses, such as DENV.

Here, I report on the design, generation, and preliminary validation of a phage-display based serological screen (phage display immunoprecipitation sequencing; PhIP-Seq) to identify ZIKV-specific epitopes that can be leveraged to identify past ZIKV infection. PhIP-Seq has been reported as a powerful tool in both autoantigen discovery and characterization of the human virome (130-134). In this screen, I utilize the entire coding sequence from ZIKV, antigenically related viruses, and pathogens that cause a similar acute febrile illness (Table 3.1) to ZIKV in order to identify samples with ZIKV-specific IgG signatures in serum.

In addition to mapping ZIKV-specific responses in sera, we hypothesized that PhIP-Seq could also be a powerful tool to epitope map monoclonal antibodies (mAbs) directed against pathogens encoded in the phage library. Indeed, we demonstrate that PhIP-Seq is a useful tool for epitope mapping HIV-specific mAbs isolated from three subjects in Kenya. Additional information on each subject and isolated mAbs is included in the results section for each subject (QA255, MG505, BG505).

Methods

Phage library design and generation

Selected viral causes of acute febrile illness in East Africa (Table 3.1), several of which are flaviviruses (DENV, WNV, YFV, JEV, TBEV) that elicit cross-reactive antibodies and complicate the serological detection of ZIKV infection, were included in the phage library. Strains of each pathogen were chosen based on their standard use in the field and, if in existence, strains isolated from East Africa / the African continent were included. Diverse HIV-1 strains were included that were used to validate PhIP-Seq by testing sera from HIV-infected humans or mAbs that target epitopes on HIV Envelope (see Table 3.1).

To generate the library, 39-amino acid sequences were generated that tiled over the coding sequences of viral genomes of interest with 20-amino acid overlap. This was done in collaborations with Katharine Crawford (Bloom laboratory, Fred Hutch). These protein sequences were reverse translated to DNA sequences and codon-optimized for expression in E. coli. Synonymous mutations were introduced to avoid EcoRI and HindIII restriction sites that were used in subsequent cloning steps. Adapter sequences (5': AGGAATTCTACGCTGAGT and 3':TGATAGCAAGCTTGCC) were added and the library was ordered on a releasable DNA microarray (Twist Biosciences) (Figure 3.1A). The library was then PCR amplified using our T7F (AATGATACGGCAGGAATTCTACGCTGAGT) and T7R (CGATCAGCAGAGGCAAGCTTGC TATCA) primers, digested with EcoRI and HindIII, cloned into the T7Select 10-3b Vector, and packaged into T7 phage and amplified according to the manufacturer's protocol (EMD Millipore) (Figure 3.1B). PCR plaque analysis was performed as previously described (131) in order to roughly examine the percentage of correct sequences in the phage library and the extent of any obvious bottlenecking.

Table 3.1. Phage library contents. See Abbreviations for full name of each virus.

Virus	Strain or Antigen	GenBank Accession No. / Source
ZIKV	H/PF/2013	KJ776791
	MR 766 Uganda	AY632535
	ArD128000	KF383117
	ArD157995	KF383118
	PRVABC59	KU501215
	Peptide #1 identified in peptide array	https://zika.labkey.com/announcements/OConnor/thread.view?rowId=101
	Peptide #2 identified in peptide array	
DENV-1	Myanmar 1996	AY722802
	Western Pacific	U88536
DENV-2	Burkina Faso 1983	EU056810
	16803	GU289914
	NewGuineaC	AF038403
	DENV-2/BR/BID-V3653/2008	GU131885
DENV-3	Mozambique 1985	FJ882575
	DENV-3/BR/BID-V2403/2008	FJ850094
DENV-4	P73-1120	JF262780
	H781363, 2011 (genotype I)	JQ513345
	BR/SJRP/850/2013 (genotype II)	KP188566
WNV	NY99	DQ211652
	WN02	KR868734
YFV	Uganda1948a	AY968065
	BeH655417, 2002	JF912190
JEV	Laos, 2009	KC196115
TBEV	MDJ-03	JF316708
CHIKV	KPA15	HQ456254 (structural proteins were translated from sequence and included in library)
	TR206/H804187, 2014	KP164572
ONNV	SG650	AF079456
RVFV	Kenya 9800523	DQ380169.1 for S DQ380196.1 for M DQ375400.1 for L
Malaria	HRP-II, Kenya	FJ871238
HIV-1	Full-length HIV	Consensus Clade A, B, C, D (LANL)
	Full-length Q23	AF004885.1 & LANL Alignments
	BF520.W14M.C2	KX168094
	BG505.W6.C2	DQ208458
	QA013 initial Env	FJ866134
	QA013 SI Env	FJ396015
	QB850 intial Env (72p.C14_A1)	MK412338
	QB850 SI Env (632p.B10)	MK412339

HIV-1 (cont.)	Q461.d1 Env	AF407155
	QC406.F3 Env	FJ866133
Rhinovirus B	Xu et al Rhinovirus B epitope (Table S2)	Xu et al, Science 2015 (133)

HIV monoclonal antibodies and HIV-infected human plasma

Monoclonal antibodies 240-D and 447-52D selected for PhIP-Seq validation were obtained from the NIH AIDS Reagent Program, Division of AIDS, NIAID. HIV-infected plasma from study participant QA013 in the Mombasa Cohort (described in Chapter II) was collected at 2282 dpi as previously described (135). Antibodies from study participants QA255, MG505, and BG505 were isolated, cloned, and produced as described previously ((122, 136) and Simonich et al, In Preparation).

Non-human primate (NHP) plasma

Plasma from seven rhesus macaques singly-infected with ZIKV was kindly provided by Dr. Daniel Streblow at Oregon Health and Science University. All ZIKV-infected NHPs were infected with a vector-relevant amount (10^5-10^7 focus forming units) of a canonical Asian-lineage ZIKV strain (PRVABC59), which is included in the phage library, and early-immune plasma (21/28 dpi) was tested in PhIP-Seq (see Methods below). Importantly, robust production of antibodies that bind and neutralize ZIKV were present in the plasma of these ZIKV-infected NHPs (90, 137). Early-immune (30 dpi) and late-immune (120-390 dpi, pooled) NHP plasma from DENV-infected NHPs (one animal per serotype) was obtained from the NIAID Biodefense and Emerging Infections Research Resources Repository.

Human plasma

Flavivirus-naïve, ZIKV-infected, or DENV-infected plasma, as defined by serology, was kindly provided by Dr. William Messer at Oregon Health and Science University or obtained from the NIAID Biodefense and Emerging Infections Research Resources Repository (see Table 3.2). Sera were further classified as primary (1˚)- or secondary (2˚)-immune depending on whether they had neutralizing activity against a single or multiple flavivirus serotypes, respectively. Secondary-immune sera indicates history of multiple flavivirus infections.

PhIP-Seq

Phage immunoprecipitation was performed as previously described (133). 96-deep-well plates (CoStar) were blocked with 3% BSA in TBST (Tris-buffered saline-Tween) by placing on a rotator overnight at 4˚C. 1 mL of amplified phage at $2x10^5$-fold representation ($1.2x10^9$ pfu/mL for a library of $5.8x10^3$ phage) was added to each well, followed by monoclonal antibody (2-20 ng) or plasma (2-20 µg total IgG). Each experimental sample was tested in technical replicate. Phage-antibody complexes were formed by rotating the plate at 4˚C for 20 hours (Figure 3.1C). To immunoprecipitate phage-antibody complexes, 40µL of a 1:1 mix of protein A and protein G Dynabeads (Invitrogen) was added to each well and rotated at 4˚C for 4 hours (Figure 3.1D). After this incubation, a magnetic plate was used to isolate the beads and perform 3 washes with 400µL of wash buffer (50mM Tris-HCl, pH 7.5, 150mM NaCl, 0.1% NP-40). The beads were resuspended in 40µL of water and isolated phage were lysed by incubating at 95˚C or 10 mins. Phage that did not undergo immunoprecipitation ('input') were also lysed to determine the baseline frequencies of each phage clone in the library (Figure 3.1E).

Isolated phage DNA was then prepared for highly multiplexed sequencing by performing two rounds of PCR with Q5 High-Fidelity DNA polymerase (New England Biolabs) to add Illumina adapters and barcodes according to the manufacturer's suggested protocol (NEB) (Figure 3.1E). The first-round PCR was performed with primers R1_F (TCGTCGGCAG

CGTCTCCAGTCAGGTGTGATGCTC) and R1_R (GTGGGCTCGGAGATGTGTATAAGA GACAGCAAGACCCGTTTAGAGGCCC). 1µL of purified first-round product was added to the second-round PCR with unique dual-indexed primers R2_F (AATGATACGGCGACC ACCGAGATCTACACxxxxxxxxTCGTCGGCAGCGTCTCCAGTC) and R2_R (CAAGCAGAA GACGGCATACGAGATxxxxxxxxGTCTCGTGGGCTCGGAGATGTGTATAAGAGACAG). In these primer sequences, "xxxxxxxx" corresponds to a unique 8-nucleotide indexing sequence. Second-round PCR products were quantified in each sample using Quant-iT PicoGreen (Thermo Fisher) according to the manufacturer's suggested protocol. Equimolar quantities of each sample were then pooled, gel isolated, and submitted for Illumina sequencing on an Illumina MiSeq.

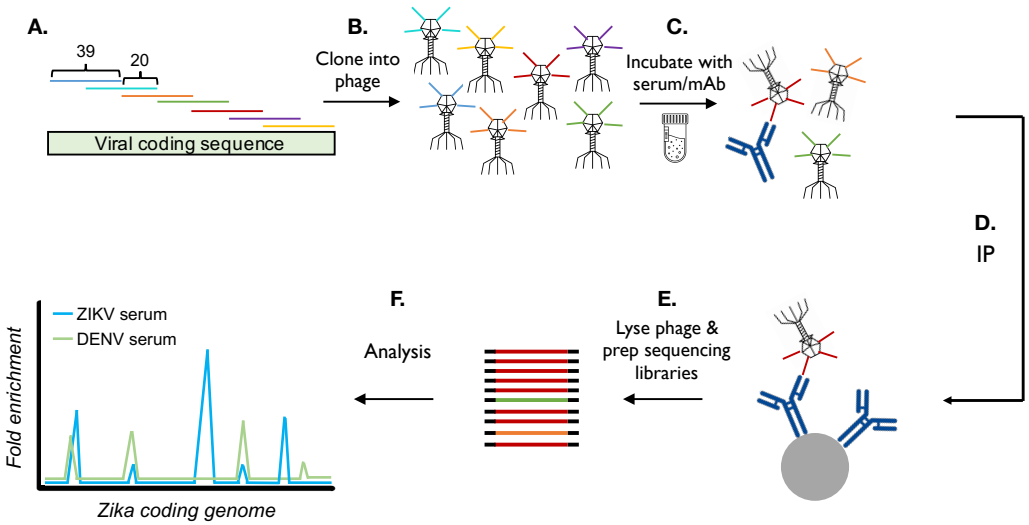

Figure 3.1. Overview of PhIP-Seq screening approach. (A-B) A phage library was designed that displays 39-residue peptide tiles across febrile pathogens with 20-residue overlap. (C) The phage library is incubated with sera or mAb of interest. (D) Immunoprecipitation is carried out with Protein A and G magnetic beads to isolate IgG-phage complexes. (E) Isolated phage are subsequently lysed and DNA is prepared for highly-multiplexed sequencing. (F) Sequencing analysis ultimately reveals peptides targeted by antibodies in the sera. The graph in this figure is an example of ZIKV and DENV-infected sera analyzed for fold-enrichment of ZIKV peptides.

Bioinformatics analysis

The fold-enrichment of phage-displayed peptides in the library by antibodies in plasma was determined by comparing sequencing counts of peptides in samples incubated with plasma

to the baseline representation of peptides before PhIP-Seq. The peptide position in the pathogen genome vs. its fold-enrichment by plasma were plotted to visualize enriched peptides by antibodies in plasma. Parts of this analysis was done in collaborations with Sidney Bell (Bedford laboratory, Fred Hutch).

For HIV mAb epitope mapping, a zero-inflated generalized Poisson significant-enrichment assignment algorithm was used to generate a –log10(p-value) for enrichment of each clone across all samples, as previously described (133). A reproducibility threshold was established to call 'hits' in technical replicate pairs by first calculating the log10(-log10(p-value)) for each clone in Replicate 1. We then surveyed these values in Replicate 2 by using a sliding window of width 0.01 from -2 to the maximum log10(-log10(p-value)) value in Replicate 1. For all clones that fell within each window, the median and median absolute deviation of log10(-log10(p-values)) in Replicate 2 were calculated and plotted against the window location. The reproducibility threshold was set as the window location where the median was greater than the median absolute deviation. The distribution of the threshold –log10(p-values) was centered around a median of 2.2 (QA255 mAbs) or 2.3 (MG505 and BG505 mAbs), since these experiments were performed and analyzed separately. In sum, we called a phage clone a 'hit' if the –log10(p value) was at least 2.2 or 2.3 in both replicates of both conditions tested (2 ng and 10 ng for QA255; 2 ng and 20 ng for MG505 and BG505). Beads-only samples, which serve as a negative control for non-specific binding of phage, were used to identify and eliminate background hits. Peptides called as hits were aligned using Clustal Omega. The shortest amino acid sequence present in all of the hits was what we defined as the "minimal epitope" of an antibody.

Results

Phage library generation and initial characterization

Peptide sequences were computationally generated from the strains in Table 3.1 (in collaboration with Katharine Crawford, Bloom laboratory, Fred Hutch). Altogether, 5,728 peptides were generated from the included pathogens, 4,473 of which were unique in peptide sequence. Oligos corresponding to these peptides were cloned and packaged into T7 phage, which resulted in a library with a titer of 1.04 x 10^7 plaque forming units (pfu) / mL (Figure 3.2A). The library was then amplified in E.Coli to obtain a phage library at a higher titer (1.83 x 10^{10} pfu/mL; Figure 3.2A) so that each peptide could be resampled at sufficient depth to define enrichment differences in PhIP-Seq (~10^5-fold representation of each peptide, as previously defined (133)). PCR plaque analysis of individual phage clones in both the packaged and amplified library revealed a high level of correct peptide sequences displayed by the phage library (70.8% packaged, 71.8% amplified; Figure 3.2B), especially as compared to prior analysis of phage libraries used in PhIP-Seq (Figure 3.2C). No clones were represented more than once in those analyzed by PCR plaque analysis within the amplified library, suggesting that there was no obvious bottlenecking of phage sequences (data not shown).

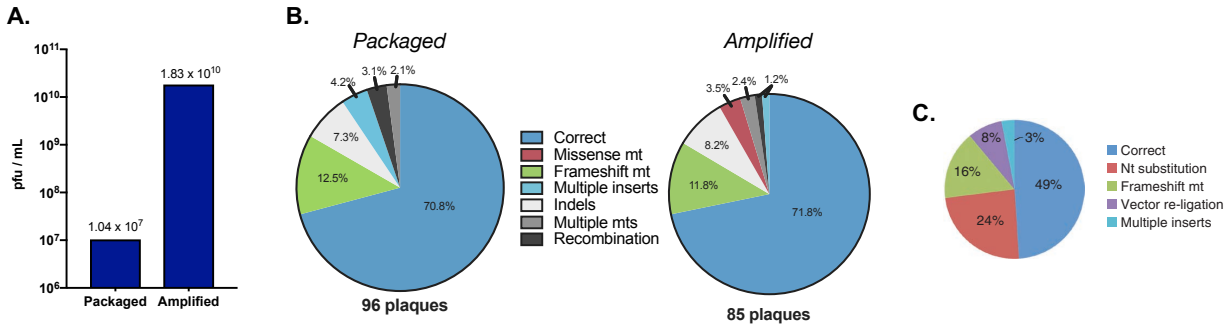

Figure 3.2. Titer and mutational profile of packaged and amplified phage libraries. (A) The titer (pfu/mL) of the packaged and amplified phage library is shown. (B) PCR plaque analysis of the packaged and amplified phage libraries reveal the mutational profile of peptides displayed by the phage. (C) Mutational profile of peptides displayed by a previously reported phage library used in PhIP-Seq. Part C of this figure is adapted from (131).

Validation of the PhIP-Seq approach with HIV-specific mAbs and HIV-infected human serum

As mentioned above, diverse HIV-1 strains were included in the phage library so that this approach could first be validated with HIV-specific mAbs and HIV-infected human sera. Thus, to assess the performance of PhIP-Seq, mAbs targeting known linear epitopes (447-52D, 240-D) on HIV Envelope (Figure 3.3) and a serum sample from an HIV-infected individual (QA013) were tested in PhIP-Seq (138-146). Based on optimized PhIP-Seq conditions (131), 2 ng of each mAb and 2 µg of IgG in sera were tested in technical duplicate. The phage library was at expected median representation (~10^5-fold) of each peptide based on sequencing data (data not shown). There was high reproducibility between technical replicates for each sample (Figure 3.4A). As expected, the mAb 240-D enriched for peptides within HIV Envelope gp41 cluster I, while the 447-52D enriched for peptides within the variable loop-3 (V3) region on HIV Envelope gp120 (Figure 3.4B). Also as expected, QA013 serum enriched for peptides from three regions on the HIV Envelope protein: gp120 V3, gp120 C5, and gp41 cluster I. No peptides appeared to be non-specifically enriched by immunoprecipitation (Figure 3.4C).

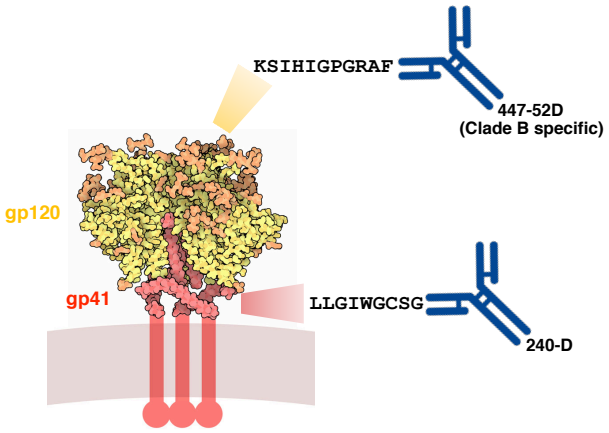

Figure 3.3. Defined epitopes of HIV-specific mAbs used in PhIP-Seq validation. The previously defined linear epitope sequence of 447-52D and 240-D is roughly mapped onto the structure of the HIV Envelope glycoprotein. The gp120 subunit is shown in yellow/orange and the gp41 subunit it shown in red. The HIV Envelope glycoprotein structure is based on BG505 SOSIP gp140 HIV-1 Env trimer and is adapted from PDB 4NC0.

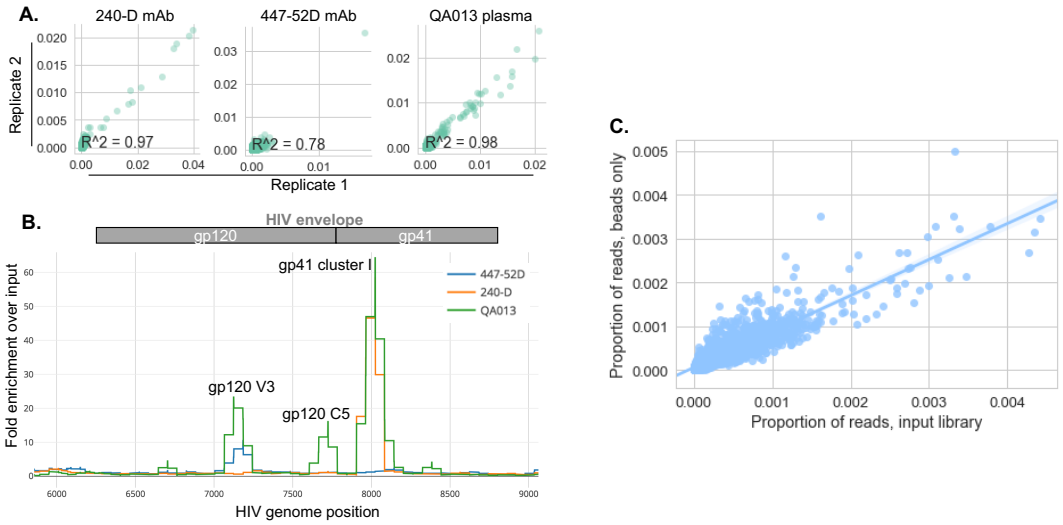

Figure 3.4. Validation of PhIP-Seq with HIV mAbs and human sera. (A) Proportion of reads assigned to phage clones is highly reproducible in each sample. (B) Testing HIV-specific mAbs with PhIP-Seq reveals their epitopes on HIV Envelope. Testing serum from an HIV-infected individual with PhIP-Seq enriches for immunodominant epitopes on HIV envelope. The fold-enrichment values plotted represent an average fold-enrichment of peptides at a given site across all HIV strains in the library. (C) Proportion of reads of each phage clone in background (beads-only, y-axis) compared to baseline (input library, x-axis) reveals lack of non-specific phage enrichment.

PhIP-Seq epitope-maps HIV-specific mAbs isolated from three Kenyan subjects

Our validation experiments with HIV-specific mAbs (Figures 3.3 and 3.4) demonstrated the potential utility of PhIP-Seq in high-throughput epitope mapping of HIV-specific mAbs. Thus, several HIV-specific mAbs isolated from three Kenyan subjects (QA255, MG505, BG505) were tested in PhIP-Seq in order to identify their epitopes.

Four novel gp41-specific ADCC-mediating mAbs (QA255.006, QA255.016, QA255.067, QA255.072) were isolated from subject QA255 (clade A HIV-infected) that arose from four independent B cell lineages (121). QA255.067 and QA255.072 all showed enrichment of HIV Envelope gp41 peptides from the phage library that encoded sequences from the C-C' loop and surrounding region. Sequences that were enriched by binding to mAb QA255.067 shared a common core sequence from 592 to 606 (based on HXB2 numbering), suggesting these amino acids are key parts of the epitope for this mAb (Figure 3.5A). QA255.072 binding enriched for an

overlapping but distinct peptide region that had a common core sequence of amino acids 596 to 609 (Figure 3.5A). MAbs QA255.006 and QA255.016 did not enrich for any peptides present in the phage library.

HIV-infected infant BG505 developed a broad neutralizing antibody response to infection (147), making the response in this infant of high interest, especially as the HIV Envelope from one virus transmitted to infant BG505 is unusually stable as a trimer and thus has been routinely used for structural and immunogen studies and BG505 Envelope protein is currently entering human clinical trials (148, 149). Sixty-nine nAbs were isolated from the only available lymphocyte sample from infant BG505 at ~ 2 years post-infection and a large number of clonal families that responded to HIV in this infant were identified (Simonich et al, In Preparation). PhIP-seq was used to identify specific linear peptides that bind the mAbs from the different clonal families. For 10 of the 18 antibody families, phage-displayed peptides were significantly enriched within the V3 region of HIV Envelope (spanning positions 304-322, based on HXB2 numbering), suggesting that this region of HIV Env comprises a key part of the epitope of these isolated antibodies (Figure 3.5B). For two of the antibodies tested (BG505.54 and BG505.56), we observed weak but significant enrichment of a smaller peptide that truncated the minimal epitope sequence suggesting this is a core part of the epitope (Figure 3.5B, blue residues). The remaining representative antibodies did not demonstrate binding to the linear epitopes present in the library.

Thirty-nine HIV-specific neutralizing monoclonal antibodies were isolated from subject MG505, the mother of BG505, at a time point just prior to vertical transmission in order to study gestational maternal antibodies since there is some evidence that they may provide some protection from vertical transmission. These nAbs belonged to 21 clonal families (122). For 9 of the 21 nAb families, phage-displayed peptides were significantly enriched within the V3 region of HIV Envelope (spanning positions 302-320, based on HXB2 numbering), suggesting that this region of HIV Envelope comprises a key part of the epitope of these isolated nAbs (Figure

3.9A). Of note, in the case of MG505.149, only a small number of peptides were significantly enriched, which likely led to lengthening of the minimal epitope sequence defined for this nAb through to position 332. Because of this, we have less confidence in the minimal peptide target of this nAb. For three of the nAbs tested (MG505.18, MG505.33, MG505.52), we observed weak but significant enrichments of a peptide that truncated the minimal epitope sequence suggesting this is a core part of the epitope (Figure 3.9A, blue residues). The remaining 12 nAb family representatives that were tested by PhIP-seq did not significantly enrich for any phage in the library.

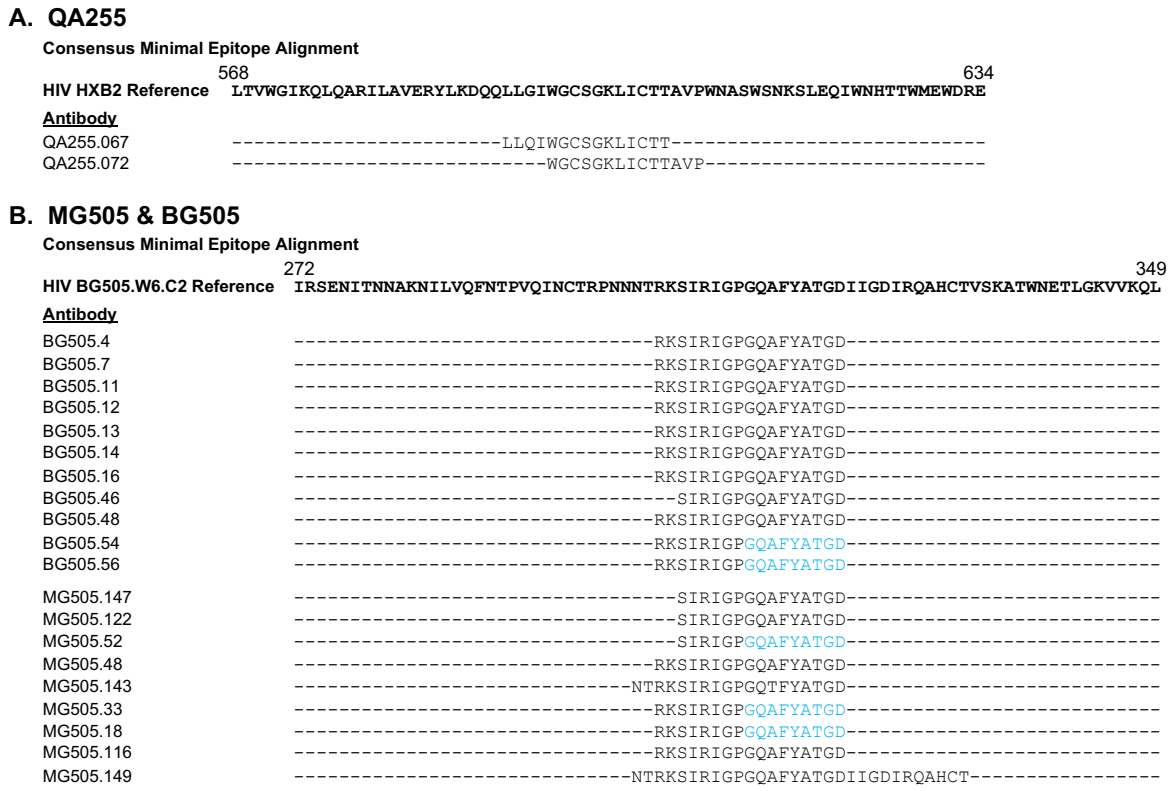

Figure 3.5. PhIP-Seq epitope mapping of HIV-specific mAbs isolated from subjects QA255, MG505, and BG505. Figure adapted from (121, 122) and Simonich et al, in preparation. Sequence alignments of the minimal consensus epitopes identified by PhIP-seq for successfully mapped (A) QA255 and (B) BG505 and MG505 mAbs. Blue residues in (B) signify where the minimal epitope was extended in cases where there was weak but significant enrichment of a peptide that truncated the minimal epitope sequence.

Preliminary identification ZIKV-specific peptides that are characteristic of ZIKV infection in non-human primate and human sera

In order to preliminarily identify ZIKV-specific peptide candidates, serum from ZIKV-infected and DENV-infected NHPs was tested in PhIP-Seq. Specifically, we tested early-immune sera (21/28 dpi) from 7 ZIKV-infected NHPs and both early-immune (30 dpi) and late-immune sera (120-390 dpi, pooled) from NHPs infected with each DENV serotype (see Methods for more details). ZIKV peptides specific to ZIKV infection were detected including three ZIKV peptides that were specifically targeted by ZIKV-infected NHP sera: E-protein residues 151-189, 211-269, and NS2B residues 29-87 (Figure 3.6). Both African- and Asian-lineage ZIKV peptides where enriched, signifying that these peptides are likely to be targeted by antibodies produced in response to infection with either lineage (data not shown). Early-immune and late-immune DENV-infected NHP sera did not strongly enrich for ZIKV peptides (Figure 3.7A and 3.8 A-D). However, as expected, each plasma sample did enrich for DENV peptides that were at distinct genomic positions as compared to the candidate ZIKV-specific peptides (Figure 3.7B-E and Figure 3.8E-H). From these initial studies, we preliminarily identified ZIKV-specific peptides that are characteristic of ZIKV infection in NHP plasma.

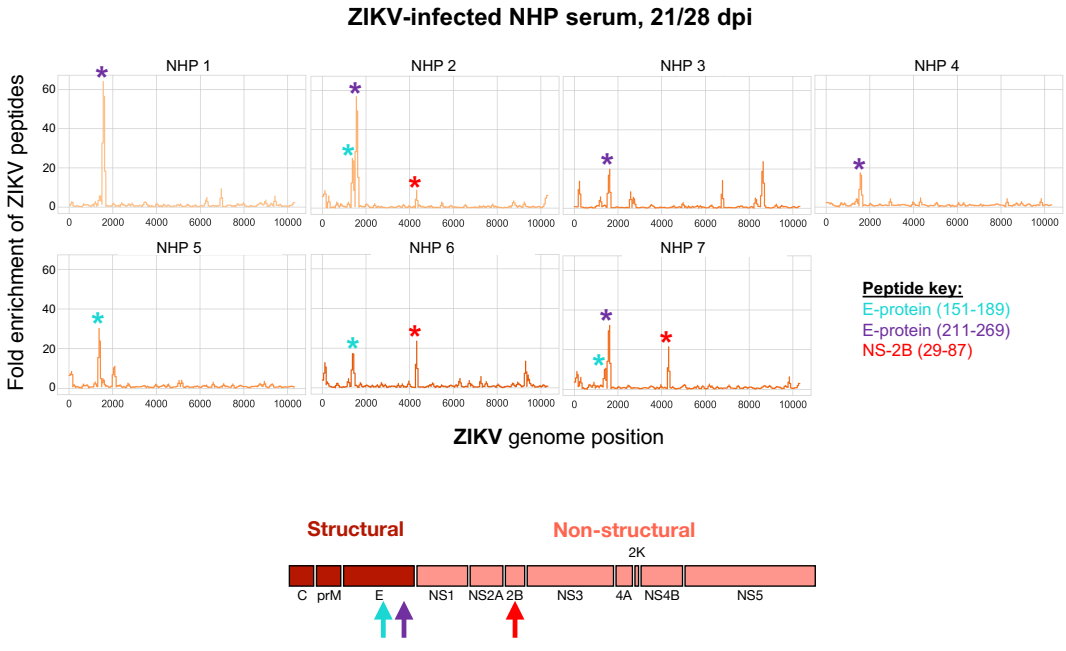

Figure 3.6. (previous page) PhIP-seq with ZIKV-infected NHP sera reveals preliminary ZIKV-specific peptide signatures. ZIKV peptide enrichment profiles for seven ZIKV-infected NHPs. Each plot represents the ZIKV peptide enrichment profile for a separate NHP. The peptide key corresponds to colored asterisks in each enrichment profile and arrows on the ZIKV genome graphic.

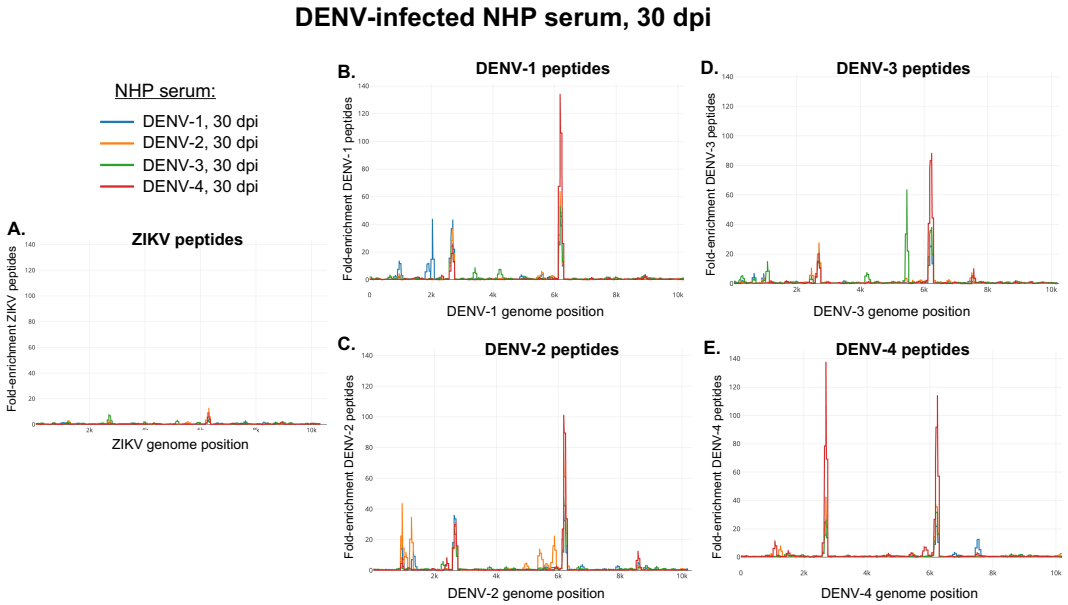

Figure 3.7. PhIP-Seq with all four serotypes of early-immune (30 dpi) DENV-infected serum reveals DENV viral peptide enrichment but lack of strong ZIKV peptide enrichment. ZIKV (A) and DENV (B-E) peptide enrichment profiles for 4 DENV-infected NHPs, 1 from each DENV serotype.

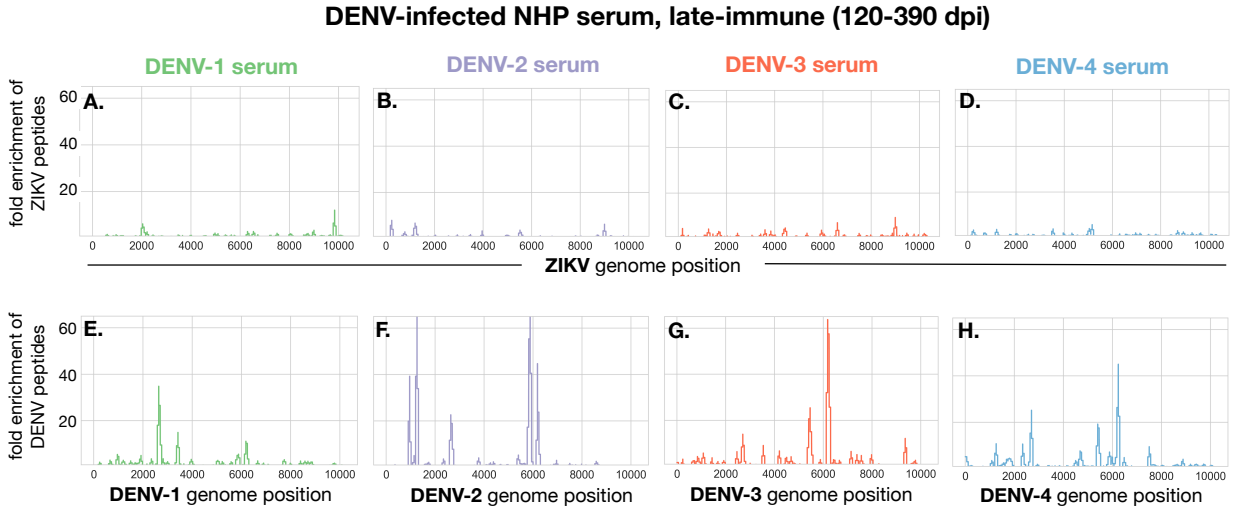

Figure 3.8. PhIP-Seq with all four serotypes of late-immune DENV serum reveals autologous viral peptide enrichment but lack of strong ZIKV peptide enrichment. ZIKV (A-D) and DENV (E-F) peptide enrichment profiles for 4 DENV-infected NHPs, 1 from each DENV serotype. Each set of two vertical plots corresponds to a separate NHP.

Discussion

This chapter shows proof-of-concept that PhIP-Seq can be used for high-throughput epitope mapping of mAbs and for examining ZIKV-specific antibody signatures in NHP serum. HIV mAbs with known epitopes as defined by either linear peptide ELISAs (447-52D; (138-140)) or structural data on antibody-antigen interactions (240-D; (141, 142)) and HIV-infected human sers were first used in validation experiments. The HIV mAbs enriched for peptides that represent the known epitopes of mAbs 240-D and 447-52D in gp41 cluster I and gp120 V3, respectively. Further, HIV-infected human serum enriched for immunodominant regions on HIV Envelope (143-146). Thus, we tested 44 HIV-specific mAbs isolated from three Kenyan subjects to see if we would map their epitopes using PhIP-Seq. In total, we were able to define the minimal epitopes of 22 HIV-specific mAbs based on overlap in the peptide sequences that were enriched by each mAb. This method requires extremely small quantities of purified mAb (2-20 ng total) and as many as 192 mAbs (or possibly more) can be epitope mapped using this method in a single experiment. Further, data on preferences for certain amino acids can be determined by examining relative fold-enrichment of peptides from various pathogen strains in the phage library (121, 122). However, the method was not able to map the epitopes for 22 mAbs. It is likely that these mAbs target more complex, discontinuous epitopes that may not be able to be mapped using PhIP-Seq, at least with the 39-mer peptides expressed by phage in the library.

Using PhIP-Seq with our febrile pathogen library, we have preliminary evidence for ZIKV-specific peptides (E-protein residues 151-189, 211-269, and NS2B residues 29-87) that are characteristic of ZIKV infection in NHP sera, at least as compared to cases of DENV infection in NHPs. The NS2B peptide we identified as ZIKV-specific by testing NHP sera was recently described as a highly specific and sensitive epitope when testing ZIKV-infected human sera, which lends support to the ZIKV-specific peptides we have identified in our initial studies (129).

Future studies examining the capacity of PhIP-Seq to specifically identify cases of prior ZIKV infection should focus on larger panels of human sera with confirmed flavivirus infection histories. To this end, we have assembled a panel of such human serum samples, although this will need to be expanded to include more samples, especially from DENV-infected and flavivirus-negative individuals (Table 3.2). The potential ZIKV-specific peptides identified in NHP sera were based on qualitative assessment of fold-enrichment plots of ZIKV and DENV peptides in each serum sample. As there are many pathogens in the phage library, the PhIP-seq data from testing each human serum sample will be highly complex. Thus, future studies should employ bioinformatics approaches that can account for this high-dimension data. There are many successful examples of such approaches, such as leave-one-out analyses employed to identify CMV exposure status based on TCR repertoire (150).

Table 3.2. Expanded panel of ZIKV-infected, DENV-infected, and flavivirus-naïve human sera that has been tested in PhIP-Seq.

ZIKV-infected (59 samples)	
Acute (3-11 days)	5 samples
Early convalescence (14-21 days)	21 samples
Late convalescence	44 samples
DENV-infected	
15 samples	
Flavivirus-negative	
20 samples	

Chapter IV

The robust restriction of Zika virus by type-I Interferon in A549 cells varies by viral lineage and is not determined by IFITM3

Sections of text in this chapter have been modified slightly from the following manuscript:

> **Gobillot TA,** Humes D, Shama A, Kikawa C, and Overbaugh J (2020) The robust restriction of Zika virus by type-I interferon in A549 cells varies by viral lineage and is not determined by IFITM3. *In preparation.*

Introduction

The recent spread and severe pathogenic features of ZIKV in the Americas have highlighted the epidemic potential of this emerging pathogen. The American outbreak clade of ZIKV strains has been linked to fetal abnormalities, a severe congenital syndrome in neonates, and adverse neurological outcomes in adults (151-154). Prior to the American epidemic, documented outbreaks of ZIKV were rare (6, 17, 155).

ZIKV was first identified in Africa over 70 years ago. There is limited evidence that African-lineage ZIKV infections are associated with the severe pathogenic profile that has been fueled by the American clade, which clusters with Asian-lineage strains. This raises the possibility that African- and Asian-lineage ZIKV strains may have distinct pathogenic properties. IFN-I is a critical component of the host innate immune response to viral infection (93). Upon recognition of viral infection, cells enter a transcriptional program that increases the production of IFN-I (IFNα and IFNβ), which establishes an anti-viral state in bystander cells and restricts viral replication in infected target cells (156). The ability of IFN-I to restrict viral replication is largely due to the activation of hundreds of ISGs that have a wide range of anti-viral functions (94, 95). IFN-I is capable of restricting ZIKV in cell culture (101, 102), and most murine models of ZIKV infection and pathogenesis require ablation of the IFN-I signaling pathway, underscoring the important role of ISGs in restricting ZIKV replication (81). One such ISG is IFITM3, which

was the first ISG described as a key effector of the IFN-I response against ZIKV in a variety of cells including A549, HeLa, 293T, HDFa, and HFF cells (111, 112, 118). IFITM3 is a small transmembrane protein that restricts a broad array of viruses and is potently induced by IFN-I (113). It is unclear whether strains of ZIKV differ in their susceptibility to IFN-I-mediated restriction and/or restriction by IFTIM3.

The goals of this study were to determine whether ZIKV strains differ in their susceptibility to restriction by IFN-I and how IFITM3 contributes to the antiviral effects of IFN-I on ZIKV replication. Using a panel of nine ZIKV strains, we found that the African-lineage viruses were less sensitive to the effects of IFN-I than the Asian-lineage viruses. We also found that IFITM3 does not explain the IFN-I-mediated restriction of African or Asian-lineage viruses in A549 cells.

Methods

Viruses

ZIKV strains were kindly provided by BEI Resources (MR 766, IbH 30656, PRVABC59, FLR, H/PAN/2016/BEI-259634, H/PAN/2015/CDC-259359) and Michael Diamond (DAK-AR-25, DAK-AR-67, DAK-AR-71). All ZIKV strains were propagated in Vero cells at an MOI of 0.01, as previously described (157). Viral titers were determined by the $TCID_{50}$ assay described below. Experiments were performed with aliquots that had undergone at most two freeze-thaw cycles, which was not found to have any discernible effect on viral titers.

Cells

A549 cells (A. Berger; ATCC) were maintained in RPMI (Invitrogren) supplemented with 10% fetal bovine serum (FBS), 2mM L-glutamine, and 1X Anti-anti (anti-microbial/anti-mycotic, Gibco). Vero cells (A. Geballe; ATCC), HEK293T cells, Jeg3 cells (ATCC), and SNB-19 cells (ATCC) were maintained in DMEM (Invitrogen) supplemented with 10% FBS, 2mM L-glutamine,

and 1X Anti-anti. SH-SY5Y cells (ATCC) were maintained in EMEM (ATCC) supplemented with 15% FBS, 2mM L-glutamine, and 1X Anti-anti.

Sequencing and phylogenetic analysis of ZIKV strains

All ZIKV stocks were sequence-confirmed by Sanger sequencing of a 1.8 – 3.4-kbp region of the ZIKV genome that encodes non-structural proteins 1 through 3. To do this, viral RNA was isolated using the QiaAMP Viral RNA Mini Kit (Qiagen) and cDNA was produced using SuperScript III First Strand Synthesis System (Invitrogen) with random hexamers according to the manufacturer's suggested protocol. The Primal Scheme primer designer software (http://primal.zibraproject.org/) was then used to design primers that tiled across the complete open reading frame in ~645 bp fragments that overlapped by ~210 bp (158). A subset of these primers were used to generate two overlapping sub-amplicons by PCR amplification of cDNA with Q5 ReadyMix (NEB) (Table 4.1). Thermocycling conditions used were:

1. 98˚C, 30 s
2. 30 cycles:
   98˚C, 15 s
   65˚C, 5 min

The sub-amplicons were then subjected to Sanger sequencing using primers that bind within each sub-amplicon and sequences were confirmed for all strains with published sequences. (Table 4.2). Full-length open-reading-frame nucleotide sequences of ZIKV strains in the panel, as well as other ZIKV strains, were used to construct a maximum-likelihood phylogenetic tree with PhyML using a general time-reversible nucleotide substitution model (159).

Table 4.1. Zika virus sub-amplicon generation primers

Sub-amplicon 1	
ZikaSeq_7_Fwd	CAAATCACTGTTTGGAGGAATGTCC
ZikaSeq_12_Rev	TTCCAAGGCCCACAGTATGACA
Sub-amplicon 2	
ZikaSeq_12_Fwd	GCCTGATATGTGCACTGGC
ZikaSeq_18_Rev	ATCATTAGCAGCGGGACTCCAA

Table 4.2. Zika virus sub-amplicon sequencing primers.

Name	Sequence (5'-3')
ZikaSeq_9_Fwd	TGACACATGGAGGCTGAAGAGG
ZikaSeq_10_Fwd	TGGAATGGAGATAAGGCCCAG
ZikaSeq_11_Fwd	TTTCAGAGCCAATTGGACACCC
ZikaSeq_12_Fwd	GCCTGATATGTGCACTGGC
ZikaSeq_13_Fwd	GAAGACTGGGAAAAGGAGTGG
ZikaSeq_14_Fwd	TCAAGACAAAGGACGGGGACAT
ZikaSeq_15_Fwd	ATGTGCCATGCCACTTTCACTT
ZikaSeq_9_Rev	CTGCGAAAGTAGCACCCATCA
ZikaSeq_10_Rev	GGGAGAGGAGCATGAACCC
ZikaSeq_11_Rev	CCTTTGAGTATGATCTCTCTCATGGG
ZikaSeq_12_Rev	TTCCAAGGCCCACAGTATGACA
ZikaSeq_13_Rev	TCCTGGTTTTTCCGGCTCC
ZikaSeq_14_Rev	GCTCTCTCTGGGACTTCCACTT
ZikaSeq_15_Rev	CTTCATCAGTCTCTGCACACCC

IFN-I sensitivity assay

To measure the impact of IFN-I treatment on ZIKV replication, $8x10^4$ A549, Jeg3, or SNB-19 cells were either left untreated or pre-treated with 1000 U/mL of IFNα-2a or IFNβ for 24 hours in each well of a 24-well plate. After pre-treatment, cells were infected at an MOI of 1 in a final volume of 250 µL of serum-free RPMI for 4-6 hours. The inoculum was then aspirated, cells were washed twice with 1X PBS, and replenished with 1 mL of complete RPMI without IFN-I or containing 1000 U/mL of IFNα-2a or IFNβ. At 48 hours post-infection (hpi), 250 uL of supernatants were harvested and cleared of cellular debris at 4ºC at 300G for 10 minutes and 2 X 100 uL aliquots were stored at -80ºC until titration by $TCID_{50}$ assay. For the data analysis, all

values were plotted and statistical analyses performed using Prism version 7 (GraphPad Software). Percent Relative Infection was determined by dividing the $TCID_{50}$ titer in the IFNα- or IFNβ-treated sample by the untreated sample.

$TCID_{50}$ assays

ZIKV titers were determined by $TCID_{50}$ assay on Vero cells in a 96-well format. One day prior to titration, Vero cells were seeded in 100 uL of complete DMEM in a flat-bottomed 96-well plate at $8x10^3$ cells per well. For each condition tested, seven serial 10-fold dilutions of viral supernatants were prepared, starting at a concentration of 1 uL/well, with each dilution including 10 replicate wells and 2 mock infected wells. Cells were infected with 50 uL of each viral dilution in serum free DMEM for 4-6 hours, before being replenished with 100 uL of DMEM with 3% FBS, for a final concentration of 2% FBS. On day 5 post-infection the wells at a given dilution were scored by light microscope for the presence or absence of cytotoxicity and the TCID50/mL was calculated using the Spearman-Karber method.

ZIKV E-protein staining

Monoclonal Anti-Flavivirus Group Antigen (4G2) antibody (ATCC) was conjugated with APC (Novus Lighting-Link) according to manufacturer's protocol. For each condition, $3x10^5$ cells were plated in a single-well of a 6-well dish. Cells were subsequently infected with 1 mL of inoculum (MOI 1) for 4-6 hours, before being replenished with 3 mL of RPMI-10% FBS-2mM L-glutamine-1X Anti-anti (anti-microbial/anti-mycotic, Gibco). Cells were harvested at 24 hours post-infection and were subsequently fixed and permeabilized with the BD Fixation/Permeabilization solution kit according to the manufacturer's protocol (BD Biosciences). Intracellular E-protein staining was then carried out with 0.25µg of APC-conjugated 4G2 antibody per condition. Cells were washed twice in Perm/Wash buffer and resuspended in PBS prior to flow cytometry analysis on a BD FACSCanto II flow cytometer. All data was analyzed using FlowJo v10 software.

Generation of stable cell lines overexpressing IFITM3

IFITM3-expressing A549 cells were generated as previously described (160). Briefly, the N-terminal FLAG-tagged IFITM3 open-reading frame was cloned into pHIV-Zsgreen (161) (Addgene plasmid # 18121, a gift from Bryan Welm & Zena Werb) directly upstream of the IRES-driven ZsGreen fluorescent reporter, thus linking IFITM3 transcript expression to ZsGreen expression. VLPs were generated in HEK293T cells by co-transfecting cells with pHIV-ZsGreen constructs (either IFITM3-encoding or empty vector as control), psPAX2 (Addgene plasmid # 12260, an HIV-based packaging plasmid gifted from Didier Trono), and pMD2.G (Addgene plasmid # 12259, vesicular stomatitis virus glycoprotein [VSV-G] envelope plasmid gifted from Didier Trono) at a ratio of 1:1:0.5 using FuGENE 6 (Promega) according to the manufacturer's protocol. Supernatants from HEK293T cells were collected 48 hours post-transfection and concentrated ~100-fold using Amicon Ultracel 100 K filters (Millipore). VLPs were then used to transduce A549 cells that has been plated 24 hours prior in a 6-well plate at $1x10^5$ cells/well in 2 mL of RPMI supplemented with 10% FBS and 2mM glutamine. A549 cells were transduced by spinoculation at 1200 x g for 90 minutes. The following day, the cells were expanded into new T75 flasks and were subsequently passaged and maintained in complete DMEM. IFITM3-expressing cells were sorted by gating cells in the fiftieth-percentile of zsGreen expression on a FACSAria II cell sorter.

Generation of clonal cell lines expressing different levels of IFITM3

Monoclonal cell populations of IFITM3-expressing A549 cells (generated as described above) were isolated by limiting dilution. Briefly, IFITM3-expressing A549 cells were seeded at a density of 1 cell per well in a 96-well plate in 150 µL of RPMI-10% FBS-2mM L-glutamine-1X Anti-anti (anti-microbial/anti-mycotic, Gibco). Seven days after plating, single colonies could be visualized and the media was changed on all wells. Ten days after plating, the number of colonies in each well were tallied and wells that contained only a single colony were selected for

further analysis. Cells from wells containing single colonies were trypsinized when they were close to confluency (~15 days after plating) and expanded into a well of a 24-well plate. Clonal cell populations were subsequently screened for zsGreen mean fluorescence intensity and two cell lines (IFITM3-rel and IFITM3-high) were selected to use in experiments.

Generation of IFITM3 and IRF9 knockout cell lines and validation by TIDE analysis

For generation of IFITM3-knockout and IRF9-knockout A549 cell lines, guide RNAs targeting the first exon of Ifitm3 and the third exon of Irf9, or non-targeting control guide RNA, were cloned into pLentiCRISPR (Addgene plasmid # 49535, a gift from Feng Zhang) (162). VLPs were generated by co-transfecting HEK 293Ts with the pLentiCRISPR plasmids, the psPAX2 packaging vector, and pMD2.G and harvested and concentrated as described above. A549 cells were transduced with pLentiCRISPR VLPs encoding and maintained as described above, except that cells were treated with 2 ug/mL puromycin to select for sgRNA and Cas9 expression two days after being moved to T75 flasks. The two IFITM3-targeting sgRNAs that yielded the most efficient knockout of IFITM3 were sgRNA1, 5'-GCAGCAGGGGTTCATGAAGA-3'; and sgRNA2, 5'-TTGAGCATCTCATAGTTGGG-3'. The IRF9-targeting sgRNA was 5'-ACAATTCCACAGGCCAGCCA-3' and the non-targeting control was 5'-ATCTCGGGTCGACTGCGGAT-3'. Gene knockout was characterized by TIDE analysis. Briefly, after three rounds of puromycin selection, genomic DNA was isolated. For IFITM3-knockout cell lines, DNA was isolated using QuickExtract DNA extraction solution (Lucigen) by resuspending cells in 100 µL of the solution, and by denaturing for 20 min at 60 °C and 20 min at 95 °C. The ifitm3 locus was amplified using the following primer set: forward 5'-ACCATCCCAGTAACCCGACCG-3' and reverse 5'-GCTGATACAGGACTCGGCTCC-3'. For IRF9-knockout cell lines, DNA was isolated using a Qiagen Blood Mini kit per the manufacturer's protocol. The Irf9 locus was amplified using the following primer set: forward 5'-CCTGCATAATCCCTTCTGAGC 3' and reverse 5'-CCCTGGAGTTTCTGCTTCCT-3'. Amplicons

were Sanger sequenced and gene editing was measured using TIDE analysis (https://tide-calculator.nki.nl/).

Western blots and quantification

Whole cell extracts were prepared by lysing the cells in RIPA cell lysis buffer (50 mM Tris pH 8.0, 0.1% SDS, 1% Triton-X, 150 mM NaCl, 1% deoxycholic acid, 2 mM PMSF). Standard Western blotting procedures were used with the following antibodies: IFITM3 (Proteintech 11714-1-AP, used at 1:1000 dilution), IFITM2 (Proteintech 66137-1-Ig, used at 1:500 dilution), FLAG (OriGene TA100023, used at 1:2000 to 1:5000 dilution), and GAPDH (BioRad MCA4739P, used at 1:5000 dilution). Protein expression was quantified by measuring the band intensities using Image J.

IAV and MLV VLP infections

IAV (generously provided by A. Russell and J. Bloom) is an mCherry-expressing reporter virus where HA is replaced with mCherry. For MLV, reporter VLPs were made by packaging the lentiGuide.mCherry vector (163) (a gift from Richard Young, AddGene plasmid #104375) with psPAX2 and pseudotyping with an amphotropic MLV envelope. For both viruses, $8x10^4$ IFITM3-expressing and control cells were plated in a 24-well plate one day prior to infections in a final volume of 1 mL of complete RPMI. For IAV, cells were infected at an MOI of 10 in 500 µL of complete RPMI for 16 hours. Cells were harvested and fixed in 1% paraformaldehyde. For MLV, cells were infected with a dilution of VLPs in complete RPMI supplemented with 10 µg/mL DEAE dextran. Cells were harvested and fixed in 1% paraformaldehyde 72 hours post infection. Both IAV and MLV-infected cells were assessed for mCherry expression using a Fortessa X50 flow cytometer and data was analyzed using FlowJo v9 software.

Data availability

The accession numbers for the ZIKV strains utilized in this study are: KU963573 (MR 766), KU963574 (IbH30656), KU955591 (DAK-AR-25), MF510857 (DAK-AR-67), KU955595 (DAK-AR-71), KX198135 (H/PAN/2016/BEI-259634), KX156774 (H/PAN/2015/CDC-259359), KX087102 (FLR), KX087101 (PRVABC59).

Results

Effect of IFN-I treatment on diverse ZIKV strains in A549 cells

In order to test the hypothesis that IFN-I sensitivity differs between African-lineage and Asian-lineage ZIKV strains, a panel of nine viruses was tested for their ability to replicate in A549 cells in the presence or absence of IFN-I. Five strains belong to the African lineage and four strains belong to the American outbreak clade within the Asian lineage (Fig 4.1, circles). The percent identity of the complete genomes of African vs. Asian lineage strains in this panel is 88-89%, which is representative of the overall diversity of isolated ZIKV strains (6). All Asian-lineage viruses were isolated from infected humans, while only one African-linage virus was isolated from an infected human (IbH 30656). Three African-lineage strains were isolated from mosquitoes (DAK-AR-25, DAK-AR-67, DAK-AR-71) and one from a sentinel rhesus macaque (MR 766) (Table 4.3). In addition, these strains have diverse passage histories. Most have undergone 3-5 passages in mosquito (AP61, C6/36) and/or African-green monkey (Vero) cell lines; however, MR 766 has been extensively passaged in mouse brain and subsequently in Vero cells. IbH 30656 has a similar but less extensive high-passage profile. The number of passages in AP61 cells for DAK-AR-67 and DAK-AR-71 is unknown.

For each strain in the panel, two independent stocks were amplified on Vero cells to account for any stock to stock variation, and the sensitivity of the viral stocks to pretreatment with IFNα-2a or IFNβ (1000 U/mL) in A549 cells was determined (Fig 4.2A). Both African-lineage and Asian-lineage viruses were more potently inhibited by IFNβ pre-treatment than

IFNα, with viral replication reduced 2 to 16-fold in response to IFNα and 20 to 407-fold in response to IFNβ (Fig 4.2A). The biggest differences were between IbH 30656 / DAK-AR-25 (both African-lineage) and H/PAN/CDC-259359 (Asian-lineage) (~8-fold) for IFNα and IbH 30656 and PRVABC59 (Asian-lineage, ~20-fold) for IFNβ. There was a range of responses within each lineage: for example, among African-lineage strains, the most sensitive MR 766 isolate was more susceptible to both IFNα and IFNβ. Among Asian-lineage strains, H/PAN/CDC-259359 was the most sensitive to IFNα, while PRVABC59 was the most sensitive to IFNβ.

As an aggregate, African-lineage ZIKV strains were significantly less susceptible to IFNα restriction than Asian-lineage strains (Fig 4.2B; p=0.049); they were also less susceptible to IFNβ, though differences in sensitivity to IFNβ (Fig 4.2B; p=0.09) were only a statistical trend.

Taken together, the data reinforces IFN-I as a potent restrictor of ZIKV replication, albeit with substantial strain-to-strain differences in susceptibility, with African-lineage strains less sensitive to IFN-I than Asian-lineage strains.

Table 4.3. Summary of characteristics of ZIKVs used in this study.

Strain	*Lineage*	*Source*	*Passage History*
MR 766	African	Rhesus (Uganda 1947)	150x mouse brain 8x Vero cells
IbH 30656		Human (Nigeria 1968)	21x mouse brain 4x Vero cells
DAK-AR-25		*Aedes africanus* (Senegal 1984)	1x AP61 cells 1x C6/36 cells 3x Vero cells
DAK-AR-67		*Aedes taylori* (Senegal 1984)	?x AP61 cells 1x C6/36 cells 2x Vero cells
DAK-AR-71		*Aedes taylori* (Senegal 1984)	?x AP61 cells 1x C6/36 cells 2x Vero cells
PRVABC59	Asian	Human (Puerto Rico 2015)	5x Vero cells
FLR		Human (Columbia 2015)	3x C6/36 cells
H/PAN/2016/BEI-259634		Human (Panama 2016)	4x Vero cells
H/PAN/2015/CDC/259359		Human (Panama 2015)	4x Vero cells

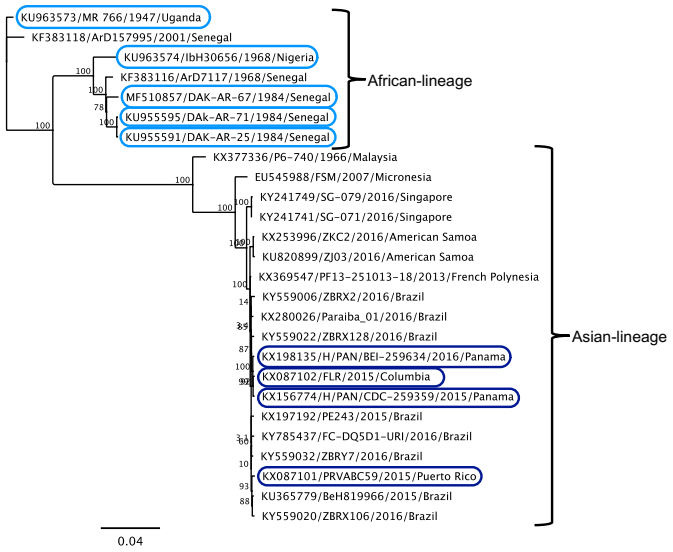

Figure 4.1. Phylogenetic relationships of Zika virus strains used in this study. Maximum-likelihood phylogeny of full-length open-reading-frame nucleotide sequences using Zika virus strains in this study (circles) and reference sequences isolated from humans, non-human primates, and mosquitoes. At least one representative strain from each documented ZIKV clade is included in the phylogenetic tree.

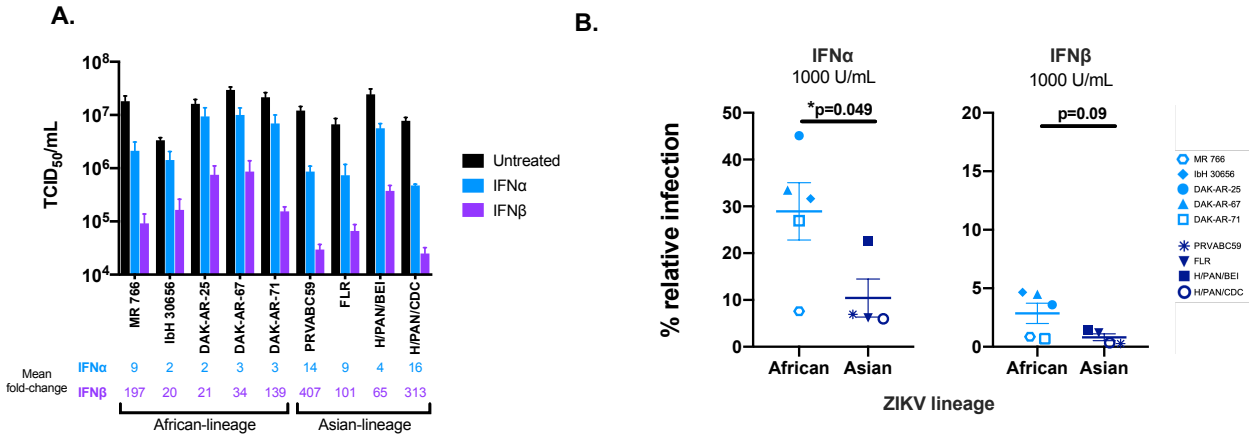

Figure 4.2. Effect of IFN-I pre-treatment on diverse Zika virus strains in A549 cells. (A) The susceptibility of each ZIKV strain to restriction by IFNα-2a or IFNβ was assessed in A549 cells. Cells were treated with 1000 U/mL IFNα-2a or IFNβ 24 hours prior to infection as well as following infection with each ZIKV strain. The titer (TCID50/mL) of each strain 48 hours post-infection in the absence of IFN-I (black), presence of IFNα-2a (blue), and presence of IFNβ (purple) is shown. All data represent the average of at least four independent experiments that were carried out with two independently-generated stocks of each ZIKV strain. Error bars represent SEM. The mean fold-reduction in viral replication of each ZIKV strain by pre-treatment with IFNα and IFNβ is listed below the graph. (B) Comparison of IFNα-2a-mediated (1000 U/mL) and IFNβ-mediated restriction (1000 U/mL) of African-lineage vs. Asian-lineage ZIKV strains. Percent relative infection (IFN+/IFN-) is plotted for African-lineage (light blue) and Asian-lineage (dark blue) ZIKV strains. Error bars indicate SEM. A two-tailed student's t-test was used to compare percent relative infection of African-lineage vs. Asian-lineage ZIKV strains for each IFN condition (*p = 0.049).

Expression of IFITM3 at levels similar to IFN-induction in A549 cells does not restrict ZIKV

Given the potent IFN-I-induced restriction of ZIKV strains in the panel, with a several hundred-fold reduction in replication for the most potently inhibited strains, we examined the contribution of the IFITM3 to this IFN-I-mediated inhibitory effect, because it was the first reported antiviral ISG against ZIKV. IFITM3 was induced by both IFNβ and IFNα in A549 cells, with slightly higher levels (~2-fold) in IFNβ than IFNα-treated cells at the same dose (1000 U/mL; Fig 4.3A). The induction was dose-dependent, as shown with increasing doses of IFNβ (Fig 4.3A). To determine whether the induction of IFITM3 expression could explain the sensitivity of ZIKV to IFN-I, an A549 cell line expressing an N-terminally FLAG-tagged IFITM3 was generated (Fig 4.3B). To ensure that the levels of IFITM3 were physiologically relevant, we sorted cells and selected cells with relatively lower levels of IFITM3 (IFITM3-low-pool cell line); these sorted A549 cells expressed similar levels of IFITM3 as IFNβ-treated A549 control cells (Fig 4.3C).

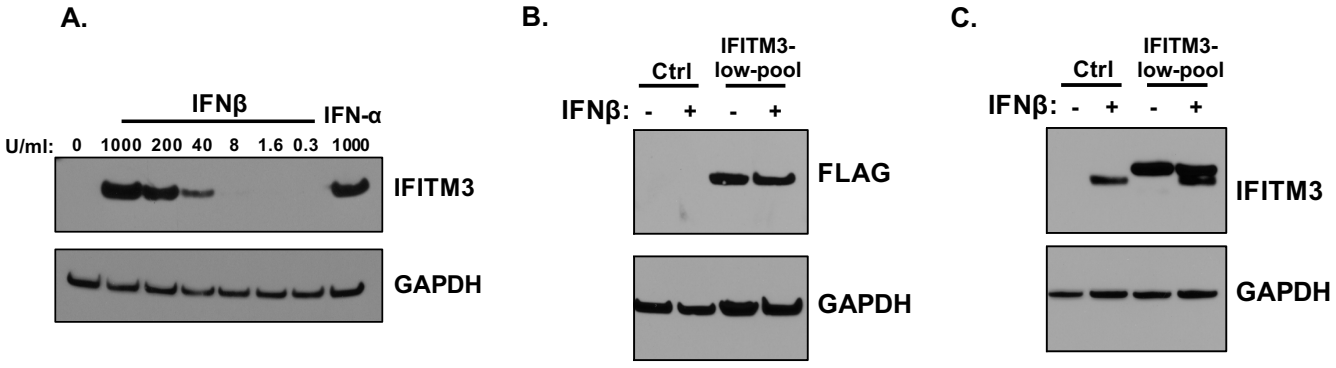

Figure 4.3. Expression of IFITM3 in A549 cells transduced with exogenous IFITM3 compared to after IFN-I-induction. (A) Western blot analysis of IFITM3 expression in A549 cells pretreated with increasing concentrations of IFNβ and 1000 U/mL IFNα for 24 hours. The concentration of IFNβ is indicated above each lane. (B) Western blot analysis of IFITM3-FLAG expression using an anti-FLAG antibody in IFITM3-low-pool A549 cell lines. Control cells were either untreated or treated with IFNβ (1000 U/mL) for 24 hours. (C) Western blot analyses of expression of IFITM3-FLAG protein compared to endogenous IFITM3 using an anti-IFITM3 antibody. Control cells were either untreated or treated with IFNβ (1000 U/mL) for 24 hours.

To assess the effect of IFITM3 expression on ZIKV replication, IFITM3-expressing and control cells were infected with African-lineage isolate MR 766 and Asian-lineage isolate PRVABC59, both of which were found to be especially susceptible to IFN-I (Fig 4.4). Viral replication was not significantly different in cells expressing IFITM3 than from control cells for either strain (Fig 4.4A). Importantly, an Influenza A reporter virus (IAV) was significantly restricted in IFITM3-expressing cells ($p<0.0001$), while virus-like particles (VLPs) expressing the murine leukemia virus (MLV) envelope protein were not significantly restricted in these cells (Fig 4.4B, 4C). This is consistent with published data showing IFITM3 restricts IAV but not MLV (164). Notably, ZIKV was potently inhibited in the same cells engineered to express IFITM3 when they were treated with IFNβ, with drastic reductions in viral replication for both strains ($1.6x10^3$ – $5.1x10^3$ –fold) when compared to infection of untreated control cells (Fig 4.4A; $p=0.007$ for MR 766, $p=0.01$ for PRVABC59). This shows that ISGs induced by IFN-I other than IFITM3 were driving the potent antiviral response to ZIKV in these cells.

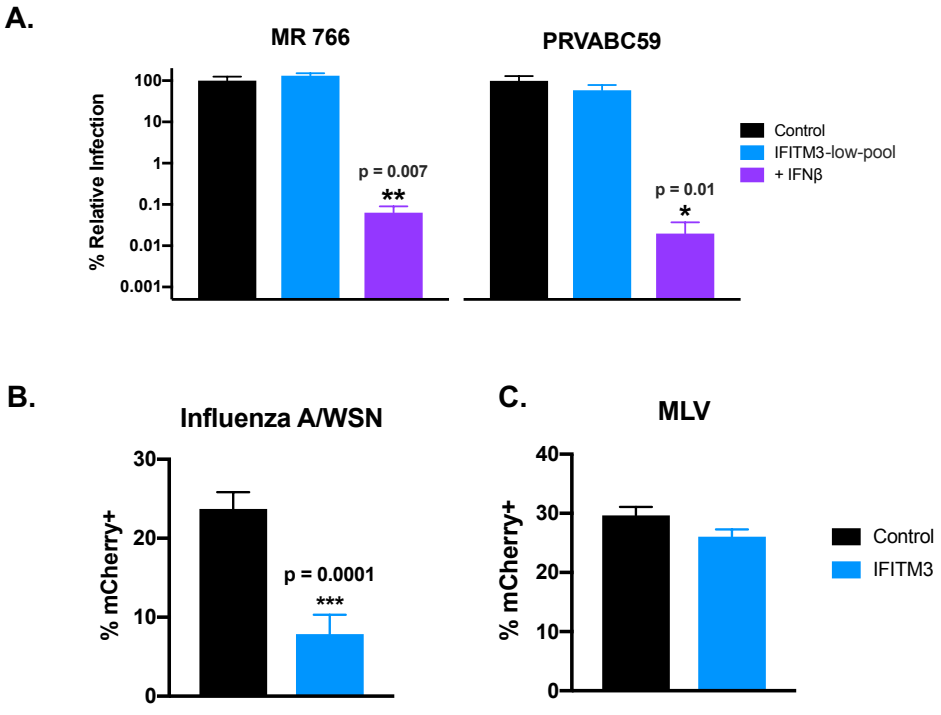

Figure 4.4. Infection of cells expressing IFITM3-FLAG in the absence and presence of IFNβ. (A) Infection of IFITM3-expressing cells with ZIKV strains MR 766 and PRVABC59. Viral titers 48 hpi in untreated (blue) or IFNβ pretreated (1000 U/mL; 24h; purple) IFITM3 cells are

shown. For each strain, percent relative infection (IFITM3-low-pool/Control or IFN+/Control) is shown. Data represent the average of four independent experiments that were carried out with two independently-generated stocks of each ZIKV strain. Error bars indicate SEM. *p = 0.01, **p = 0.007 (one-way analysis of variance (ANOVA) followed by Dunnett's post-hoc test for multiple comparisons) (B, C) Infection of IFITM3-expressing cells with mCherry-expressing (B) IAV and (C) VLPs expressing MLV envelope protein. Data represent the average of at least four independent experiments. Error bars indicate SEM. ***p = 0.0001 (two-tailed student's t-test).

Overexpression of IFITM3 above IFN-I-induced levels in A549 cells restricts ZIKV

Our results indicating that IFITM3 did not restrict ZIKV replication in our system contrasted with results of several studies that have described IFITM3 as a ZIKV restriction factor. These studies tended to utilize systems that overexpress IFITM3 at levels that are higher than seen upon IFN-I induction (111, 112). To determine if these differences in expression levels could explain the differences in results, clonal A549 cell lines were generated that either overexpress IFITM3 above IFN-I-induced levels (5.1-fold higher; IFITM3-high cell line, Fig 4.5A) or express IFITM3 to levels that were closer and thus more relevant to those induced by treatment with IFN-I (1.7-fold higher; IFITM3-rel cell line, "-rel" for IFN-I-relevant, Fig 4.5A). These cells were infected with MR 766 in parallel to empty vector-transduced A549 control cells. While viral replication was not significantly different between control and IFITM3-rel cells, there was a significant reduction of viral replication in IFITM3-high cells (16-fold, p=0.003; Fig 4.5B).

Because the prior studies that suggested IFITM3 inhibits early stages of ZIKV replication used different time points and assays to study IFITM3-mediated restriction of ZIKV (111, 112), we next determined whether we missed the activity of IFITM3 at earlier times or because of our methods of measuring virus. For this, we examined the percent of infected cells in control, IFITM3-rel, and IFITM3-high cells by E-protein staining at 24 hours post-infection (Fig 4.5C). There was no difference in percent E-protein-positive cells between control and the low-expressing IFITM3-rel cells, while there was a 12-fold reduction in percent E-protein-positive cells in high-expressing IFITM3-high cells ($p < 0.0001$).

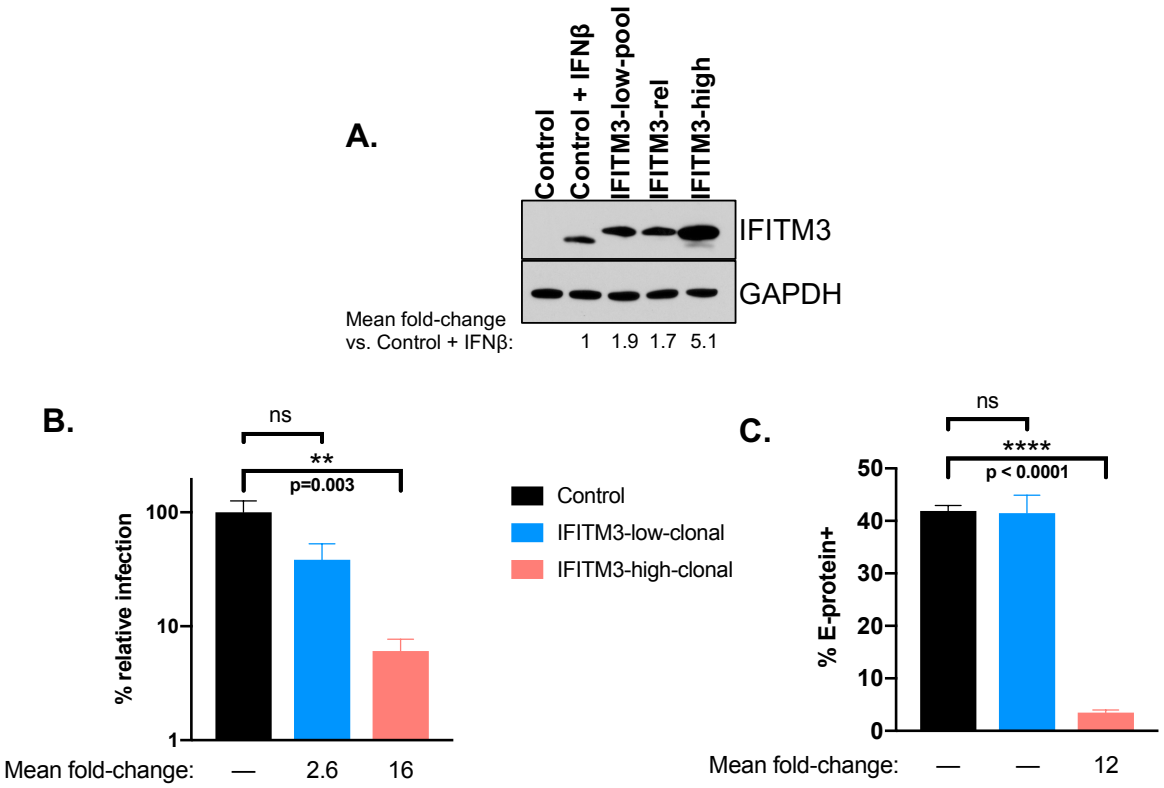

Figure 4.5. Infection of clonal A549 cells expressing IFN-relevant levels of IFITM3-FLAG or overexpressing IFITM3-FLAG. (A) Western blot analysis of IFITM3 expression using an anti-IFITM3 antibody in A549 clonal cell lines and control cells. Control cells were either untreated or treated with 1000 U/mL IFNβ for 24 hours. The fold-change in IFITM3 expression compared to controls cells treated with IFNβ (normalized to GAPDH expression) is noted below the Western blot which was quantified by measuring the band intensities across three different exposures of the same Western blot and calculating the mean. IFITM3-rel cells are named for their IFN-I-relevant levels of IFITM3 expression, while IFITM3-high cells are named for their overexpression of IFITM3 above levels observed by IFN-I induction. (B, C) Infection of clonal cell lines and control cells with ZIKV strain MR 766. The percent relative TCID50 titer of MR 766 measured at 48 hpi (B) and percent of E-protein-positive cells at 24 hpi (C) is shown. All data represent the average of at least four independent experiments. The mean fold-reduction in viral replication (b) or percent E-protein-positive cells (C) in each cell line as compared to control cells (Control/IFITM3-rel or Control/IFITM3-high) is presented below each graph. Error bars represent SEM. **p = 0.003, ****p < 0.0001 (one-way analysis of variance (ANOVA) followed by Tukey's post-hoc test for multiple comparisons).

To rule out that the reason physiological levels of IFITM3 are not associated with restriction of ZIKV in A549 cells is because they are unusually low, we compared their IFN-I-induced IFITM3 levels to other cells, including glial (SNB-19), neuronal (SH-SY5Y), and placental cells (Jeg3 cells) which play important roles in the vertical transmission and

neurological pathogenesis of ZIKV-infected neonates (165-168). IFN-I-induced levels of IFITM3 in Jeg3 were similar to those observed in A549 cells, while SNB-19 and SH-SY5Y cells had lower levels of IFN-I-induced IFITM3 induction (0.3-0.4-fold; Fig 4.6A).

Collectively, these results indicate the neither cell type nor assay differences explain differences in results among studies. Rather, the differences reflect an inhibitory effect of IFITM3 at very high levels that does not reflect what happens at physiological levels.

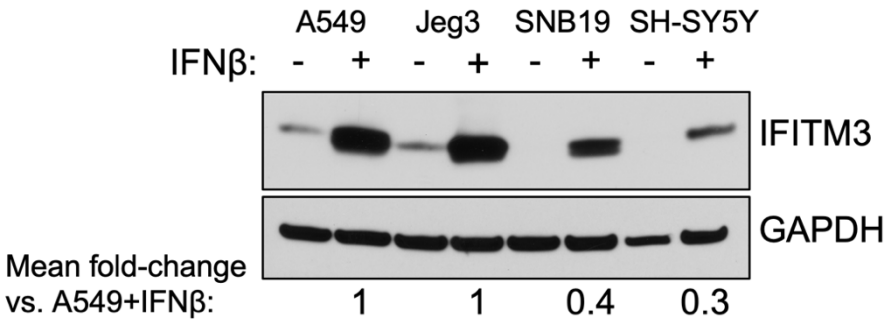

Figure 4.6. Effect of IFN-I pre-treatment on expression of IFITM3 in Jeg3, SNB-19, and SH-SY5Y cells. (a) Western blot analysis of IFITM3 expression using an anti-IFITM3 antibody in A549, Jeg3, SNB-19, and SH-SY5Y cells. Cells were either untreated or treated with 1000 U/mL IFNα or IFNβ for 24 hours. For each cell line, the level of IFITM3 expression by IFNβ treatment as compared to IFNβ-treated A549 cells (normalized to GAPDH expression) is noted below the Western blot.

CRISPR-Cas9 inactivation of IFITM3 does not ablate the effect of IFN-I on ZIKV replication in A549 cells

To better define the contribution of IFITM3 to the overall IFN-I response against ZIKV replication, we employed a complementary CRISPR-Cas9 gene editing approach to knock out IFITM3. In parallel, we inactivated IRF9 because it is an essential component of the IFN-I signaling cascade and thus serves as a control for ablation of the IFN-I response. The transduced cell lines had high percent total editing , including with two different sgRNAs to IFITM3 (IFITM3 sgRNA1: 96%; IFITM3 sgRNA2: 88%; IRF9: 100%). Cells transduced with IFITM3-targeting sgRNA1 or sgRNA2 were depleted in IFITM3 expression as compared to NTC

cells, both basally and when treated with IFNβ (Fig 4.7A). Due to the high level of sequence identity between IFITM2 and IFITM3, IFITM2 expression was also knocked out in cells transduced with IFITM3-targeted sgRNAs (Fig 4.7B). Thus, the IFITM3-knockout cell lines could detect the loss of activity of either IFITM3 or IFITM2 against ZIKV. Cells transduced with the IRF9-targeting sgRNA were depleted in IRF9 expression (Fig 4.7C).

IFITM3-knockout, IRF9-knockout, and NTC cells were infected with an African-lineage (MR 766) or Asian-lineage (PRVABC59) virus at an MOI of 1. In untreated cells, there was a modest but statistically significant (2.5-fold; p=0.0008) increase in virus replication of MR 766 in sgRNA1 IFITM3-knockout cells that was not observed in sgRNA2 IFITM3-knockout cells or in either of the IFITM3-knockout cells infected with PRVABC59. In IFN-treated cells, there was no significant impact on the level of IFNβ inhibition with the ablation of IFITM3 expression. Viral titers were reduced by very similar amounts in control cells (380-fold) compared to IFITM3 knock-out cells (300 and 360-fold) for MR766 infection and in control cells (680-fold) and IFITM3 knock-out cells (510- and 500-fold) for PRVABC59, (Fig 4.7D, purple bars). The effect of IFNβ was completely abrogated in IRF9-knockout cells, as expected (Fig 4.7E).

We also examined whether the time of infection or assay read-out impacted the results in our IFITM3 knockout cells by examining E-protein staining at 24 hours post-infection (Fig 4.7F). In these experiments, two lower doses (50, 150 U/mL) of IFNβ were used to enhance the dynamic range of the assay. In NTC cells, E-protein staining was 3.1- and 8.8-fold lower at 50 U/mL and 150 U/mL IFNβ, respectively. We observed a similar level of inhibition in IFITM3 knockout cells: 2.7- (sgRNA1) and 2.4-fold (sgRNA2) inhibition at 50 U/mL; 6.3- (sgRNA1) and 5.6-fold (sgRNA2) inhibition at 150 U/mL (Fig 4.7F). The differences between untreated or IFN-treated conditions between NTC and IFITM3-knockout cells were not significant. IFNβ-mediated restriction of ZIKV at both IFNβ concentrations was again abrogated in IRF9-knockout cells as compared to NTC cells ($p<0.0001$ at both IFN concentrations).

Taken together, these data suggest at best a very modest contribution of IFITM3 to the overall IFN-I response to ZIKV in A549 cells, which is consistent with the results in cells exogenously expressing IFITM3. Thus, the several order of magnitude restriction to ZIKV replication, including both African and Asian lineage strains in A549 cells is due to ISGs other than IFITM3.

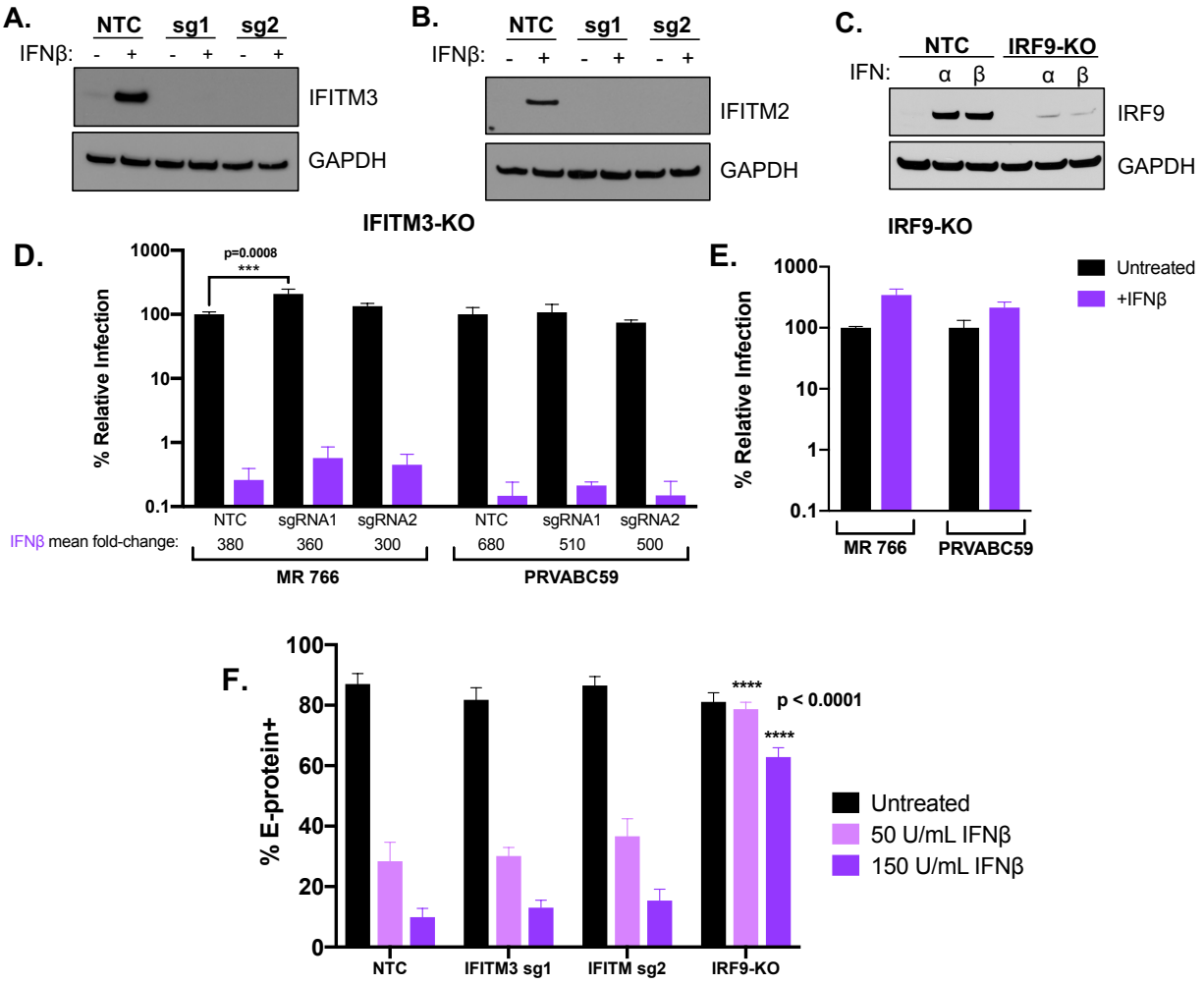

Figure 4.7 Analysis and infection results of IFITM3 and IRF9 knock-out cells. (a, b) Western blot analysis of IFITM3 (A) and IFITM2 (B) expression in untreated or IFNβ pretreated (1000 U/mL; 24h) A549 cells transduced with NTC, sgRNA1 (sg1), or sgRNA2 (sg2). The sgRNA used to transduce each cell line is indicated above each lane. (C) Western blot analysis of IRF9 expression in untreated, IFNα pretreated (1000 U/mL; 24h), or IFNβ pretreated (1000 U/mL; 24h) A549 cells transduced with NTC or an IRF9-targeting sgRNA. (D, E) Infection results with MR 766 and PRVABC59 showing viral titers 48 hpi in IFITM3-knockout (D) and IRF9-knockout (E) A549 cells. The percent relative infection (normalized to untreated NTC) of each strain in the absence of IFN-I (black) and presence of 1000 U/mL of IFNβ (purple; 24h pretreatment) is shown in each indicated cell type. All data represent the average of four independent experiments. Error bars indicate SEM. ***p = 0.0008 (two-way analysis of variance (ANOVA) followed by Dunnet's post-hoc test for multiple comparisons). (F) Infection results with MR 766 showing percent E-protein-positive cells 24 hpi in IFITM3-knockout, IRF9-knockout, and NTC A549 cells. The percent E-protein-positive cells in the absence of IFN-I (black) and presence of 50 U/mL IFNβ (light purple ; 24h pretreatment) and 150 U/mL IFNβ (dark purple; 24h pretreatment) is shown in each indicated cell type. All data represent the average of four independent experiments. Error bars indicate SEM. All data comparisons were made to identical conditions in the NTC. ****p < 0.0001 (one-way ANOVA followed by Dunnett's post-hoc test for multiple comparisons).

Discussion

The emergence of more prevalent and severe pathogenic outcomes associated with ZIKV infection has brought renewed interested in the study of this virus over the past few years. Given the importance of IFN-I in the antiviral response, we asked whether African- and Asian-lineage ZIKV strains differ in their IFN-I sensitivity and whether the previously defined ZIKV antiviral protein IFITM3 plays a critical role in the IFN-I response. ZIKV strains were potently inhibited by IFN-I in A549 cells, although they had a range of susceptibilities and African-lineage strains were less sensitive to IFN-I-mediated restriction than Asian-lineage strains. The potent IFN-I antiviral activity was not due to IFITM3 in A549 cells, suggesting that these cells could shed light on novel ISGs with the potential to restrict ZIKV replication, including those that determine lineage-dependent differences in the IFN-I antiviral effect.

African-lineage strains were significantly less sensitive to the effects of IFNα and showed a trend for a difference with IFNβ compared to Asian-lineage strains. This was at first counter-intuitive given the fact that it is Asian-lineage strains that cause severe neuropathologic outcomes in fetuses, neonates, and adults. However, the data are in line with several recent studies that have demonstrated that infection with African-lineage strains resulted in enhanced replication kinetics, virus production, cytopathicity, and disease progression in murine models (75-87, 126). Further, one such study showed that induction of IFN-I is higher following infection with African-lineage strains in murine models (87). While IFN-Is are potent antiviral proteins, they also play important roles in immune activation and for this reason can have dual roles in viral infection outcomes. One hypothesis to explain these data is that decreased virulence, reduced immune activation, and IFN-I sensitivity may be conducive to establishing persistent infections within certain tissues and that rapid, self-limiting virus replication may minimize opportunities to establish infected cell sanctuaries. Indeed, others have suggested that Asian-lineage strains may be better able to establish chronic infection of neural progenitor cells, undergo more efficient vertical transmission, and establish viral reservoirs in the central nervous

system, lymph nodes, and gastrointestinal and genitourinary tracts (84, 89-92). A caveat to all of these studies, including ours, is the divergent passage histories of the strains that are available for study, and we cannot rule out that this drives some of the observed differences. Future studies with larger numbers of low-passage strains involving important target cell types of ZIKV tropism and pathogenesis will be critical in strengthening our understanding of these relationships.

All ZIKV strains were more potently restricted by IFNβ than IFNα at 1000 U/mL. Although IFNα and IFNβ signal through the same heterodimeric IFN receptor (IFNAR), IFNβ has been reported to possess higher binding affinities for IFNAR and can independently bind one IFNAR chain (IFNAR1), which triggers the downstream expression of a unique set of ISGs (169, 170). A combination of these factors likely influences the stronger potency of IFNβ-mediated viral restriction we and others have observed (171). Of note, we focused on two (IFNα-2a and IFNβ) subtypes that are expressed during ZIKV infection in more relevant cell types, such as human-induced neuroprogenitor cells and the neuroblastoma SH-SY5Y cell line (172), because these IFNs are likely part of the innate antiviral response to ZIKV. However, there are many subtypes of IFN-I that have been shown to have specific and distinct biological effects that may also contribute to IFN-I-induced restriction of ZIKV (170, 173-175).

It is noteworthy that while the African-lineage strains were overall less sensitive to IFNα than the Asian-lineage strains, one commonly used African isolate, MR 766, was very sensitive to both IFNα and IFNβ. This may reflect the extensive passage history of MR 766, which could have selected for a virus that is, as a result, not adapted to evade innate immune pressures. Of note, the differences between African-lineage and Asian-lineage groups in terms of both their IFNα and IFNβ sensitivity would have been even stronger if MR 766 were not included in our panel ($p=0.0054$ for IFNα; $p=0.039$ for IFNβ). In addition, it is interesting that two of the African-lineage isolates tested, MR 766 and DAK-AR-25, are not very divergent (Fig 4.1) with only 38 amino-acid differences between the two isolates throughout their entire coding sequences, yet

DAK-AR-25 was one of the least IFN-I-sensitive viruses. The key sequence determinants for increased evasion of IFN-I signaling in NS1 and for replication in immunocompetent mice in NS4B (72, 176) do not differ between MR766 and DAK-AR-25 and therefore do not explain their differences. Thus, we have identified viruses that show differences in IFN sensitivity that could be leveraged to identify key sequence determinants that predict relative sensitivity to IFN-I.

IFITM3 has recently been reported as an important ZIKV-restricting host factor that blocks an early stage of the ZIKV replication cycle (111, 112). The current findings provide evidence that while IFITM3 has the potential to restrict ZIKV, it does not contribute to the very potent IFN-I-mediated antiviral response to ZIKV in A549 cells. Two ZIKV isolates belonging to each lineage (MR 766 and PRVABC59) that were highly sensitive to IFN-I were not significantly restricted by IFITM3 when it was expressed at physiologically relevant levels. ZIKV replication by IFNβ treatment was potent and unaffected by IFITM3-expression at levels similar to those induced by IFN-I, underscoring the critical contribution of ISGs other than IFITM3 in the IFN-I-mediated restriction of ZIKV. ZIKV restriction also remained unchanged in IFNβ-treated cells in which endogenous IFITM3 had been knocked out, providing further support that endogenous levels of IFITM3 induced by IFN-I do not play a critical role in restricting ZIKV replication. Knocking out IFITM3 expression also abrogated IFITM2 expression. Thus, because there were not significant differences in viral replication between IFITM2/3-deficient cells and control cells, the data is consistent with a prior study reporting that IFITM2 does not play an important role in the IFN-I-induced restriction of ZIKV (111).

We used several experimental approaches to understand why the current findings differ from previous studies that have described an important role for IFITM3 in restricting ZIKV. First, we used two different methods to measure virus, both TCID50 and E-protein staining, as the latter was used in previous studies (111, 112). We did not detect evidence of a role for restriction by IFITM3 at physiological levels by either method. Importantly, we used an MOI of 1 and measured viral replication at 48 hpi, which is consistent with most experiments performed in

these previous studies. To explore whether IFITM3 is active at earlier stages, we examined virus production at 24 hours post-infection and the results were the same as what was observed at 48 hours post-infection, suggesting that a transient effect of IFITM3 is not likely to explain differences in results among studies. Rather, our results indicate that the differences between studies are likely due to the use of overexpression of IFITM3 above physiological levels, as we show that IFITM3 can inhibit ZIKV when overexpressed even though it does not have an impact at levels similar to those induced by IFN-I. It is also worth noting that ours is one of only two studies to examine IFITM3-mediated restriction of ZIKV using a complete CRISPR-Cas9-mediated knockout strategy as opposed to a shRNA/siRNA-mediated knockdown approach (111, 112). Interestingly, the CRISPR-Cas9 inactivation study of Spence et al was conducted in HeLa cells and their combination of knock-out and reconstitution studies show a small (~7 – 10-fold) inhibitory effect of IFITM2 and IFITM3 on ZIKV replication in HeLa cells, although it is unclear what fraction of the overall IFN-I response this explained in these cells (118). Our knock-out studies confirm that in A549 cells, where there is a robust, several order of magnitude inhibitory effect of IFN-I, IFITM3 is not a major player.

While our study clarifies that IFITM3 does not contribute to the IFN-I response in A549 cells, we cannot rule out that IFITM3 contributes to the inhibitory effect of IFN-I in other cell types (HeLa, 293T, HDFa, HFF, MEF), as suggested by other studies (111, 112). However, these studies did not focus on analyzing physiological levels of IFITM3 and instead overexpressed IFITM3 to levels much higher than seen upon IFN-I induction (111, 112). Here, we rule out the possibility that A549s are an anomaly due to unusually low-level induction of IFITM3 – in fact we found that IFN-I-induced expression of IFITM3 in cells relevant to the neuropathogenesis and vertical transmission of ZIKV the same or lower than in A549 cells. Thus, our findings serve as a caution in interpreting these findings in the context of the overall antiviral effect of IFN-I.

Our results hint at a possible threshold of IFITM3 activity because ZIKV was not significantly inhibited in A549 cells expressing IFITM3 at levels slightly higher than those induced by IFN-I (~1.7-1.9 fold higher than IFN-I treated cells) but was inhibited in cells expressing ~3-fold more IFITM3 (~5-fold more than IFN-I-treated cells). This could be relevant if there are cell types that express high levels of IFITM3 expressed upon IFN treatment. Although this is not the case for Jeg3, SNB-19, or SH-SY5Y cells, there is recent evidence that stem cells express much higher levels of IFITM3, among other known antiviral proteins, than their corresponding untreated or IFNβ-treated differentiated cell types (177). This high level of intrinsic IFITM3 expression imparted a unique antiviral resistance to stem cell populations as compared to their differentiated counterparts. This could be the case for ZIKV, given that IFITM3 can restrict ZIKV when present at high levels.

Overall, the results of this study demonstrate that the effects of IFN-I on ZIKV replication in A549 cells are lineage-dependent in our panel of ZIKV strains. The inter-strain variation in IFN-I sensitivity across all viruses in the panel is intriguing and future studies using these strains may identify determinants of IFN-I sensitivity and/or resistance. Finally, the findings suggest that the potent IFN-I effect against ZIKV in A549 cells is not due to IFITM3. Thus, continued investigations of ISGs that restrict ZIKV at physiologically-relevant protein levels, including those that have been recently identified (114-116, 178), are needed to understand the antiviral ISGs and the innate immune responses important in ZIKV replication and pathogenesis.

Chapter V

Development of a CRISPR-death screen for comprehensive identification of interferon stimulated genes that restrict Zika virus in A549 cells

Introduction

IFN-I robustly restricts ZIKV replication in A549 cells as well as in other relevant cell types to ZIKV pathogenesis (see Chapter IV). While these findings underscore the important role of downstream ISGs in restricting ZIKV replication, the identity and contribution of specific ISGs that restrict ZIKV remain poorly characterized (Figure 5.1). Several individual ISGs (IFITM3, PARP12, Viperin/RSAD2, IFI6) have been reported to have activity against ZIKV, although no studies to date have examined the contribution of these ISGs to the overall IFN-I response against ZIKV (see Chapter I). There has only been a single published large-scale screen designed specifically to identify ZIKV-restricting ISGs (107). Dukhovny et al employed a genome-wide CRISPR-activation strategy where all targeted genes were overexpressed. Based on our findings that IFITM3 is only capable of restricting ZIKV when overexpressed above levels induced by IFN-I treatment in Chapter IV, it is likely that this overexpression screen does not accurately recapitulate the IFN-I response for many targeted genes in this study.

Here, we report on the development and validation of a CRISPR screen to interrogate the contribution of ISGs to the IFN-I-mediated restriction of ZIKV. Our CRISPR library targets 1,905 ISGs based on gene expression datasets from IFN-I-stimulated cells, including A549 cells (179). The screening method takes advantage of the cytopathic effect of ZIKV in A549 cells (166), where cells harboring inactivated ISGs that normally inhibit ZIKV are more susceptible to ZIKV-induced cell death (Figure 5.2A). We identified enriched sgRNAs in IFN-stimulated, ZIKV-infected dying/dead cells to define potential ZIKV-restricting ISGs (Figure 5.2B). In this chapter, I present and discuss the data we have collected to-date to develop and execute this screening strategy.

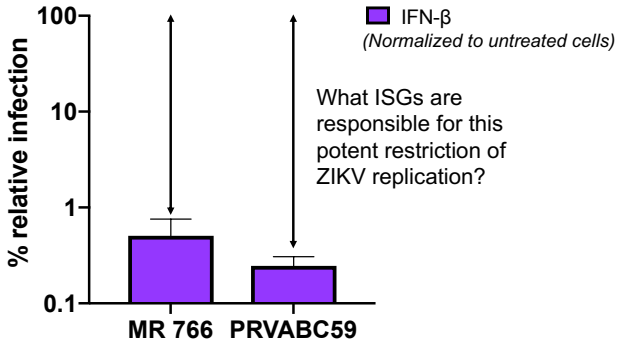

Figure 5.1. IFN-I-mediated restriction of two ZIKV strains and motivating question for this Chapter. The percent relative infection of MR 766 and PRVABC59 in IFN-treated A549 cells (normalized to untreated cells) is shown. The central question of this chapter is presented. ZIKV strain PRVABC59 is used in this chapter.

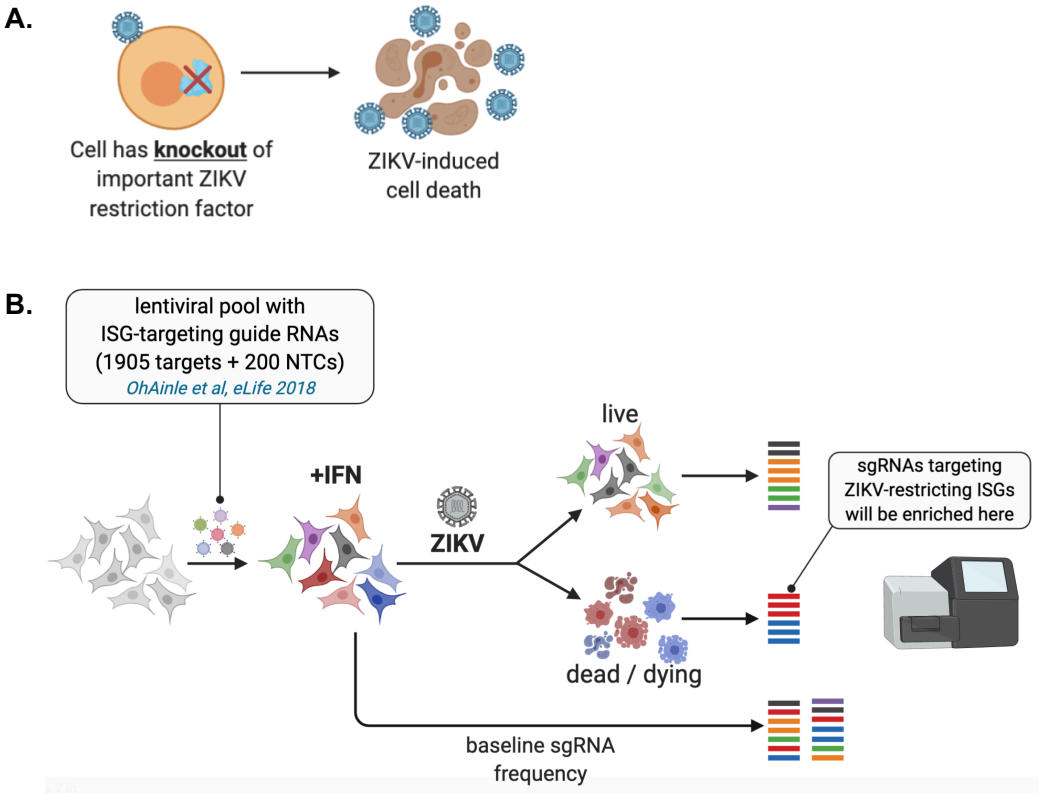

Figure 5.2. Overview of CRISPR-death screening strategy. (A) CRISPR screening strategy used in this chapter, where we have hypothesized that cells harboring a knock-out of a ZIKV-restricting ISG will preferentially succumb to ZIKV-induced cell death. (B) A549 cells are transduced with a lentiviral CRISPR pool (described in (179)). After puromycin selection, transduced A549 cells (A549-ISG-KO cells) undergo a 24-hour IFNβ pre-treatment and are subsequently infected with ZIKV. Following infection, dead/dying cells are isolated from the supernatant and sgRNA frequencies from this population are compared to the live and/or baseline population. Enriched sgRNAs in the dead/dying cell population are of interest as potentially ZIKV-restricting ISGs.

Methods

Cells

A549 cells were obtained from Alice Berger (ATCC) and were maintained in RPMI (Invitrogren) supplemented with 10% fetal bovine serum (FBS), 2mM L-glutamine, and 1X Anti-anti (anti-microbial/anti-mycotic, Gibco).

Viruses

ZIKV strain PRVABC59 was kindly provided by BEI resources. All ZIKV strains were propagated in Vero cells at an MOI of 0.01, as previously described (157). Viral titers were determined by the $TCID_{50}$ assay (see Chapter IV). For all experiments in this chapter, an MOI of 3 was used.

CRISPR ISG library design

The CRISPR library was designed as previously described (179). In brief, ISGs were identified from gene expression profiles of IFN-stimulated cells, including A549 cells (105, 180). A total of 8 sgRNAs were randomly selected for each ISG target, 4 from the Brunello library (181) and 4 from the from Genome-scale CRISPR Knock-Out (GeCKO v2) library (162, 182). The Moffat (183) and Sabatini/Lander libraries (184, 185) were used in cases where 8 unique sgRNAs could not be obtained from the Brunello and GeCKO v2 libraries. There were a total of 12 genes that contained no sgRNAs in any of the aforementioned libraries and, for these genes, 8 sgRNAs were designed using the sgRNA Designer from the Broad Institute (http://portals.broadinstitute.org/gpp/public/analysis-tools/sgrna-design). In total, 15,348 unique sgRNA sequences were synthesized.

Generation of A549 cells with a comprehensive ISG KO (A549-ISG-KO)

Lentiviruses were made by transduction of 293T cells, as previously described (179), with the following exception: $5x10^5$ 293-T cells were plated in 2 mL in 6-well plates and the following day

were transduced with lentiCRISPRv2 plasmid (Addgene plasmid # 52961, a gift from Feng Zhang), 667 ng lentiviral plasmid (with unrepaired 3' long terminal repeat), 500 ng psPAX2 (Addgene plasmid # 12260, an HIV-based packaging plasmid gifted from Didier Trono), and 162.5 ng pMD2.G (Addgene plasmid # 12259, vesicular stomatitis virus glycoprotein [VSV-G] envelope plasmid gifted from Didier Trono). The comprehensive ISG CRISPR library was titered by colony forming unit assay on A549 cells and used to transduce A549 cells at an MOI of 0.5. Cells were selected in puromycin (1 μg/mL, based on kill-curve experiment in A549 cells) for 14 days. Following selection, aliquots of $1x10^7$ cells/mL (> 500-fold representation) were frozen and subsequently stored in liquid nitrogen until ZIKV ISG screening. When cultured, cells were maintained in RPMI complete containing 1 μg/mL puromycin at ≥ 500-fold representation to avoid bottlenecking the library.

Annexin-V staining

Annexin-V staining was performed using the FITC Annexin V Apoptosis Detection Kit I (BD Biosciences) as per the manufacturer's protocol. Cells were analyzed by flow cytometry on a BD FACSCanto II flow cytometer. All data was analyzed using FlowJo v10 software.

ZIKV ISG screening

To perform the ZIKV ISG screen, $2.5x10^7$ cells were plated in a 5-layer flask (Corning Falcon) in 125 mL RPMI complete (Gibco) containing 1000 U/mL IFNβ (PBL Assay Science) and placed at 37˚C. At the time of plating, $1x10^7$ cells were spun down at 650 x g for 5 minutes and frozen at -80˚C for use as "Baseline" sample (see Figure 5.2B). Twenty-four hours after plating and IFNβ pre-treatment, cells were infected with ZIKV (PRVABC59) at an MOI of 3 for 4 hours in a total of 50 mL of serum-free RPMI inoculum. Following infection with ZIKV, the inoculum was removed and replaced with 125 mL of fresh RPMI complete containing 1000

U/mL IFNβ and placed at 37˚C. At 42 hours post-infection, the supernatant (125 mL) was collected and evenly distributed across 5 x 50 mL conical tubes. A PBS wash was performed by adding 50 mL of 1x PBS (Gibco) to the multi-layer flask and rotating the flask so the PBS spread across all layers several times. The PBS was collected and added evenly across the conical tubes holding the supernatant. The Supernatant & PBS Wash (S/W) was spun at 1500 x g for 10 mins at room temperature. Following the spin, the supernatant was poured off and the pellets from the 5 x 50 mL conical tubes were resuspended in PBS and combined into a single Eppendorf tube. The Eppendorf tube was spun again at 1500 x g for 10 mins. The supernatant was then aspirated and the pellet was frozen at -80˚C until further processing. For collection of Live cells (see Figure 5.2B), 12.5 mL 0.05% Trypsin-EDTA was added to the multi-layer flask after collection of S/W. Live cells were collected, counted using a hemocytometer, and $1x10^7$ Live cells were spun down at 650 x g for 4-5 minutes and stored at -80˚C until further processing.

Once cell pellets for all conditions were collected and frozen at -80˚C, genomic DNA (gDNA) isolation was performed. To reduce the likelihood of contamination, gDNA isolation was performed for S/W samples first using a Qiagen DNA mini kit, per the manufacturer's protocol, with the exception that water was used in place of buffer AE for elution. For gDNA purification from Live and Baseline samples, a Qiagen DNA midi kit was used as per the manufacturer's protocol, with the following modifications: each population of $1x10^7$ cells was purified over two columns to maximize recovery of gDNA; Water was used in place of Buffer AE for gDNA elutions; and two elutions were performed for each column so that a second elution containing less ethanol could be obtained that would be well-suited for downstream sequencing purposes.

Following successful gDNA purification, the gDNA was prepared for Illumina sequencing. Again, to reduce contamination from Live and Baseline samples, the Illumina library preparation was first carried out on S/W samples followed by Live and Baseline samples. Illumina library preparation was performed by two rounds of PCR using Herculase II Fusion

DNA Polymerase (Agilent), as previously described (179). For sequencing primers and thermocycling conditions, see (179). For the S/W samples, all purified gDNA was amplified in an attempt to sequence all isolated gDNA. For Live and Baseline cells, as much as 52 µg gDNA was amplified (range of 28-52 µg so that a maximum of 192 first-round PCRs are performed) because this roughly corresponds to 500-fold representation of each sgRNA, as per previously published methods (179). A maximum of 2 µg of gDNA was used per first-round PCR reaction. Following the first-round PCR, all PCRs corresponding to the same sample were pooled and up to 12 first-round PCR reactions were purified on a single Qiaquick PCR purification column (Qiagen), as per the manufacturer's protocol. Four second-round PCRs were performed per sample (10 µL PCR-purified first-round product as template). The second-round PCRs were then pooled and run on a 2% TBE gel to ensure successful amplification of a ~230 bp product. Following this, a 0.7x right-sided AMPure XP (Beckman-Coulter) bead purification was performed as per the manufacturer's protocol using a 96-well plate magnet (Thermo Fischer). The bead-purified products were run on a 2% TBE gel to verify clean-up and their concentration was quantified using the QuBit dsDNA HS assay kit as per the manufacturer's protocol. An equimolar pool was made from all the samples, gel-purified using a 2% TBE gel, and sequenced on an Illumina HiSeq.

Due to different conditions included in each screen (Figure 5.5), there were some modification to the above methods in certain cases. In Screen 2, additional time points (12, 24, 26, 48 hpi) were harvested in the same manner as described above. In Screens 2 and 3, Mock-infected conditions were performed identically to methods described above except no virus was added to the 50 mL serum-free RPMI inoculum. In Screen 3, the Untreated Mock sample was plated without any IFNβ in the media. For "sup toss" conditions in Screen 3 (not described elsewhere in this Chapter), $1.5x10^7$ were plated in order to avoid over-confluency of cells prior to harvesting.

Bioinformatics analyses

Bioinformatics analysis was performed as previously described (179). Baseline, Live, and Mock-infected samples (see Figure 5.2B) were compared to S/W samples to quantitate log_2 fold-enrichment of individual sgRNAs and gene enrichment scores using the MAGeCK statistical package (186) in the S/W samples.

Results

A549-ISG-KO cells succumb to ZIKV-induced cell death

To determine if it was possible to utilize ZIKV-induced cell death as a screening strategy and examine the temporal dynamics of ZIKV-induced cell death in A549-ISG-KO cells, ZIKV-infected untreated and IFNβ-treated A549-ISG-KO cells were stained with Annexin-V every 6 hours from 24 to 48 hpi (Figure 5.3). Annexin-V labels apoptotic (dying/dead) cells by binding to phosphatidylserine, which is selectively present on the outer leaflet of dying/dead cell membranes. Indeed, others have used Annexin-V to label A549 and neural progenitor cells succumbing to DENV- and ZIKV-induced cell death, respectively (187, 188).

There was clear ZIKV-induced cell death in untreated A549-ISG-KO cells, and the percent of Annexin-V+ cells increased throughout the time course (Figure 5.3, black line). Cells pre-treated with IFNβ (1000 U/mL) were protected from ZIKV-induced cell death and resembled mock-infected A549-ISG-KO cells throughout the time course. From this data, it seemed suitable to perform a screen using ZIKV-induced cell death at/after 36 hpi, when the level of ZIKV-induced cell death was clearly above the IFN-treated and mock-infected conditions, which would allow us to detect cells that preferentially succumbed to ZIKV-induced cell death due to inactivation of ISGs that inhibit ZIKV. The 42 hpi time point was selected for piloting a ZIKV ISG screen.

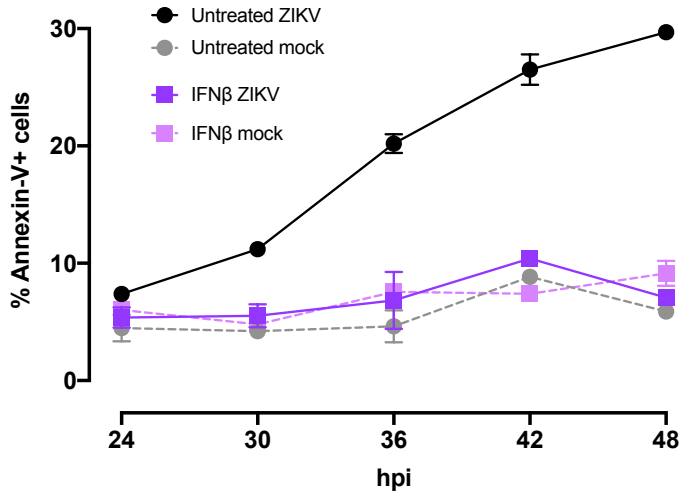

Figure 5.3. Annexin-V staining over a time course of ZIKV infection in Untreated and IFNβ-treated A549-ISG-KO cells. The percent Annexin-V+ cells in Untreated or IFNβ-treated, ZIKV-infected or Mock-infected A549-ISG-KO cells is shown every 6 hours from 24 to 48 hpi.

Harvesting non-adherent cells from IFN-treated, ZIKV-infected cells enriches for dying/dead cells

Given that Annexin-V staining had supported using ZIKV-induced cell death as a screening strategy on/after 36 hpi (Figure 5.3), it was critical to develop a method to isolate dying/dead cells so that we could ultimately quantify enrichment of sgRNAs in this population. We hypothesized that we could harvest the supernatant along with a single PBS wash (S/W; Figure 5.4A; see Methods), to isolate dying/dead A549 cells. To test this approach, S/W was harvested from IFN-treated ZIKV-infected A549-ISG-KO cells at 42 hpi and the Annexin-V+ staining profile was compared to all (adherent and supernatant) cells in the flask. There was a clear and strong enrichment of Annexin-V cells in the S/W population, suggesting that dying/dead cells were highly enriched in the S/W (Figure 5.4B).

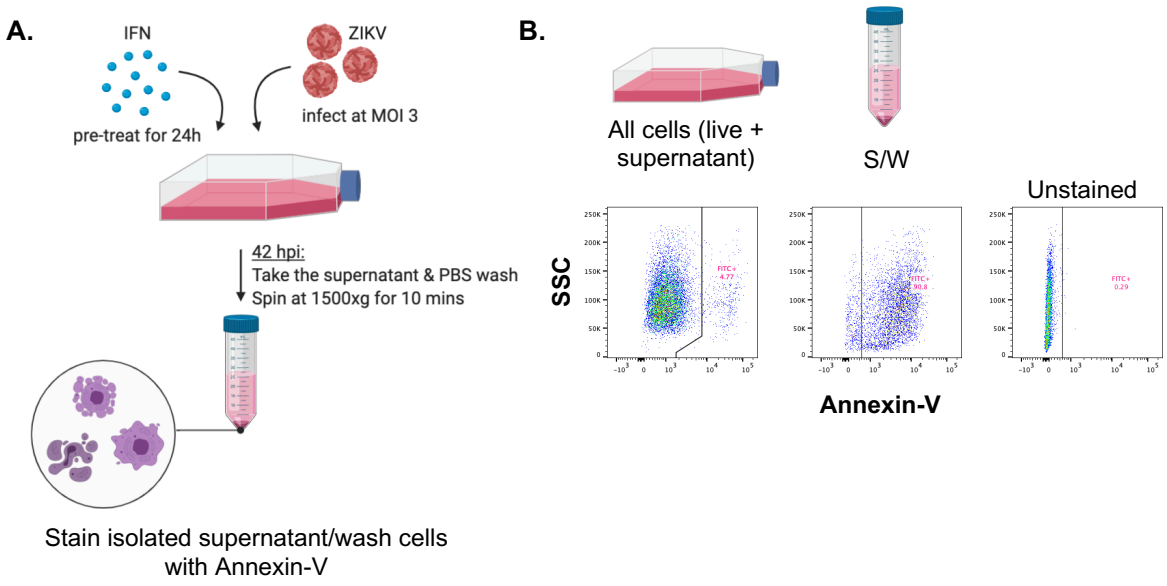

Figure 5.4. Isolation of dying/dead cells by harvesting S/W from IFN-treated, ZIKV-infected A549-ISG-KO cells at 42 hpi. (A) Outline of experimental approach to examine whether harvesting S/W was sufficient to isolate dying/dead (Annexin-V+) cells. (B) Annexin-V staining data by flow cytometry is presented for each different condition. Note that the Annexin-V+ gate in "All cells" is different from the other two gates because the Annexin-V- group was broader in this population of cells.

Screen 1: A pilot screen identifies positive control genes as top hits

With the profile of ZIKV-induced cell death defined and a method for isolation of dying/dead cells validated, a pilot screenwas performed to determine the utility of this screening approach in potentially identifying ZIKV-restricting ISGs (Figure 5.5, Screen 1). In this screen, we examined the 42 hpi time point that was determined to be optimal based on the Annexin-V staining time course of ZIKV-infected cells (Figure 5.3) and compared S/W to Baseline cells (Figure 5.2B). There were two central goals for this pilot screen. First, it was necessary to quantify the extent of enrichment of sgRNAs targeting positive control genes in S/W. Within the lentiviral CRISPR library, a number of genes within the IFN-I signaling cascade are targeted that serve as positive controls for the success of the screening strategy. Specifically, sgRNAs targeting IFNAR1, STAT1, STAT2, and IRF9 are present in the library (Figure 5.6). If the screen is working as expected, guides targeting these genes should be some of the most enriched in

S/W because they inactivate the IFN-I signaling pathway and, thus, these genes should have some of the highest -$\log_{10}$(MAGeCK scores). Second, we wanted to examine the reproducibility of the data between the two screening replicates (Figure 5.5, Screen 1).

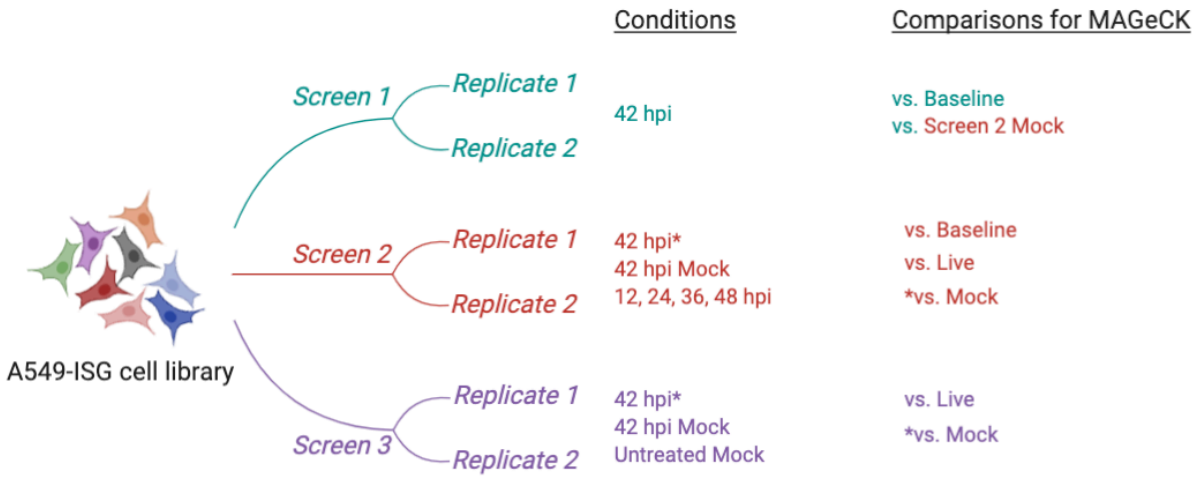

Figure 5.5. Overview of ZIKV ISG screens performed to date. Three screens have been performed with the A549-ISG-KO cell library. Each screen is comprised of two replicates that are performed on separate days. The conditions tested in each screen are listed on the right and the comparisons made to S/W for each condition for MAGeCK analysis are also listed.

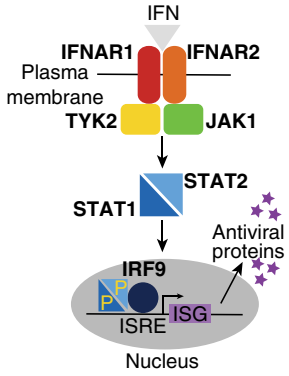

Figure 5.6. Overview of the IFN-I signaling cascade. Figure from (116). The signaling cascade initiated by IFN-I binding to its heterodimeric receptor is shown. Within the CRISPR library, sgRNAs targeting IFNAR1 (red), STAT1 and STAT2 (light blue), and IRF9 (dark blue) are present. These serve as positive controls in the screen, as they should be highly enriched in the dying/dead cell population if the screen is working as expected.

The profile of sgRNA representation in Baseline and S/W samples was highly reproducible between the two replicates (Figure 5.8; R^2=0.96 for Baseline; R^2=0.94 for S/W). In both Baseline and S/W, a high percentage (>80%) of reads aligned to reference sgRNA sequences in the library. Of the 15,348 sgRNAs present in the library, most (>99%) were detected in the sequencing data. As expected, analysis of individual sgRNA fold-enrichment in S/W as compared to Baseline revealed that sgRNAs were both enriched and depleted, ranging 16-fold in either direction (Figure 5.9). The sgRNA fold-enrichment data was filtered to the most-enriched NTC sgRNA to determine the level of background in the dataset (Figure 5.10, red bar). The most-enriched NTC was enriched in S/W by 1.7-fold. Encouragingly, several sgRNAs targeting positive control genes (Figure 5.10, green bars) as well as sgRNAs targeting other genes (Figure 5.10, gray bars) had higher levels of enrichment than this NTC sgRNA. Finally, a $-\log_{10}$(MAGeCK score) was calculated for each targeted gene in the library (Figure 5.11). Encouragingly, the positive control genes STAT1, STAT2, and IFNAR1 were the highest scoring genes in the library (Figure 5.11, green bars). IRF9, another positive control gene, was also highly scoring but to a lesser extent than the other positive control genes. In contrast to the fold-enrichment analysis of individual sgRNAs (Figure 5.10), genes corresponding to randomly-generated sets of non-targeting control guides (NTC_324, NTC_1178; Figure 5.9, red bars) appeared within the top ~20 scoring genes, suggesting that the background signal in the screen may be somewhat high when analyzing screening data using this method. There were a number of high-scoring genes in this pilot screen, some of which have been reported to code for proteins with anti-viral functions (ADAR, OASL) (189, 190).

Baseline	S/W
% of reads aligned:	
Replicate 1: 81.9%	Replicate 1: 81.2%
Replicate 2: 82%	Replicate 2: 81.4%
Distinct guides detected (15,348 total)	
Replicate 1: 15,309	Replicate 1: 15,313
Replicate 2: 15,319	Replicate 2: 15,297

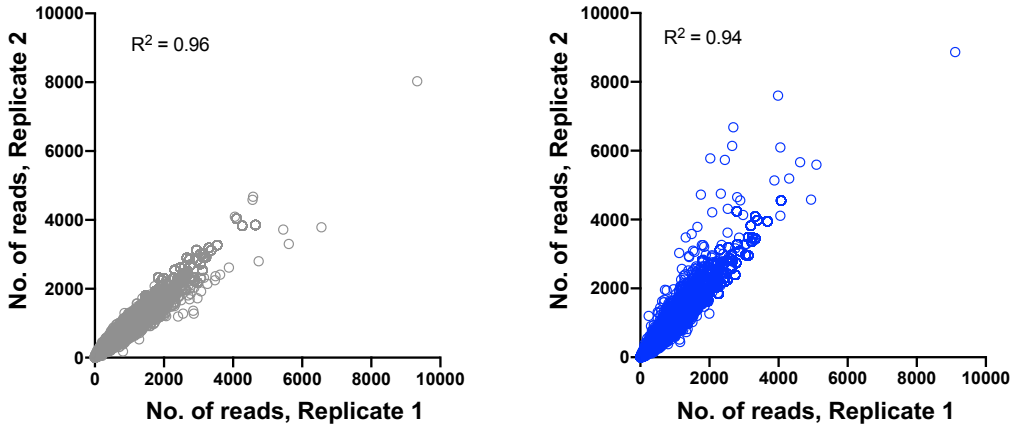

Figure 5.7. Library representation and reproducibility profiles from Baseline and S/W samples in ZIKV ISG Screen 1. For both conditions, the percent of sequencing reads aligned and number of distinct guides detected are presented. In the reproducibility plots below, each dot corresponds to an sgRNA in the CRISPR library.

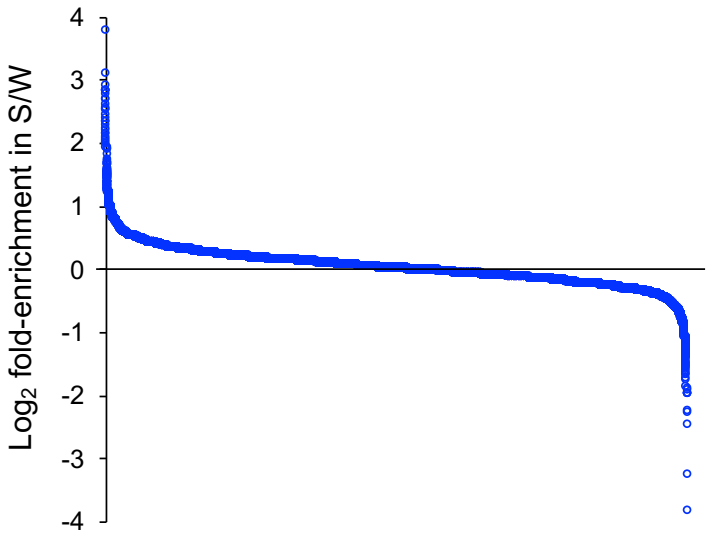

Figure 5.8. Waterfall plot of sgRNA enrichment in S/W vs. Baseline in Screen 1. The log_2 fold-enrichment enrichment of sgRNAs in S/W is shown as compared to Baseline. Each blue dot represents a guide in the CRISPR library.

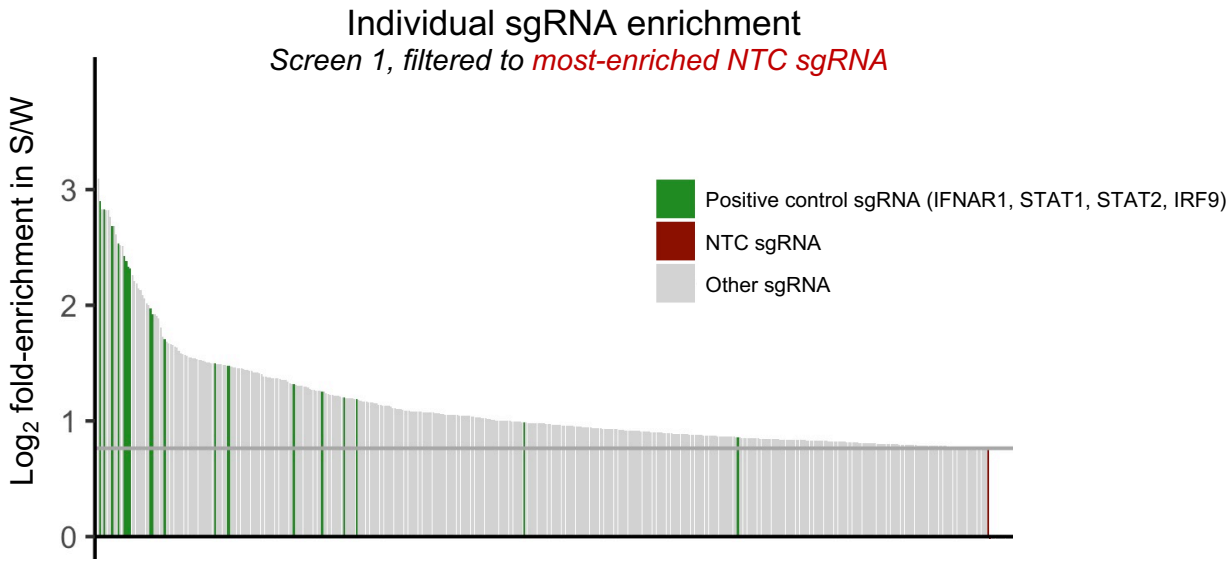

Figure 5.9. Enrichment of sgRNAs in S/W vs. Baseline in Screen 1 filtered to the most-enriched NTC sgRNA. The $\log_2$ fold-change enrichment of sgRNAs in S/W (dying/dead cell population) is shown as compared to Baseline. Each bar represents a separate sgRNA in the CRISPR library, with sgRNAs targeting positive control genes in green and the most-enriched non-targeting control sgRNAs in red. The data is cut off at the highest-enriched non-targeting control sgRNA, the fold-enrichment of which is represented by the horizontal gray bar.

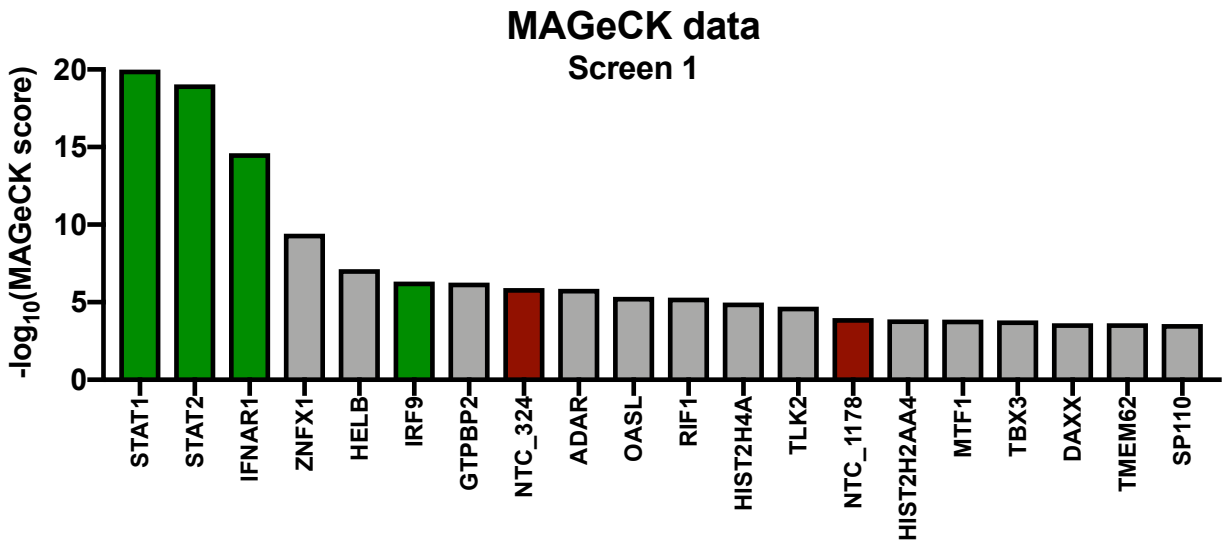

Figure 5.10. Top 20 MAGeCK-scoring genes in Screen 1. The top 20 scoring genes are shown in descending order by $-\log_{10}$(MAGeCK score). Positive control genes are in green and genes corresponding to randomly-generated sets of NTC sgRNAs are shown in red.

Screen 2: Mock-infected screening conditions highlight and adjust for background from non-specific cell death

Given the promising results from the pilot screen (Screen 1), a second screen (Figure 5.6, Screen 2) was performed to assess the reproducibility between independent screens and to incorporate additional conditions, as detailed below.

Adenosine Deaminase Acting on RNA (ADAR) was a top-scoring hit in Screen 1. However, it is known to cause cell death when inactivated in A549 cells (191), suggesting that its high score in Screen 1 may reflect non-specific cell death instead of ZIKV-restricting capacity. Thus, a mock-infected condition was added to Screen 2 to examine and broadly control for non-specific cell death. In addition, S/W was harvested at 12, 24, 36, and 48 hpi to examine additional time points because Screen 1 only assessed S/W at a single time point (42 hpi) and there may be differences in results at different times after ZIKV infection. Mock-infected conditions were not performed for these additional timepoints because otherwise the screen would become too unwieldy. Lastly, Live cells (those adherent on the plate at the end of the screen) were harvested since it was hypothesized that comparing sgRNA frequency in this population to that in S/W may allow for stronger detection of sgRNA enrichment than comparing S/W to Baseline (Figure 5.3)

There was not a significant difference in the MAGeCK scores of positive control genes when making comparisons between S/W vs. Baseline and S/W vs. Live cells at 42 hpi, suggesting that there is not a significant difference in sgRNA frequency in Baseline and Live cell populations that would allow for stronger detection of sgRNA enrichment in S/W (Figure 5.12). The $-\log_{10}$(MAGeCK score) for genes in Screen 2 were compared to those in Screen 1 at 42 hpi (Figure 5.13). Positive control genes were consistently high scoring, with IRF9 lower scoring than the other 3 positive control genes. There were 7 genes that were amongst the 20 highest-scoring genes in both screens (Figure 5.13, blue bars). However, 11 top-scoring genes in Screen 2 were also in the top 20 scoring genes within the Mock condition at 42 hpi (Figure 5.14,

orange bars), signifying a high level of non-specific cell death leading to the results from both screens. However, sgRNAs targeting the positive control genes were some of the most depleted in S/W from the Mock condition (data not shown).

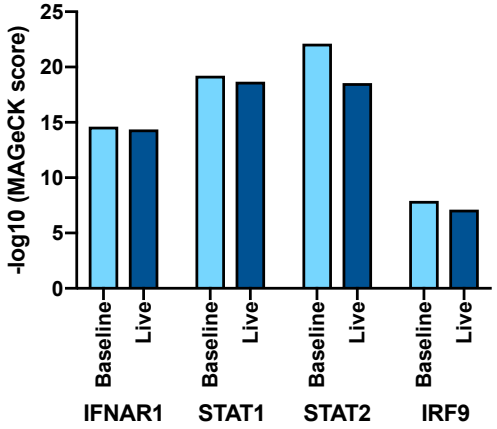

Figure 5.11. MAGeCK scores of positive control genes in comparisons of S/W to Baseline or Live populations at 42 hpi. The -$\log_{10}$(MAGeCK) score is shown for each positive control gene when MAGeCK comparisons were made between S/W vs. Baseline (light blue) or S/W vs. Live (dark blue). See Figure Figure 5.3 for more details on these conditions.

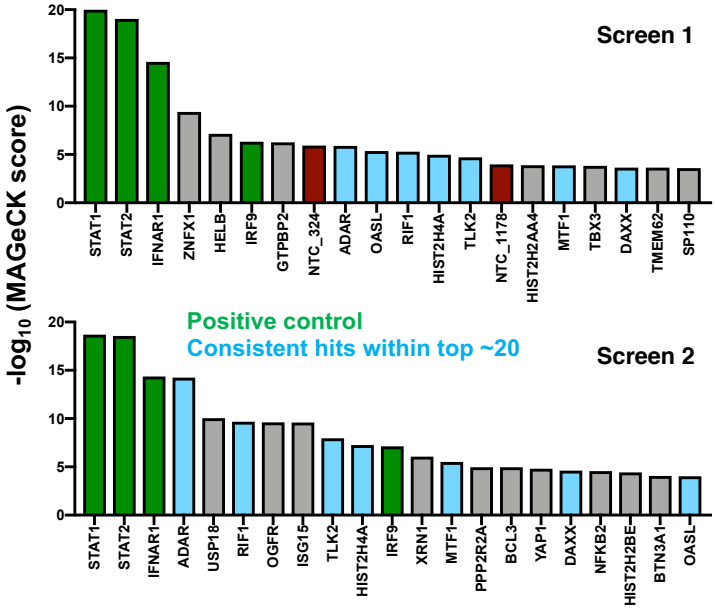

Figure 5.12. MAGeCK scores for the top ~20 scoring genes of Screen 2 as compared to Screen 1 at 42 hpi. The highest scoring ~20 genes for Screen 1 and Screen 2 are shown. Positive control genes are highlighted in green, genes from randomly-generated sets of NTC sgRNAs are shown in red, and consistent hits within the top ~20 scoring genes are in blue.

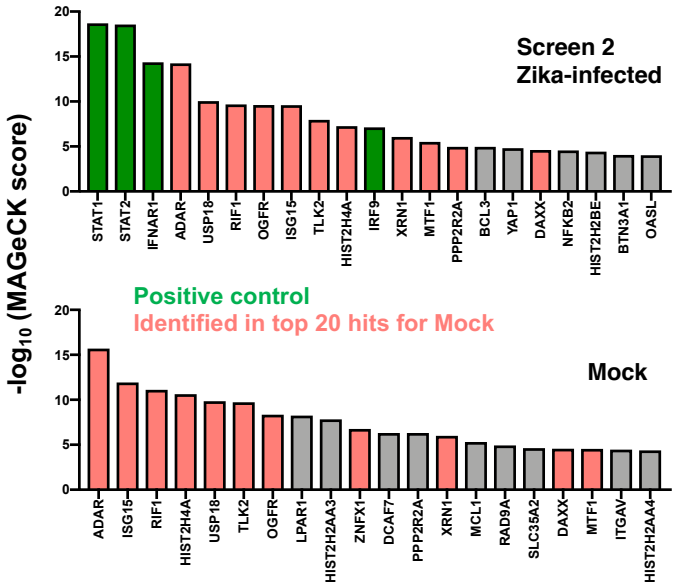

Figure 5.13. MAGeCK scores of top ~20 scoring genes in Screen 2 as compared to Mock condition at 42 hpi. The highest scoring ~20 genes for ZIKV-infected (top) and Mock-infected conditions (bottom) in Screen 2 are shown. Positive control genes are highlighted in green and genes within the top ~20 for both conditions are highlighted in orange.

To quantitatively adjust for non-specific cell death, a new MAGeCK analysis was completed where sequencing data from the Mock-infected condition was compared to detect enrichment in the S/W sample (Figure 5.15). In this mock-adjusted dataset, the positive controls (including IRF9) were the highest scoring genes in the library. All other high scoring genes that were present in both ZIKV-infected and Mock-infected conditions were absent in this Mock-adjusted data.

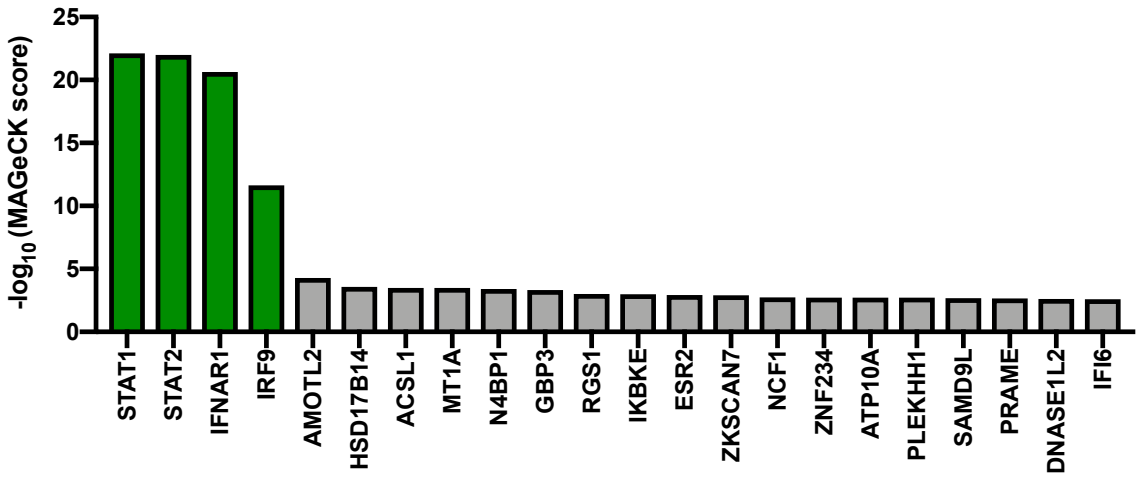

Figure 5.14. Mock-adjusted MAGeCK scores from Screen 2 at 42 hpi. The highest scoring ~20 genes from the mock-adjusted Screen 2 analyses are shown. Positive control genes are highlighted in green.

Finally, MAGeCK analyses were performed on the additional time points (Figure 5.17). Intriguingly, no positive control genes were among the top-scoring 25 genes at 12 hpi. While they appeared in the top-scoring 25 genes at 24 hpi, they were not the highest-scoring genes until 36 hpi. Interestingly, many genes that were the highest scoring in the Mock-infected condition (Figure 5.14) were top-scoring as early as 12 hpi and continued to score highly throughout the rest of the time course (Figure 5.18).

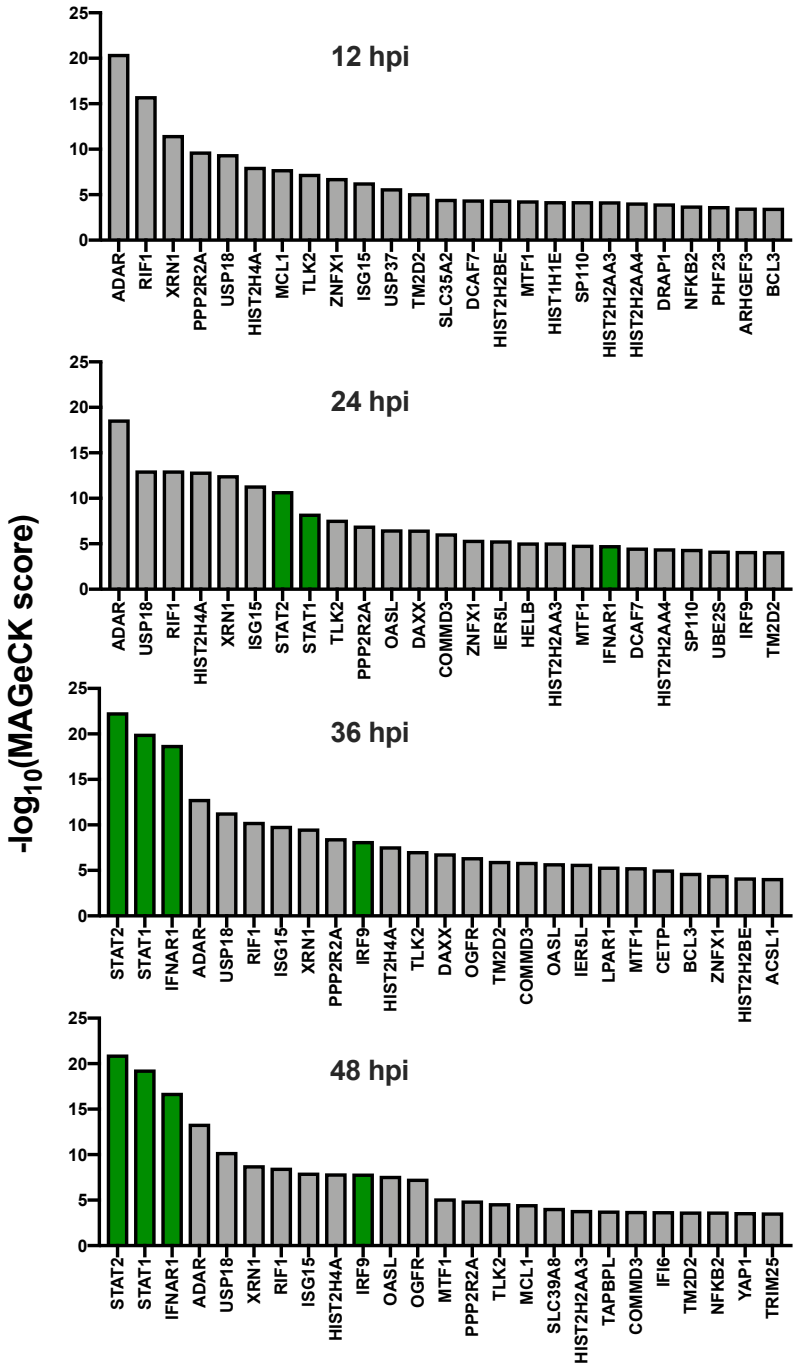

Figure 5.15. MAGeCK scores of top 25 scoring genes at 12, 24, 36, and 48 hpi. The highest scoring 25 genes for each time point in Screen 2 are shown. Positive control genes are highlighted in green.

Taken together, data from Screen 2 highlighted the importance of controlling for non-specific cell death with Mock-infected conditions and performing the screen on/after 36 hpi where positive-control genes are highest-scoring in the screen. We next set out to perform a replicate mock-adjusted screen at 42 hpi to assess the reproducibility of this approach. In addition, given the drawback of non-specific cell death in the screen, we sought to more closely examine several mock-infected conditions to understand the cause of background and inform future methods to reduce its impact.

Screen 3: Mock-adjusted results from two screens identify both previously-described and novel hits as potential ZIKV-restricting ISGs

Based on the importance of mock-adjustment in the results from Screen 2, we modified our CRISPR screening strategy to specifically focus on comparisons between ZIKV-infected and mock-infected S/W samples (Figure 5.16). Mock-adjusted MAGeCK scores from a third screen at 42 hpi were compared to those from Screen 2 (Figure 5.17). As expected, positive control genes (IFNAR1, STAT1, STAT2, IRF9) were reproducibly high scoring (Figure 5.17A, green points). Next, the scores of non-positive control genes were examined from both screens (5.17A, blue box). Within this set of genes, we identified both previously described (IFI6) (107, 116) and novel IFN-induced genes that may restrict ZIKV. *AMOTL2* and *GBP3* were the highest scoring reproducible non-positive control genes in both screens. AMOTL2*,* which has been shown to play important roles in angiogenesis among other functions (192), does not have reported anti-viral activity. GBP3, a guanylate binding protein, has been reported to restrict influenza virus replication and transcription (193), and other members of the IFN-induced GBP protein family have known anti-viral roles (Reviewed in (194)). Interestingly, previously reported ZIKV restriction factors IFITM3 and PARP12 were not hits in either screen, while RSAD2 (Viperin) was a low-scoring hit above NTC only in Screen 2 (Figure 5.17B, red points).

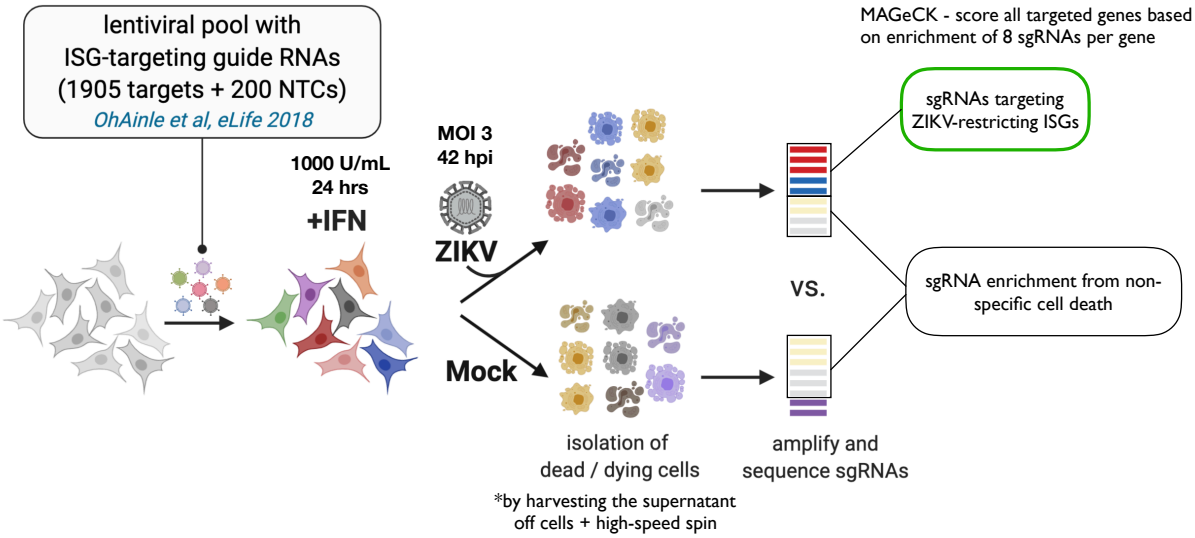

Figure 5.16. Revised ZIKV ISG screening strategy focused on adjusted by Mock-infected IFN-treated conditions. A549-ISG-KO cells undergo a 24-hour IFNβ pre-treatment and are subsequently infected with ZIKV or are Mock-infected. Dead/dying cells from ZIKV-infected condition are isolated from the supernatant and sgRNA frequencies from this population are compared to those in the Mock-infected dead/dying cell population. Enriched sgRNAs in the ZIKV-infected dead/dying cell population are of interest as potentially ZIKV-restricting ISGs.

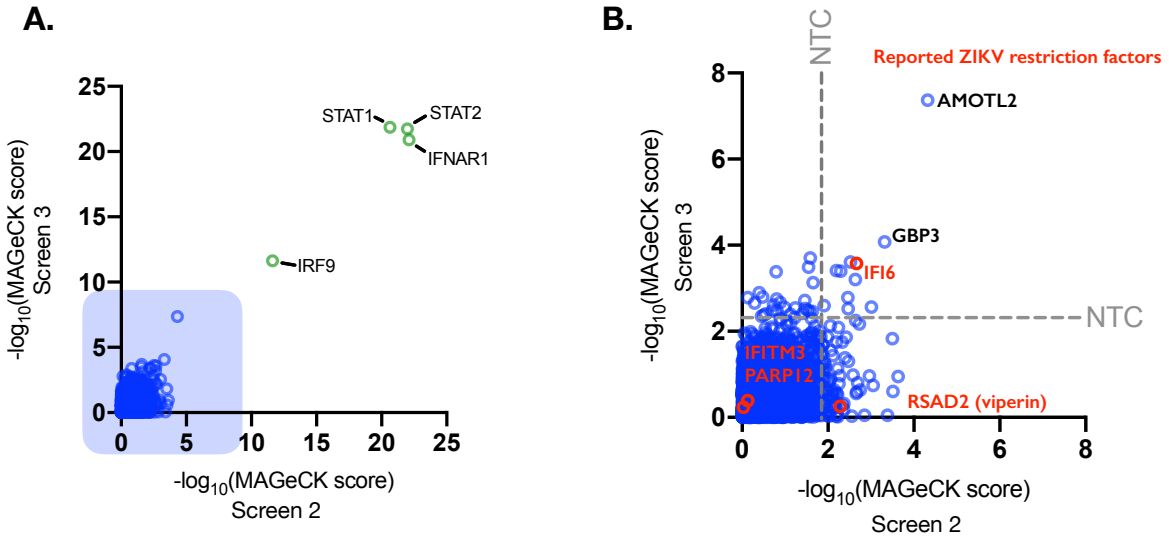

Figure 5.17. Comparison of mock-adjusted MAGeCK score datasets from Screen 2 and Screen 3 at 42 hpi. (A) The mock-adjusted Screen 2 (x-axis) and Screen 3 (y-axis) MAGeCK score datasets are shown. Each dot represents a different gene targeted in the CRISPR library. Green dots correspond to positive control genes as labeled on the graph. (B) Mock-adjusted MAGeCK dataset from blue box in (A).

To more closely examine non-specific cell death in the screen, S/W was harvested from both untreated (Screen 3) and IFN-treated (Screen 2 & Screen 3) mock-infected cells and MAGeCK scores were generated for both conditions by comparing S/W to live cells at the end of mock infection (Figure 5.18). To examine the reproducibility of IFN-treated mock-infected results, we compared MAGeCK scores between these conditions in Screen 2 and Screen 3 and found that they were reproducible (R=0.69; Figure 5.18A). However, there was weak correlation when comparing Screen 2 or Screen 3 IFN-treated mock-infected results to those from untreated mock-infected cells in Screen 3 (R=0.11 and R=0.13, respectively), suggesting that the groups of gene knockouts that lead to cell death with vs. without IFN treatment are largely distinct. These data also reveal that most of the high MAGeCK scoring background originates in the IFN-treated mock-infected condition, as evidenced by the differences in MAGeCK score range between Untreated (0-8) vs. IFN-treated (0-20) mock-infected conditions (Figure 5.18B,C; x-axis range vs. y-axis range). This suggests that our mock-adjusted screening approach (Figure 5.16) accounts for most of the background since the mock-infected condition is IFN-treated. However, the highest-scoring gene in the untreated mock-infected sample is *AMOTL2* (Figure 5.18B,C), suggesting that its high score in the mock-adjusted dataset in Figure 5.17B is a result of background not captured by comparing to mock-infected IFN-treated samples. No other high-scoring hits in the untreated sample appeared as hits of interest in the mock-adjusted screen data (Figure 5.17B), further underscoring the current mock-adjustment approach using an IFN-treated mock-infected sample (Figure 5.16).

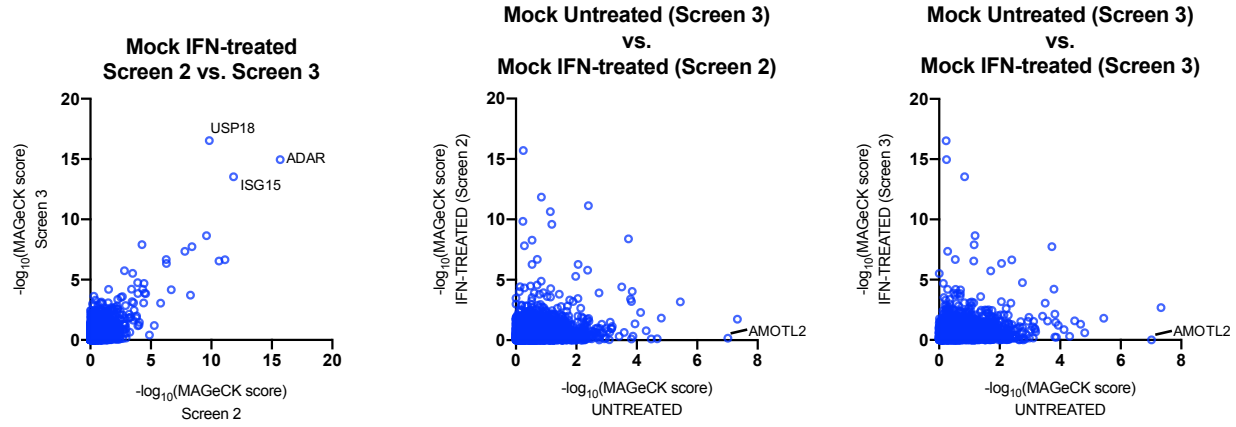

Figure 5.18. Comparison of non-specific cell death in Mock-infected Untreated vs. Mock-infected IFN-treated conditions at 42 hpi. (A) MAGeCK scores (S/W vs. Live) from Mock-infected IFN-treated cells in Screen 2 and Screen 3 are shown. (B, C) MAGeCK scores (S/W vs. Live) from Mock-infected Untreated cells in Screen 3 vs. Mock-infected IFN-treated cells in Screen 2 (B) or Screen 3 (C) is shown.

Variability in sgRNA enrichment for positive control genes underscores need for optimization of sgRNA design and/or bioinformatics approaches

While positive control genes have been consistently the highest scoring genes in the library in both Screen 1 and Screen 2 by multiple analyses, IRF9 is consistently lower scoring than the others. This is particularly intriguing given our $TCID_{50}$ (Figure 4.7E) and E-protein staining (Figure 4.7F) which demonstrated that IRF9 knockout ablates the IFN-mediated restriction of ZIKV. The MAGeCK scores presented this Chapter are based on the level of enrichment of all 8 sgRNAs that target a each gene. Thus, we examined the enrichment of all 8 sgRNAs targeting positive control genes from both Screen 1 and Screen 2 in S/W at 42 hpi to determine if a difference in sgRNA enrichment between the positive control genes could be driving differences in MAGeCK scores (Figure 5.18). Indeed, while all 8 sgRNAs targeting STAT1, STAT2, and IFNAR1 were enriched with small variation, there was significantly more variability in enrichment across the 8 sgRNAs targeting IRF9 likely leading to lower MAGeCK

scores. This suggests that IRF9-targeting sgRNAs that are not as highly enriched are not editing the IRF9 locus as efficiently, although more detailed studies are certainly needed to confirm this.

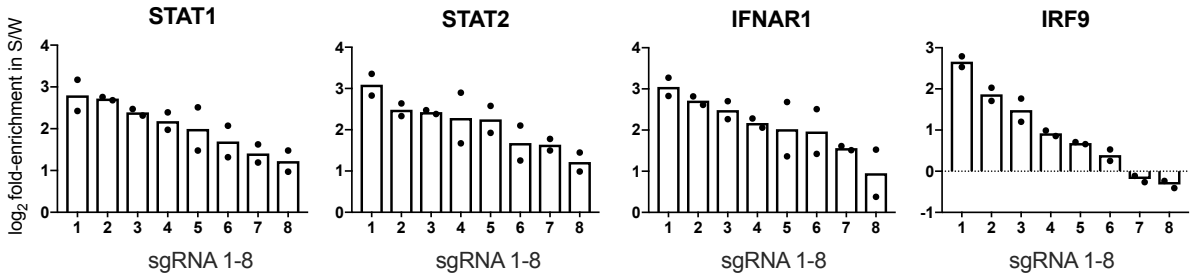

Figure 5.19. Individual sgRNA enrichment profiles for positive control genes in Screen 1 and Screen 2 at 42 hpi. The $\log_2$ fold-enrichment (y-axis) of each sgRNA (x-axis) for each positive control gene in the library is shown for both Screen 1 and Screen 2 (individual black dots).

Discussion

The preliminary findings outlined in this chapter demonstrate the promise of a CRISPR-Cas9-based screen developed to identify ZIKV-restricting ISGs in A549 cells. A strength of this approach lies in its simplicity. By harvesting and sequencing the sgRNAs in S/W from IFN-stimulated, ZIKV-infected cells, enriched sgRNAs can be identified that potentially target ZIKV-restricting ISGs. In fact, several recent screens have successfully used cell survival as a method to screen for ZIKV restriction (107) and ZIKV host/dependency factors (108-110). Cell survival-based screening strategies have also been employed to study other cytopathic viruses, such as CHIKV (195).

In its current state, the screen has a significant level of background attributed to non-specific cell death. However, we have incorporated a mock-infected condition that is able to adjust for this background. In our mock-adjusted data from two screens (Screen 2 and Screen 3), we identified genes that were reproducibly high-scoring above non-targeting control, including expected positive-control genes in the IFN-signaling pathway. Of the previously-reported IFN-induced ZIKV restriction factors (see Chapter I), we identified IFI6 as reproducible hit. IFI6 was identified in a screen for YFV restriction factors and was shown to have activity against ZIKV when overexpressed. IFI6 was also a reproducible top-scoring hit in a genome-wide overexpression screen for ZIKV restriction factors, which is the only published study to date that has specifically screened for ZIKV restriction factors. The preliminary data from our screen suggests that these published findings are likely not artifacts of overexpression since we identified IFI6 in this CRISPR-KO screen. In support of our findings in Chapter IV, IFITM3 was not a hit in the screen. Intriguingly, PARP12 was also not a hit in our screen. This is a surprising result since PARP12 was identified using a targeted knockout approach in A549 cells. RSAD2 (Viperin) scored above NTC in Screen 2 but not in Screen 3. Studies examining the IFN-mediated restriction of ZIKV in single targeted IFI6-KO, PARP12-KO, and RSAD2-KO A549 cells are currently underway and will allow us to validate our screen findings.

We identified several novel genes as hits in the screen. GBP3, the highest-scoring reproducible hit, has reported anti-viral functions against influenza in A549 cells (193). Future studies of IFN-mediated restriction of ZIKV in GBP3-KO A549 cells will be necessary to validate the screen findings. We also identified eight other reproducible high-scoring hits above NTC in our mock-adjusted screen (Figure 5.17B; ST3GAL6, RMI2, HELZ2, DNASE1L2, BTN3A1, CBWD6, IKBKE, ICAM1). These genes will also be individually validated in single knockout A549 cell lines to verify their importance to the IFN response (see Chapter VI).

Future work will also focus on development of methods to reduce background from non-specific cell death, including longer pre-treatment periods with IFN prior to infection in order to increase the likelihood of discarding cells that non-specifically die from IFN treatment. The high level of non-specific cell death could be taking up a significant amount of sequencing space, making it more difficult to detect differences in the enrichment of the remaining genes of interest. If this is the case, a potential alternative approach could be to synthesize a new CRISPR lentiviral library that does not target top-scoring hits in the Mock-infected condition. In building a new CRISPR library, updated sgRNA design metrics could be used that may address issues of inadequate gene editing for some sgRNAs in the library, as seen in the case of IRF9. Novel bioinformatics approaches, such as MAGeCKFlute (196) which accounts for sgRNA editing efficiency and allows for better comparisons amongst different conditions, can also be easily implemented without designing an entirely new library.

Chapter VI

Conclusions and Future Directions

The recent emergence of ZIKV and its associated morbidity and mortality are novel features of this previously understudied virus that was discovered in East Africa more than 70 years ago. Significant efforts on a global scale have been focused on elucidating factors underlying novel aspects of ZIKV transmission and pathogenesis in the Americas. Many of these efforts are complicated by a lack of ZIKV data from the African continent, where the level of ZIKV prevalence and the properties of strains that circulate there are unknown (28-30). This thesis details intriguing discoveries made by examining both ZIKV seroepidemiology in Kenya and the role of the type-I interferon response in restriction of diverse ZIKV strains (Figure 6.1). Technological developments are also described in this thesis that may enable exciting scientific discovery in each of these areas in the future. In Chapter II, we found a low but detectable level of ZIKV prevalence within cohorts from two urban centers in Kenya over a period of ~20 years (Figure 6.1, left). Our findings set an important baseline for future ZIKV surveillance in the major urban regions of Kenya, especially as outbreaks fueled by Asian-lineage ZIKV strains continue their geographic expansion on the African continent (119, 120). where arbovirus infections are common. In Mombasa, where the burden of DENV infections were also high, it was more challenging to distinguish infection histories, which speaks to the many current challenges of distinguishing ZIKV (and other flavivirus) infections (38). In Chapter III, we developed and initiated testing of a method (PhIP-Seq) to identify ZIKV-specific antibody responses in plasma samples (Figure 6.1, left). We extended the utility of PhIP-Seq to map the epitopes of HIV-specific monoclonal antibodies isolated from HIV-infected individuals from Kenya. It has been postulated that the strains of ZIKV that circulate in the Americas may have different properties than African-lineage ZIKV strains circulating on the African continent, where severe neuropathogenic outcomes of ZIKV infection have not been documented (92). In Chapter IV, we

found that African-lineage ZIKV strains were more resistant to IFN-I-mediated restriction as compared to American ZIKV isolates, which may contribute to differences in ZIKV pathogenesis in Africa vs. the Americas (Figure 6.1, right; Figure 6.2). Further, IFITM3 does not contribute to the IFN-I-mediated restriction of ZIKVs from either lineage (Figure 6.1, right). Finally, in Chapter V, we developed a CRISPR screen that shows promise in identifying ISGs that restrict ZIKV. The technological developments detailed in Chapter III (PhIP-Seq) and Chapter V (ZIKV ISG screen) require further validation which is described in detail in this Chapter.

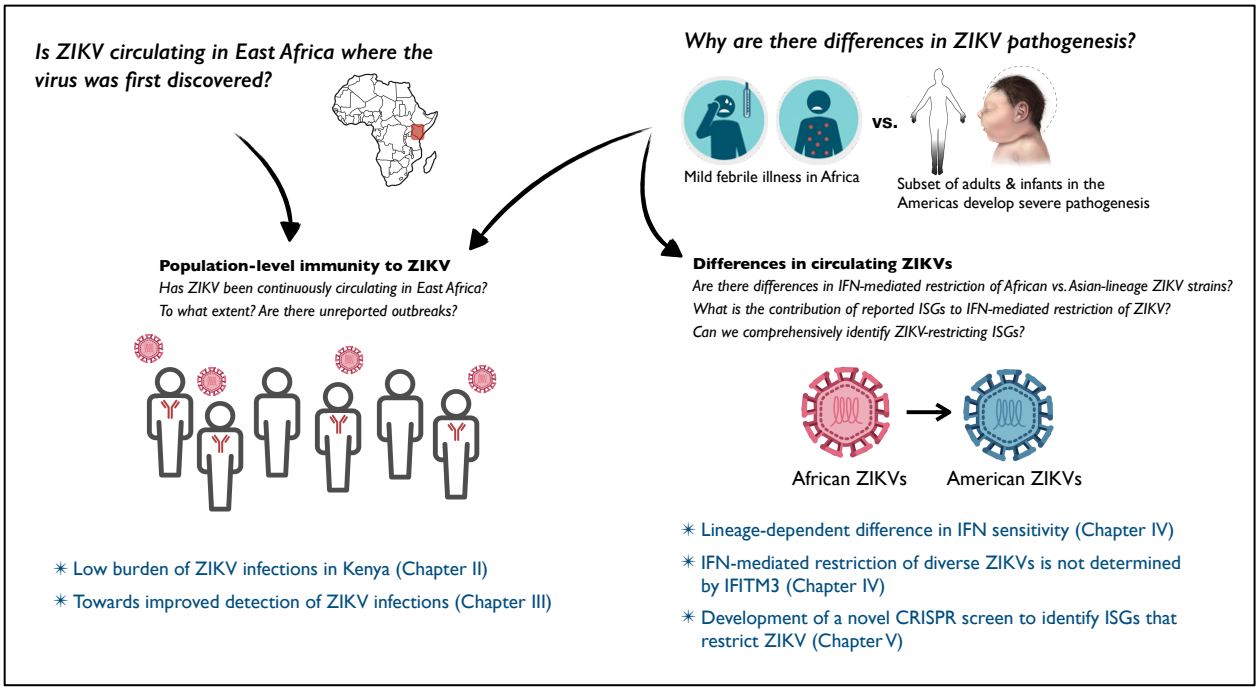

Figure 6.1. Summary schematic of thesis findings. In this thesis, we examine population-level immunity to ZIKV in Kenya (left) and the IFN-I-mediated restriction of African and American ZIKV strains (right). The main findings from this thesis and corresponding chapters are listed in blue at the bottom of each section.

Low burden of ZIKV infections in urban centers in Kenya

In Chapter II, we identified low seroprevalence of ZIKV (0.5-1.6%) from cohorts in two densely populated urban centers in Kenya. The durability of the binding and neutralizing antibody responses against ZIKV over long time periods is not well known. In Chapter II, we identified one ZIKV-infected subject who had a durable nAb response against ZIKV over a 10-year period. However, it is possible that such a durable nAb response is not a common feature of the antibody response to ZIKV infection and instead the response waned overtime is a subset or most ZIKV-infected individuals. If this is the case, we and others (58, 60, 61) would be underestimating ZIKV exposure in these regions. Future studies utilizing samples from pediatric cohorts in Africa can address if there is a difference in ZIKV seroprevalence in age groups perhaps due to binding or neutralizing antibody waning, although this does not appear to be the case at least in pediatric cohorts in Central Africa (63). Nonetheless, given that ZIKV appears to be present at low levels in large population centers in Kenya, our study highlights the need for continued arboviral surveillance and improved platforms for arboviral detection.

As discussed in Chapter I, the gold standard for detection of ZIKV infection (as well as infection with many viruses) is molecular detection of viral RNA. In addition to the convalescent samples outlined in Chapter II, plasma was collected from each included subject at/closest to the time of febrile illness (“acute sample”), when there is the highest likelihood of capturing viral RNA. Future work to detect and amplify viral RNA from these samples will add to and broaden our serological studies in Chapter II. This can be carried out in a multiplex method for simultaneous detection of RNA from multiple viruses (i.e. ZIKV, DENV, CHIKV) using validated qRT-PCR methods (197) or by leveraging collaborations with the Blood Systems Research Institute (BSRI), who is currently implementing a multiplex Aptima assay similar to the highly-sensitive Hologic Aptima ZIKV assay that is capable of detecting both Asian and African ZIKV strains (198). For samples where ZIKV RNA is detected by the Aptima test, coding-sequencing-complete genomes can be generated by utilizing a multiplex PCR-viral genome enrichment

strategy coupled with Illumina sequencing developed in-part by the Bedford lab (158). If ZIKV RNA is detected, amplified, and sequenced in acute plasma, the findings will allow for the first phylogenetic characterization of circulating ZIKV sub-lineages in humans in Kenya.

Finally, future studies examining ZIKV pathogenesis on the African continent will better define the impact of ZIKV circulation in this region. In fact, a group who recently published their findings of continuous ZIKV circulation in West Africa (25) is currently leading an prospective cohort study to examine the prevalence of ZIKV (as well as DENV and CHIKV) in pregnant women and the pathologic risks imparted to infants born to ZIKV-infected women in north-central Nigeria (199).

Towards improved detection of ZIKV infections

The design and preliminary validation of PhIP-Seq as a tool to detect ZIKV infections in plasma samples was presented in Chapter III. In Chapter III, PhIP-Seq was tested with non-human primate sera. To determine the capacity of PhIP-seq to discriminate ZIKV infections from other flavivirus infections, a larger panel of control human sera that are ZIKV-infected, DENV-infected, or flavivirus-naïve has been assembled (Table 3.2) and tested in PhIP-seq. Novel bioinformatics approaches that account for the high dimensionality of this dataset are needed to accomplish this task. This panel is still lacking in non-ZIKV flavivirus-infected samples, which are critical in determining the discriminatory capacity of PhIP-Seq. Collaborations with the laboratory of Dr. William Messer at OHSU, who runs a travel-associated infection cohort, may allow us to access these sample types. The samples we have characterized from our studies of Kenyan cohorts in Chapter II will also be a valuable set of plasma to include in future PhIP-seq experiments.

Finally, the ability of PhIP-Seq to epitope map monoclonal antibodies has been further advanced by another graduate student in the Overbaugh lab with the development of Phage-Deep Mutational Scanning (Phage-DMS). This approach surveys mAb preference of all twenty

amino acids at each position along its epitope, enabling more fine-scale epitope mapping as compared to the HIV mAb epitope mapping efforts described in Chapter II.

The role of the type-I IFN response in the restriction of diverse ZIKV strains

In Chapter IV, we discovered that the restriction mediated by IFN-I varied by viral lineage. As discussed in detail in Chapter IV, this was initially surprising given that African-lineage viruses are not associated with the severe neuropathologic outcomes linked to infection with Asian-lineage strains. However, our findings in Chapter IV, when taken together with several studies that have found that infection with African-lineage strains results in enhanced replication kinetics, virus production, cytopathicity, and disease progression in murine models (75-88), suggests a potential model where Asian-lineage strains may be better able to establish chronic infection of neural progenitor cells, undergo more efficient vertical transmission, and establish viral reservoirs in the central nervous system, lymph nodes, and gastrointestinal and genitourinary tracts (84, 89-92) (Figure 6.2). Our understanding of this model would be further strengthened by future studies with larger numbers of low-passage ZIKV strains from both viral lineages.

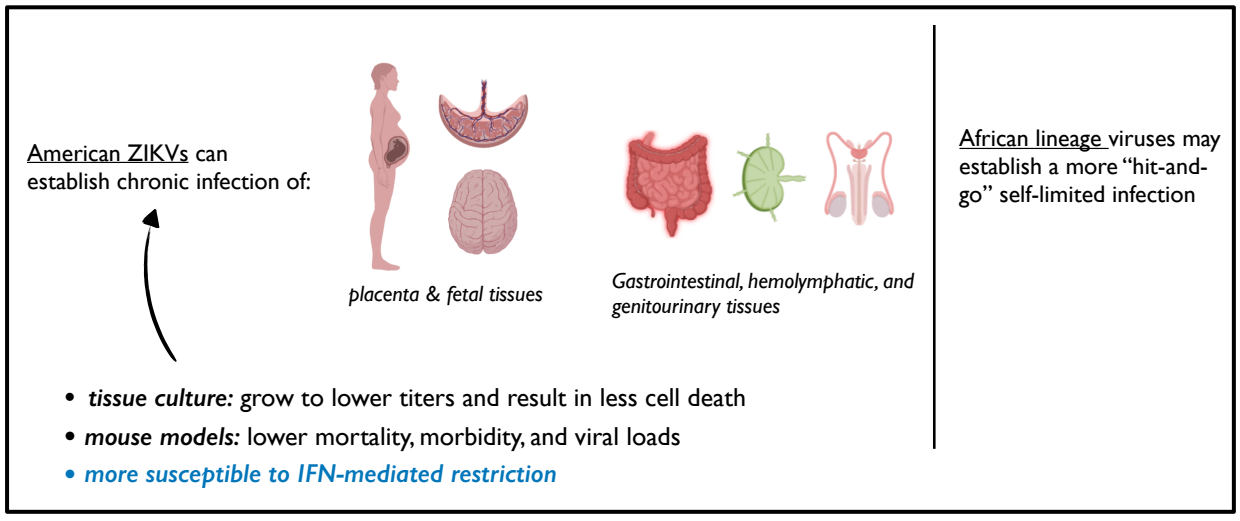

Figure 6.2. A potential model of African- vs. Asian-lineage viral characteristics and their relevance to differential infection outcomes.

Defining ISGs that inhibit ZIKV

In Chapter IV, we examined the contribution of IFITM3 to the IFN-I response against highly IFN-sensitive ZIKV strains. We found that IFITM3 was only active against ZIKV when overexpressed above levels induced by IFN-I in A549 cells. Further, our findings suggest that IFITM3 also does not play a role in cell types relevant to the vertical transmission and neuropathogenesis of ZIKV associated with infections in the American outbreak. This serves a cautionary tale when interpreting studies that describe restriction factors in the context of overexpression (Table 1.2). Ongoing studies in the Overbaugh lab are examining the contribution of other the reported ZIKV-restricting ISGs to the overall IFN-I response against ZIKV in A549 cells. PARP12 is particularly interesting in this respect, as it was discovered in a targeted knockout screen in A549 cells (114).

In Chapter V, we describe a CRISPR-knockout based ZIKV ISG screen where ~2,000 ISGs are surveyed. Our data from three screens highlight both the promise and potential challenges of this screening approach. Importantly, we have identified genes to target and validate in single knock-out cell lines using validated approaches discussed throughout this thesis (E-protein staining, $TCID_{50}$) as well as new approaches that are in development in the Overbaugh lab (ZIKV RNA quantification (200)). Importantly, ZIKV-restricting ISGs discovered in future endeavors with this screening platform may have activity against other related flaviviruses (i.e., DENV, YFV, WNV) that cause a significant global burden of disease. There are a number of genes that are also depleted in the screens we have completed to date, which may hold clues as to important host/dependency factors for ZIKV infection. Further, this screen is likely adaptable to other important unrelated cytopathic viruses, such as cytomegalovirus, influenza, or vesicular stomatitis virus, as well as in other cell lines that succumb to ZIKV-induced cell death.

Conclusion

By examining both the population-level immunity to ZIKV in Kenya and the role of a critical antiviral response in its restriction, we have not only made important insights into the susceptibility of populations in East Africa where ZIKV was discovered and is thought to be endemic, but also describe differences in basic virologic characteristics of ZIKV strains that circulate in the Americas and Africa. Further, the methods described in this thesis will enable more detailed and high-throughput studies of ZIKV seroepidemiology and IFN-I-mediated restriction in the future.

References

1. Lowe R, Barcellos C, Brasil P, Cruz OG, Honorio NA, Kuper H, Carvalho MS. The Zika Virus Epidemic in Brazil: From Discovery to Future Implications. Int J Environ Res Public Health. 2018;15(1). Epub 2018/01/10. doi: 10.3390/ijerph15010096. PubMed PMID: 29315224; PMCID: PMC5800195.
2. Heukelbach J, Alencar CH, Kelvin AA, de Oliveira WK, Pamplona de Goes Cavalcanti L. Zika virus outbreak in Brazil. J Infect Dev Ctries. 2016;10(2):116-20. Epub 2016/03/02. doi: 10.3855/jidc.8217. PubMed PMID: 26927450.
3. Campos GS, Bandeira AC, Sardi SI. Zika Virus Outbreak, Bahia, Brazil. Emerg Infect Dis. 2015;21(10):1885-6. Epub 2015/09/25. doi: 10.3201/eid2110.150847. PubMed PMID: 26401719; PMCID: PMC4593454.
4. Cardoso CW, Paploski IA, Kikuti M, Rodrigues MS, Silva MM, Campos GS, Sardi SI, Kitron U, Reis MG, Ribeiro GS. Outbreak of Exanthematous Illness Associated with Zika, Chikungunya, and Dengue Viruses, Salvador, Brazil. Emerg Infect Dis. 2015;21(12):2274-6. Epub 2015/11/20. doi: 10.3201/eid2112.151167. PubMed PMID: 26584464; PMCID: PMC4672408.
5. Zanluca C, Melo VC, Mosimann AL, Santos GI, Santos CN, Luz K. First report of autochthonous transmission of Zika virus in Brazil. Mem Inst Oswaldo Cruz. 2015;110(4):569-72. Epub 2015/06/11. doi: 10.1590/0074-02760150192. PubMed PMID: 26061233; PMCID: PMC4501423.
6. Musso D, Gubler DJ. Zika Virus. Clin Microbiol Rev. 2016;29(3):487-524. Epub 2016/04/01. doi: 10.1128/CMR.00072-15. PubMed PMID: 27029595; PMCID: PMC4861986.
7. Willison HJ, Jacobs BC, van Doorn PA. Guillain-Barre syndrome. Lancet. 2016;388(10045):717-27. Epub 2016/03/08. doi: 10.1016/S0140-6736(16)00339-1. PubMed PMID: 26948435.
8. Teixeira MG, Costa Mda C, de Oliveira WK, Nunes ML, Rodrigues LC. The Epidemic of Zika Virus-Related Microcephaly in Brazil: Detection, Control, Etiology, and Future Scenarios. Am J Public Health. 2016;106(4):601-5. Epub 2016/03/10. doi: 10.2105/AJPH.2016.303113. PubMed PMID: 26959259; PMCID: PMC4816003.
9. World Health Organization. Situation report: Zika virus microcephaly Guillain-Barré syndrome World Health Organization2017 [updated 20 Janurary 2017; cited 2018 25 March 2018]. Available from: http://apps.who.int/iris/bitstream/10665/253604/1/zikasitrep20Jan17-eng.pdf?ua=1.
10. Musso D, Ko AI, Baud D. Zika Virus Infection - After the Pandemic. N Engl J Med. 2019;381(15):1444-57. Epub 2019/10/10. doi: 10.1056/NEJMra1808246. PubMed PMID: 31597021.
11. Hills SL, Fischer M, Petersen LR. Epidemiology of Zika Virus Infection. J Infect Dis. 2017;216(suppl_10):S868-S74. Epub 2017/12/22. doi: 10.1093/infdis/jix434. PubMed PMID: 29267914; PMCID: PMC5853392.
12. Affairs USDoS-BoC. Zika Virus Information for Travelers2018. Epub August 16, 2018.
13. Pomar L, Vouga M, Lambert V, Pomar C, Hcini N, Jolivet A, Benoist G, Rousset D, Matheus S, Malinger G, Panchaud A, Carles G, Baud D. Maternal-fetal transmission and

adverse perinatal outcomes in pregnant women infected with Zika virus: prospective cohort study in French Guiana. BMJ. 2018;363:k4431. Epub 2018/11/02. doi: 10.1136/bmj.k4431. PubMed PMID: 30381296; PMCID: PMC6207920 at www.icmje.org/coi_disclosure.pdf (available on request from the corresponding author) and declare: no support from any organisation for the submitted work; no financial relationships with any organisations that might have an interest in the submitted work in the previous three years; no other relationships or activities that could appear to have influenced the submitted work.

14. Rice ME, Galang RR, Roth NM, Ellington SR, Moore CA, Valencia-Prado M, Ellis EM, Tufa AJ, Taulung LA, Alfred JM, Perez-Padilla J, Delgado-Lopez CA, Zaki SR, Reagan-Steiner S, Bhatnagar J, Nahabedian JF, 3rd, Reynolds MR, Yeargin-Allsopp M, Viens LJ, Olson SM, Jones AM, Baez-Santiago MA, Oppong-Twene P, VanMaldeghem K, Simon EL, Moore JT, Polen KD, Hillman B, Ropeti R, Nieves-Ferrer L, Marcano-Huertas M, Masao CA, Anzures EJ, Hansen RL, Jr., Perez-Gonzalez SI, Espinet-Crespo CP, Luciano-Roman M, Shapiro-Mendoza CK, Gilboa SM, Honein MA. Vital Signs: Zika-Associated Birth Defects and Neurodevelopmental Abnormalities Possibly Associated with Congenital Zika Virus Infection - U.S. Territories and Freely Associated States, 2018. MMWR Morb Mortal Wkly Rep. 2018;67(31):858-67. Epub 2018/08/10. doi: 10.15585/mmwr.mm6731e1. PubMed PMID: 30091967; PMCID: PMC6089332.

15. van der Linden V, Pessoa A, Dobyns W, Barkovich AJ, Junior HV, Filho EL, Ribeiro EM, Leal MC, Coimbra PP, Aragao MF, Vercosa I, Ventura C, Ramos RC, Cruz DD, Cordeiro MT, Mota VM, Dott M, Hillard C, Moore CA. Description of 13 Infants Born During October 2015-January 2016 With Congenital Zika Virus Infection Without Microcephaly at Birth - Brazil. MMWR Morb Mortal Wkly Rep. 2016;65(47):1343-8. Epub 2016/12/03. doi: 10.15585/mmwr.mm6547e2. PubMed PMID: 27906905.

16. Ventura CV, Ventura LO. Ophthalmologic Manifestations Associated With Zika Virus Infection. Pediatrics. 2018;141(Suppl 2):S161-S6. Epub 2018/02/14. doi: 10.1542/peds.2017-2038E. PubMed PMID: 29437049; PMCID: PMC5795515 conflicts of interest to disclose.

17. Duffy MR, Chen TH, Hancock WT, Powers AM, Kool JL, Lanciotti RS, Pretrick M, Marfel M, Holzbauer S, Dubray C, Guillaumot L, Griggs A, Bel M, Lambert AJ, Laven J, Kosoy O, Panella A, Biggerstaff BJ, Fischer M, Hayes EB. Zika virus outbreak on Yap Island, Federated States of Micronesia. N Engl J Med. 2009;360(24):2536-43. Epub 2009/06/12. doi: 10.1056/NEJMoa0805715. PubMed PMID: 19516034.

18. Cao-Lormeau VM, Roche C, Teissier A, Robin E, Berry AL, Mallet HP, Sall AA, Musso D. Zika virus, French polynesia, South pacific, 2013. Emerg Infect Dis. 2014;20(6):1085-6. Epub 2014/05/27. doi: 10.3201/eid2006.140138. PubMed PMID: 24856001; PMCID: PMC4036769.

19. Musso D, Roche C, Nhan TX, Robin E, Teissier A, Cao-Lormeau VM. Detection of Zika virus in saliva. J Clin Virol. 2015;68:53-5. Epub 2015/06/14. doi: 10.1016/j.jcv.2015.04.021. PubMed PMID: 26071336.

20. Faria NR, Quick J, Claro IM, Theze J, de Jesus JG, Giovanetti M, Kraemer MUG, Hill SC, Black A, da Costa AC, Franco LC, Silva SP, Wu CH, Raghwani J, Cauchemez S, du Plessis L, Verotti MP, de Oliveira WK, Carmo EH, Coelho GE, Santelli A, Vinhal LC, Henriques CM, Simpson JT, Loose M, Andersen KG, Grubaugh ND, Somasekar S, Chiu CY, Munoz-Medina JE, Gonzalez-Bonilla CR, Arias CF, Lewis-Ximenez LL, Baylis SA, Chieppe AO, Aguiar SF, Fernandes CA, Lemos PS, Nascimento BLS, Monteiro HAO,

Siqueira IC, de Queiroz MG, de Souza TR, Bezerra JF, Lemos MR, Pereira GF, Loudal D, Moura LC, Dhalia R, Franca RF, Magalhaes T, Marques ET, Jr., Jaenisch T, Wallau GL, de Lima MC, Nascimento V, de Cerqueira EM, de Lima MM, Mascarenhas DL, Neto JPM, Levin AS, Tozetto-Mendoza TR, Fonseca SN, Mendes-Correa MC, Milagres FP, Segurado A, Holmes EC, Rambaut A, Bedford T, Nunes MRT, Sabino EC, Alcantara LCJ, Loman NJ, Pybus OG. Establishment and cryptic transmission of Zika virus in Brazil and the Americas. Nature. 2017;546(7658):406-10. Epub 2017/05/26. doi: 10.1038/nature22401. PubMed PMID: 28538727; PMCID: PMC5722632.

21. Dick GW, Kitchen SF, Haddow AJ. Zika virus. I. Isolations and serological specificity. Trans R Soc Trop Med Hyg. 1952;46(5):509-20. Epub 1952/09/01. doi: 10.1016/0035-9203(52)90042-4. PubMed PMID: 12995440.

22. Macnamara FN. Zika virus: a report on three cases of human infection during an epidemic of jaundice in Nigeria. Trans R Soc Trop Med Hyg. 1954;48(2):139-45. Epub 1954/03/01. doi: 10.1016/0035-9203(54)90006-1. PubMed PMID: 13157159.

23. Fagbami AH. Zika virus infections in Nigeria: virological and seroepidemiological investigations in Oyo State. J Hyg (Lond). 1979;83(2):213-9. PubMed PMID: 489960; PMCID: PMC2129900.

24. Faye O, Freire CC, Iamarino A, Faye O, de Oliveira JV, Diallo M, Zanotto PM, Sall AA. Molecular evolution of Zika virus during its emergence in the 20(th) century. PLoS Negl Trop Dis. 2014;8(1):e2636. doi: 10.1371/journal.pntd.0002636. PubMed PMID: 24421913; PMCID: PMC3888466.

25. Herrera BB, Chang CA, Hamel DJ, Mboup S, Ndiaye D, Imade G, Okpokwu J, Agbaji O, Bei AK, Kanki PJ. Continued Transmission of Zika Virus in Humans in West Africa, 1992-2016. J Infect Dis. 2017;215(10):1546-50. doi: 10.1093/infdis/jix182. PubMed PMID: 28398562.

26. Moore DL, Causey OR, Carey DE, Reddy S, Cooke AR, Akinkugbe FM, David-West TS, Kemp GE. Arthropod-borne viral infections of man in Nigeria, 1964-1970. Ann Trop Med Parasitol. 1975;69(1):49-64. PubMed PMID: 1124969.

27. Simpson DI. Zika Virus Infection in Man. Trans R Soc Trop Med Hyg. 1964;58:335-8. PubMed PMID: 14175744.

28. Meda N, Salinas S, Kagone T, Simonin Y, Van de Perre P. Zika virus epidemic: Africa should not be neglected. Lancet. 2016;388(10042):337-8. doi: 10.1016/S0140-6736(16)31103-5. PubMed PMID: 27477155.

29. Nutt C, Adams P. Zika in Africa-the invisible epidemic? Lancet. 2017;389(10079):1595-6. doi: 10.1016/S0140-6736(17)31051-6. PubMed PMID: 28593839.

30. Wetsman N. The missing pieces: Lack of Zika data from Africa complicates search for answers. Nat Med. 2017;23(8):904-6. doi: 10.1038/nm0817-904. PubMed PMID: 28777794.

31. Robinson ML, Manabe YC. Reducing Uncertainty for Acute Febrile Illness in Resource-Limited Settings: The Current Diagnostic Landscape. Am J Trop Med Hyg. 2017;96(6):1285-95. doi: 10.4269/ajtmh.16-0667. PubMed PMID: 28719277; PMCID: PMC5462561.

32. Goncalves A, Peeling RW, Chu MC, Gubler DJ, de Silva AM, Harris E, Murtagh M, Chua A, Rodriguez W, Kelly C, Wilder-Smith A. Innovative and New Approaches to Laboratory

Diagnosis of Zika and Dengue: A Meeting Report. J Infect Dis. 2018;217(7):1060-8. Epub 2018/01/03. doi: 10.1093/infdis/jix678. PubMed PMID: 29294035; PMCID: PMC6279137.

33. van Boheemen S, Tas A, Anvar SY, van Grootveld R, Albulescu IC, Bauer MP, Feltkamp MC, Bredenbeek PJ, van Hemert MJ. Quasispecies composition and evolution of a typical Zika virus clinical isolate from Suriname. Sci Rep. 2017;7(1):2368. Epub 2017/05/26. doi: 10.1038/s41598-017-02652-w. PubMed PMID: 28539654; PMCID: PMC5443807.

34. Paz-Bailey G, Rosenberg ES, Doyle K, Munoz-Jordan J, Santiago GA, Klein L, Perez-Padilla J, Medina FA, Waterman SH, Gubern CG, Alvarado LI, Sharp TM. Persistence of Zika Virus in Body Fluids - Preliminary Report. N Engl J Med. 2017. doi: 10.1056/NEJMoa1613108. PubMed PMID: 28195756.

35. Ngono AE, Shresta S. Immune Response to Dengue and Zika. Annu Rev Immunol. 2018;36:279-308. Epub 2018/01/19. doi: 10.1146/annurev-immunol-042617-053142. PubMed PMID: 29345964; PMCID: PMC5910217.

36. Pierson TC, Fremont DH, Kuhn RJ, Diamond MS. Structural insights into the mechanisms of antibody-mediated neutralization of flavivirus infection: implications for vaccine development. Cell Host Microbe. 2008;4(3):229-38. Epub 2008/09/10. doi: 10.1016/j.chom.2008.08.004. PubMed PMID: 18779049; PMCID: PMC2678546.

37. Tonnerre P, Melgaco JG, Torres-Cornejo A, Pinto MA, Yue C, Blumel J, de Sousa PSF, de Mello VDM, Moran J, de Filippis AMB, Wolski D, Grifoni A, Sette A, Barouch DH, Hoogeveen RC, Baylis SA, Lauer GM, Lewis-Ximenez LL. Evolution of the innate and adaptive immune response in women with acute Zika virus infection. Nat Microbiol. 2020;5(1):76-83. Epub 2019/12/04. doi: 10.1038/s41564-019-0618-z. PubMed PMID: 31792427.

38. Munoz-Jordan JL. Diagnosis of Zika Virus Infections: Challenges and Opportunities. J Infect Dis. 2017;216(suppl_10):S951-S6. doi: 10.1093/infdis/jix502. PubMed PMID: 29267922.

39. Rabe IB, Staples JE, Villanueva J, Hummel KB, Johnson JA, Rose L, Mts, Hills S, Wasley A, Fischer M, Powers AM. Interim Guidance for Interpretation of Zika Virus Antibody Test Results. MMWR Morb Mortal Wkly Rep. 2016;65(21):543-6. doi: 10.15585/mmwr.mm6521e1. PubMed PMID: 27254248.

40. Ricciardi MJ, Magnani DM, Grifoni A, Kwon YC, Gutman MJ, Grubaugh ND, Gangavarapu K, Sharkey M, Silveira CGT, Bailey VK, Pedreno-Lopez N, Gonzalez-Nieto L, Maxwell HS, Domingues A, Martins MA, Pham J, Weiskopf D, Altman J, Kallas EG, Andersen KG, Stevenson M, Lichtenberger P, Choe H, Whitehead SS, Sette A, Watkins DI. Ontogeny of the B- and T-cell response in a primary Zika virus infection of a dengue-naive individual during the 2016 outbreak in Miami, FL. PLoS Negl Trop Dis. 2017;11(12):e0006000. doi: 10.1371/journal.pntd.0006000. PubMed PMID: 29267278; PMCID: PMC5755934.

41. Busch MP, Kleinman SH, Tobler LH, Kamel HT, Norris PJ, Walsh I, Matud JL, Prince HE, Lanciotti RS, Wright DJ, Linnen JM, Caglioti S. Virus and antibody dynamics in acute west nile virus infection. J Infect Dis. 2008;198(7):984-93. doi: 10.1086/591467. PubMed PMID: 18729783.

42. Manz RA, Hauser AE, Hiepe F, Radbruch A. Maintenance of serum antibody levels. Annu Rev Immunol. 2005;23:367-86. doi: 10.1146/annurev.immunol.23.021704.115723. PubMed PMID: 15771575.

43. Dowd KA, DeMaso CR, Pelc RS, Speer SD, Smith ARY, Goo L, Platt DJ, Mascola JR, Graham BS, Mulligan MJ, Diamond MS, Ledgerwood JE, Pierson TC. Broadly Neutralizing Activity of Zika Virus-Immune Sera Identifies a Single Viral Serotype. Cell Rep. 2016;16(6):1485-91. Epub 2016/08/03. doi: 10.1016/j.celrep.2016.07.049. PubMed PMID: 27481466; PMCID: PMC5004740.

44. Robbiani DF, Bozzacco L, Keeffe JR, Khouri R, Olsen PC, Gazumyan A, Schaefer-Babajew D, Avila-Rios S, Nogueira L, Patel R, Azzopardi SA, Uhl LFK, Saeed M, Sevilla-Reyes EE, Agudelo M, Yao KH, Golijanin J, Gristick HB, Lee YE, Hurley A, Caskey M, Pai J, Oliveira T, Wunder EA, Jr., Sacramento G, Nery N, Jr., Orge C, Costa F, Reis MG, Thomas NM, Eisenreich T, Weinberger DM, de Almeida ARP, West AP, Jr., Rice CM, Bjorkman PJ, Reyes-Teran G, Ko AI, MacDonald MR, Nussenzweig MC. Recurrent Potent Human Neutralizing Antibodies to Zika Virus in Brazil and Mexico. Cell. 2017;169(4):597-609 e11. Epub 2017/05/06. doi: 10.1016/j.cell.2017.04.024. PubMed PMID: 28475892; PMCID: PMC5492969.

45. Robbiani DF, Olsen PC, Costa F, Wang Q, Oliveira TY, Nery N, Jr., Aromolaran A, do Rosario MS, Sacramento GA, Cruz JS, Khouri R, Wunder EA, Jr., Mattos A, de Paula Freitas B, Sarno M, Archanjo G, Daltro D, Carvalho GBS, Pimentel K, de Siqueira IC, de Almeida JRM, Henriques DF, Lima JA, Vasconcelos PFC, Schaefer-Babajew D, Azzopardi SA, Bozzacco L, Gazumyan A, Belfort R, Jr., Alcantara AP, Carvalho G, Moreira L, Araujo K, Reis MG, Keesler RI, Coffey LL, Tisoncik-Go J, Gale M, Jr., Rajagopal L, Adams Waldorf KM, Dudley DM, Simmons HA, Mejia A, O'Connor DH, Steinbach RJ, Haese N, Smith J, Lewis A, Colgin L, Roberts V, Frias A, Kelleher M, Hirsch A, Streblow DN, Rice CM, MacDonald MR, de Almeida ARP, Van Rompay KKA, Ko AI, Nussenzweig MC. Risk of Zika microcephaly correlates with features of maternal antibodies. J Exp Med. 2019;216(10):2302-15. Epub 2019/08/16. doi: 10.1084/jem.20191061. PubMed PMID: 31413072; PMCID: PMC6781003.

46. Mukherjee S, Pierson TC, Dowd KA. Pseudo-infectious reporter virus particles for measuring antibody-mediated neutralization and enhancement of dengue virus infection. Methods Mol Biol. 2014;1138:75-97. Epub 2014/04/04. doi: 10.1007/978-1-4939-0348-1_6. PubMed PMID: 24696332.

47. Wahala WM, Silva AM. The human antibody response to dengue virus infection. Viruses. 2011;3(12):2374-95. doi: 10.3390/v3122374. PubMed PMID: 22355444; PMCID: PMC3280510.

48. Heinz FX, Stiasny K. The Antigenic Structure of Zika Virus and Its Relation to Other Flaviviruses: Implications for Infection and Immunoprophylaxis. Microbiol Mol Biol Rev. 2017;81(1). Epub 2017/02/10. doi: 10.1128/MMBR.00055-16. PubMed PMID: 28179396; PMCID: PMC5312239.

49. Kostyuchenko VA, Lim EX, Zhang S, Fibriansah G, Ng TS, Ooi JS, Shi J, Lok SM. Structure of the thermally stable Zika virus. Nature. 2016;533(7603):425-8. Epub 2016/04/20. doi: 10.1038/nature17994. PubMed PMID: 27093288.

50. Barba-Spaeth G, Dejnirattisai W, Rouvinski A, Vaney MC, Medits I, Sharma A, Simon-Loriere E, Sakuntabhai A, Cao-Lormeau VM, Haouz A, England P, Stiasny K, Mongkolsapaya J, Heinz FX, Screaton GR, Rey FA. Structural basis of potent Zika-dengue virus antibody cross-neutralization. Nature. 2016;536(7614):48-53. Epub 2016/06/25. doi: 10.1038/nature18938. PubMed PMID: 27338953.

51. Dejnirattisai W, Wongwiwat W, Supasa S, Zhang X, Dai X, Rouvinski A, Jumnainsong A, Edwards C, Quyen NTH, Duangchinda T, Grimes JM, Tsai WY, Lai CY, Wang WK,

Malasit P, Farrar J, Simmons CP, Zhou ZH, Rey FA, Mongkolsapaya J, Screaton GR. A new class of highly potent, broadly neutralizing antibodies isolated from viremic patients infected with dengue virus. Nat Immunol. 2015;16(2):170-7. Epub 2014/12/17. doi: 10.1038/ni.3058. PubMed PMID: 25501631; PMCID: PMC4445969.

52. Priyamvada L, Quicke KM, Hudson WH, Onlamoon N, Sewatanon J, Edupuganti S, Pattanapanyasat K, Chokephaibulkit K, Mulligan MJ, Wilson PC, Ahmed R, Suthar MS, Wrammert J. Human antibody responses after dengue virus infection are highly cross-reactive to Zika virus. Proc Natl Acad Sci U S A. 2016;113(28):7852-7. Epub 2016/06/30. doi: 10.1073/pnas.1607931113. PubMed PMID: 27354515; PMCID: PMC4948328.

53. Swanstrom JA, Plante JA, Plante KS, Young EF, McGowan E, Gallichotte EN, Widman DG, Heise MT, de Silva AM, Baric RS. Dengue Virus Envelope Dimer Epitope Monoclonal Antibodies Isolated from Dengue Patients Are Protective against Zika Virus. MBio. 2016;7(4). Epub 2016/07/21. doi: 10.1128/mBio.01123-16. PubMed PMID: 27435464; PMCID: PMC4958264.

54. Collins MH, McGowan E, Jadi R, Young E, Lopez CA, Baric RS, Lazear HM, de Silva AM. Lack of Durable Cross-Neutralizing Antibodies Against Zika Virus from Dengue Virus Infection. Emerg Infect Dis. 2017;23(5):773-81. Epub 2017/04/19. doi: 10.3201/eid2305.161630. PubMed PMID: 28418292; PMCID: PMC5403059.

55. Montoya M, Collins M, Dejnirattisai W, Katzelnick LC, Puerta-Guardo H, Jadi R, Schildhauer S, Supasa P, Vasanawathana S, Malasit P, Mongkolsapaya J, de Silva AD, Tissera H, Balmaseda A, Screaton G, de Silva AM, Harris E. Longitudinal Analysis of Antibody Cross-neutralization Following Zika Virus and Dengue Virus Infection in Asia and the Americas. J Infect Dis. 2018;218(4):536-45. Epub 2018/04/05. doi: 10.1093/infdis/jiy164. PubMed PMID: 29618091; PMCID: PMC6047418.

56. Balmaseda A, Stettler K, Medialdea-Carrera R, Collado D, Jin X, Zambrana JV, Jaconi S, Cameroni E, Saborio S, Rovida F, Percivalle E, Ijaz S, Dicks S, Ushiro-Lumb I, Barzon L, Siqueira P, Brown DWG, Baldanti F, Tedder R, Zambon M, de Filippis AMB, Harris E, Corti D. Antibody-based assay discriminates Zika virus infection from other flaviviruses. Proc Natl Acad Sci U S A. 2017;114(31):8384-9. doi: 10.1073/pnas.1704984114. PubMed PMID: 28716913; PMCID: PMC5547631.

57. Slon Campos JL, Mongkolsapaya J, Screaton GR. The immune response against flaviviruses. Nat Immunol. 2018;19(11):1189-98. Epub 2018/10/20. doi: 10.1038/s41590-018-0210-3. PubMed PMID: 30333606.

58. Chepkorir E, Tchouassi DP, Konongoi SL, Lutomiah J, Tigoi C, Irura Z, Eyase F, Venter M, Sang R. Serological evidence of Flavivirus circulation in human populations in Northern Kenya: an assessment of disease risk 2016-2017. Virol J. 2019;16(1):65. Epub 2019/05/19. doi: 10.1186/s12985-019-1176-y. PubMed PMID: 31101058; PMCID: PMC6525424.

59. Kayiwa JT, Nankya AM, Ataliba IJ, Mossel EC, Crabtree MB, Lutwama JJ. Confirmation of Zika virus infection through hospital-based sentinel surveillance of acute febrile illness in Uganda, 2014-2017. J Gen Virol. 2018;99(9):1248-52. Epub 2018/07/06. doi: 10.1099/jgv.0.001113. PubMed PMID: 29975185.

60. Kisuya B, Masika MM, Bahizire E, Oyugi JO. Seroprevalence of Zika virus in selected regions in Kenya. Trans R Soc Trop Med Hyg. 2019;113(12):735-9. Epub 2019/10/23. doi: 10.1093/trstmh/trz077. PubMed PMID: 31639184.

61. Mengesha Tsegaye M, Beyene B, Ayele W, Abebe A, Tareke I, Sall A, Yactayo S, Shibeshi ME, Staples E, Belay D, Lilay A, Alemu A, Alemu E, Kume A, A HM, Ronveaux O, Tefera M, Kassa W, Bekele Weyessa A, Jima D, Kebede A, Tayachew A. Sero-prevalence of yellow fever and related Flavi viruses in Ethiopia: a public health perspective. BMC Public Health. 2018;18(1):1011. Epub 2018/08/16. doi: 10.1186/s12889-018-5726-9. PubMed PMID: 30107830; PMCID: PMC6092792.

62. Soghaier MA, Abdelgadir DM, Abdelkhalig SM, Kafi H, Zarroug IMA, Sall AA, Eldegai MH, Elageb RM, Osman MM, Khogali H. Evidence of pre-existing active Zika virus circulation in Sudan prior to 2012. BMC Res Notes. 2018;11(1):906. Epub 2018/12/21. doi: 10.1186/s13104-018-4027-9. PubMed PMID: 30567583; PMCID: PMC6299991.

63. Willcox AC, Collins MH, Jadi R, Keeler C, Parr JB, Mumba D, Kashamuka M, Tshefu A, de Silva AM, Meshnick SR. Seroepidemiology of Dengue, Zika, and Yellow Fever Viruses among Children in the Democratic Republic of the Congo. Am J Trop Med Hyg. 2018;99(3):756-63. Epub 2018/07/11. doi: 10.4269/ajtmh.18-0156. PubMed PMID: 29988000; PMCID: PMC6169194.

64. Ellis EM, Neatherlin JC, Delorey M, Ochieng M, Mohamed AH, Mogeni DO, Hunsperger E, Patta S, Gikunju S, Waiboic L, Fields B, Ofula V, Konongoi SL, Torres-Velasquez B, Marano N, Sang R, Margolis HS, Montgomery JM, Tomashek KM. A household serosurvey to estimate the magnitude of a dengue outbreak in Mombasa, Kenya, 2013. PLoS Negl Trop Dis. 2015;9(4):e0003733. Epub 2015/04/30. doi: 10.1371/journal.pntd.0003733. PubMed PMID: 25923210; PMCID: PMC4414477.

65. Kariuki Njenga M, Nderitu L, Ledermann JP, Ndirangu A, Logue CH, Kelly CH, Sang R, Sergon K, Breiman R, Powers AM. Tracking epidemic Chikungunya virus into the Indian Ocean from East Africa. J Gen Virol. 2008;89(Pt 11):2754-60. Epub 2008/10/22. doi: 10.1099/vir.0.2008/005413-0. PubMed PMID: 18931072; PMCID: PMC3347796.

66. Ndenga BA, Mutuku FM, Ngugi HN, Mbakaya JO, Aswani P, Musunzaji PS, Vulule J, Mukoko D, Kitron U, LaBeaud AD. Characteristics of Aedes aegypti adult mosquitoes in rural and urban areas of western and coastal Kenya. PLoS One. 2017;12(12):e0189971. Epub 2017/12/21. doi: 10.1371/journal.pone.0189971. PubMed PMID: 29261766; PMCID: PMC5736227.

67. McClelland RS, Richardson BA, Cherutich P, Mandaliya K, John-Stewart G, Miregwa B, Odem-Davis K, Jaoko W, Kimanga D, Overbaugh J. A 15-year study of the impact of community antiretroviral therapy coverage on HIV incidence in Kenyan female sex workers. AIDS. 2015;29(17):2279-86. Epub 2015/08/04. doi: 10.1097/QAD.0000000000000829. PubMed PMID: 26237099; PMCID: PMC4640974.

68. Kinuthia J, Drake AL, Matemo D, Richardson BA, Zeh C, Osborn L, Overbaugh J, McClelland RS, John-Stewart G. HIV acquisition during pregnancy and postpartum is associated with genital infections and partnership characteristics. AIDS. 2015;29(15):2025-33. Epub 2015/09/10. doi: 10.1097/QAD.0000000000000793. PubMed PMID: 26352880; PMCID: PMC4692052.

69. Wang L, Valderramos SG, Wu A, Ouyang S, Li C, Brasil P, Bonaldo M, Coates T, Nielsen-Saines K, Jiang T, Aliyari R, Cheng G. From Mosquitos to Humans: Genetic Evolution of Zika Virus. Cell Host Microbe. 2016;19(5):561-5. Epub 2016/04/20. doi: 10.1016/j.chom.2016.04.006. PubMed PMID: 27091703; PMCID: PMC5648540.

70. Hu T, Li J, Carr MJ, Duchene S, Shi W. The Asian Lineage of Zika Virus: Transmission and Evolution in Asia and the Americas. Virol Sin. 2019;34(1):1-8. Epub 2019/01/27. doi: 10.1007/s12250-018-0078-2. PubMed PMID: 30684211; PMCID: PMC6420435.

71. Liu Y, Liu J, Du S, Shan C, Nie K, Zhang R, Li XF, Zhang R, Wang T, Qin CF, Wang P, Shi PY, Cheng G. Evolutionary enhancement of Zika virus infectivity in Aedes aegypti mosquitoes. Nature. 2017;545(7655):482-6. Epub 2017/05/18. doi: 10.1038/nature22365. PubMed PMID: 28514450; PMCID: PMC5885636.

72. Xia H, Luo H, Shan C, Muruato AE, Nunes BTD, Medeiros DBA, Zou J, Xie X, Giraldo MI, Vasconcelos PFC, Weaver SC, Wang T, Rajsbaum R, Shi PY. An evolutionary NS1 mutation enhances Zika virus evasion of host interferon induction. Nat Commun. 2018;9(1):414. Epub 2018/01/31. doi: 10.1038/s41467-017-02816-2. PubMed PMID: 29379028; PMCID: PMC5788864.

73. Yuan L, Huang XY, Liu ZY, Zhang F, Zhu XL, Yu JY, Ji X, Xu YP, Li G, Li C, Wang HJ, Deng YQ, Wu M, Cheng ML, Ye Q, Xie DY, Li XF, Wang X, Shi W, Hu B, Shi PY, Xu Z, Qin CF. A single mutation in the prM protein of Zika virus contributes to fetal microcephaly. Science. 2017;358(6365):933-6. Epub 2017/10/04. doi: 10.1126/science.aam7120. PubMed PMID: 28971967.

74. Aliota MT, Bassit L, Bradrick SS, Cox B, Garcia-Blanco MA, Gavegnano C, Friedrich TC, Golos TG, Griffin DE, Haddow AD, Kallas EG, Kitron U, Lecuit M, Magnani DM, Marrs C, Mercer N, McSweegan E, Ng LFP, O'Connor DH, Osorio JE, Ribeiro GS, Ricciardi M, Rossi SL, Saade G, Schinazi RF, Schott-Lerner GO, Shan C, Shi PY, Watkins DI, Vasilakis N, Weaver SC. Zika in the Americas, year 2: What have we learned? What gaps remain? A report from the Global Virus Network. Antiviral Res. 2017;144:223-46. Epub 2017/06/10. doi: 10.1016/j.antiviral.2017.06.001. PubMed PMID: 28595824; PMCID: PMC5920658.

75. Anfasa F, Siegers JY, van der Kroeg M, Mumtaz N, Stalin Raj V, de Vrij FMS, Widagdo W, Gabriel G, Salinas S, Simonin Y, Reusken C, Kushner SA, Koopmans MPG, Haagmans B, Martina BEE, van Riel D. Phenotypic Differences between Asian and African Lineage Zika Viruses in Human Neural Progenitor Cells. mSphere. 2017;2(4). doi: 10.1128/mSphere.00292-17. PubMed PMID: 28815211; PMCID: PMC5555676.

76. Bowen JR, Quicke KM, Maddur MS, O'Neal JT, McDonald CE, Fedorova NB, Puri V, Shabman RS, Pulendran B, Suthar MS. Zika Virus Antagonizes Type I Interferon Responses during Infection of Human Dendritic Cells. PLoS Pathog. 2017;13(2):e1006164. doi: 10.1371/journal.ppat.1006164. PubMed PMID: 28152048; PMCID: PMC5289613.

77. Dowall SD, Graham VA, Rayner E, Hunter L, Atkinson B, Pearson G, Dennis M, Hewson R. Lineage-dependent differences in the disease progression of Zika virus infection in type-I interferon receptor knockout (A129) mice. PLoS Negl Trop Dis. 2017;11(7):e0005704. doi: 10.1371/journal.pntd.0005704. PubMed PMID: 28672028; PMCID: PMC5510909.

78. Esser-Nobis K, Aarreberg LD, Roby JA, Fairgrieve MR, Green R, Gale M, Jr. Comparative Analysis of African and Asian Lineage-Derived Zika Virus Strains Reveals Differences in Activation of and Sensitivity to Antiviral Innate Immunity. J Virol. 2019;93(13). Epub 2019/04/26. doi: 10.1128/JVI.00640-19. PubMed PMID: 31019057; PMCID: PMC6580957.

79. Gabriel E, Ramani A, Karow U, Gottardo M, Natarajan K, Gooi LM, Goranci-Buzhala G, Krut O, Peters F, Nikolic M, Kuivanen S, Korhonen E, Smura T, Vapalahti O, Papantonis

A, Schmidt-Chanasit J, Riparbelli M, Callaini G, Kronke M, Utermohlen O, Gopalakrishnan J. Recent Zika Virus Isolates Induce Premature Differentiation of Neural Progenitors in Human Brain Organoids. Cell Stem Cell. 2017;20(3):397-406 e5. doi: 10.1016/j.stem.2016.12.005. PubMed PMID: 28132835.

80. Hamel R, Ferraris P, Wichit S, Diop F, Talignani L, Pompon J, Garcia D, Liegeois F, Sall AA, Yssel H, Misse D. African and Asian Zika virus strains differentially induce early antiviral responses in primary human astrocytes. Infect Genet Evol. 2017;49:134-7. doi: 10.1016/j.meegid.2017.01.015. PubMed PMID: 28095299.

81. Lazear HM, Govero J, Smith AM, Platt DJ, Fernandez E, Miner JJ, Diamond MS. A Mouse Model of Zika Virus Pathogenesis. Cell Host Microbe. 2016;19(5):720-30. doi: 10.1016/j.chom.2016.03.010. PubMed PMID: 27066744; PMCID: PMC4866885.

82. Liu S, DeLalio LJ, Isakson BE, Wang TT. AXL-Mediated Productive Infection of Human Endothelial Cells by Zika Virus. Circ Res. 2016;119(11):1183-9. doi: 10.1161/CIRCRESAHA.116.309866. PubMed PMID: 27650556; PMCID: PMC5215127.

83. McGrath EL, Rossi SL, Gao J, Widen SG, Grant AC, Dunn TJ, Azar SR, Roundy CM, Xiong Y, Prusak DJ, Loucas BD, Wood TG, Yu Y, Fernandez-Salas I, Weaver SC, Vasilakis N, Wu P. Differential Responses of Human Fetal Brain Neural Stem Cells to Zika Virus Infection. Stem Cell Reports. 2017;8(3):715-27. doi: 10.1016/j.stemcr.2017.01.008. PubMed PMID: 28216147; PMCID: PMC5355569.

84. Sheridan MA, Balaraman V, Schust DJ, Ezashi T, Roberts RM, Franz AWE. African and Asian strains of Zika virus differ in their ability to infect and lyse primitive human placental trophoblast. PLoS One. 2018;13(7):e0200086. doi: 10.1371/journal.pone.0200086. PubMed PMID: 29985932; PMCID: PMC6037361 Board member. This does not alter the authors' adherence to PLOS ONE Editorial policies and criteria.

85. Sheridan MA, Yunusov D, Balaraman V, Alexenko AP, Yabe S, Verjovski-Almeida S, Schust DJ, Franz AW, Sadovsky Y, Ezashi T, Roberts RM. Vulnerability of primitive human placental trophoblast to Zika virus. Proc Natl Acad Sci U S A. 2017;114(9):E1587-E96. doi: 10.1073/pnas.1616097114. PubMed PMID: 28193876; PMCID: PMC5338554.

86. Simonin Y, Loustalot F, Desmetz C, Foulongne V, Constant O, Fournier-Wirth C, Leon F, Moles JP, Goubaud A, Lemaitre JM, Maquart M, Leparc-Goffart I, Briant L, Nagot N, Van de Perre P, Salinas S. Zika Virus Strains Potentially Display Different Infectious Profiles in Human Neural Cells. EBioMedicine. 2016;12:161-9. doi: 10.1016/j.ebiom.2016.09.020. PubMed PMID: 27688094; PMCID: PMC5078617.

87. Tripathi S, Balasubramaniam VR, Brown JA, Mena I, Grant A, Bardina SV, Maringer K, Schwarz MC, Maestre AM, Sourisseau M, Albrecht RA, Krammer F, Evans MJ, Fernandez-Sesma A, Lim JK, Garcia-Sastre A. A novel Zika virus mouse model reveals strain specific differences in virus pathogenesis and host inflammatory immune responses. PLoS Pathog. 2017;13(3):e1006258. doi: 10.1371/journal.ppat.1006258. PubMed PMID: 28278235; PMCID: PMC5373643.

88. Zhang F, Hammack C, Ogden SC, Cheng Y, Lee EM, Wen Z, Qian X, Nguyen HN, Li Y, Yao B, Xu M, Xu T, Chen L, Wang Z, Feng H, Huang WK, Yoon KJ, Shan C, Huang L, Qin Z, Christian KM, Shi PY, Xu M, Xia M, Zheng W, Wu H, Song H, Tang H, Ming GL, Jin P. Molecular signatures associated with ZIKV exposure in human cortical neural progenitors. Nucleic Acids Res. 2016;44(18):8610-20. doi: 10.1093/nar/gkw765. PubMed PMID: 27580721; PMCID: PMC5063002.

89. Aid M, Abbink P, Larocca RA, Boyd M, Nityanandam R, Nanayakkara O, Martinot AJ, Moseley ET, Blass E, Borducchi EN, Chandrashekar A, Brinkman AL, Molloy K, Jetton D, Tartaglia LJ, Liu J, Best K, Perelson AS, De La Barrera RA, Lewis MG, Barouch DH. Zika Virus Persistence in the Central Nervous System and Lymph Nodes of Rhesus Monkeys. Cell. 2017;169(4):610-20 e14. doi: 10.1016/j.cell.2017.04.008. PubMed PMID: 28457610; PMCID: PMC5426912.

90. Hirsch AJ, Smith JL, Haese NN, Broeckel RM, Parkins CJ, Kreklywich C, DeFilippis VR, Denton M, Smith PP, Messer WB, Colgin LM, Ducore RM, Grigsby PL, Hennebold JD, Swanson T, Legasse AW, Axthelm MK, MacAllister R, Wiley CA, Nelson JA, Streblow DN. Zika Virus infection of rhesus macaques leads to viral persistence in multiple tissues. PLoS Pathog. 2017;13(3):e1006219. doi: 10.1371/journal.ppat.1006219. PubMed PMID: 28278237; PMCID: PMC5344528.

91. Sarno M, Sacramento GA, Khouri R, do Rosario MS, Costa F, Archanjo G, Santos LA, Nery N, Jr., Vasilakis N, Ko AI, de Almeida AR. Zika Virus Infection and Stillbirths: A Case of Hydrops Fetalis, Hydranencephaly and Fetal Demise. PLoS Negl Trop Dis. 2016;10(2):e0004517. doi: 10.1371/journal.pntd.0004517. PubMed PMID: 26914330; PMCID: PMC4767410.

92. Simonin Y, van Riel D, Van de Perre P, Rockx B, Salinas S. Differential virulence between Asian and African lineages of Zika virus. PLoS Negl Trop Dis. 2017;11(9):e0005821. doi: 10.1371/journal.pntd.0005821. PubMed PMID: 28934211; PMCID: PMC5608167.

93. Ivashkiv LB, Donlin LT. Regulation of type I interferon responses. Nat Rev Immunol. 2014;14(1):36-49. doi: 10.1038/nri3581. PubMed PMID: 24362405; PMCID: PMC4084561.

94. Schneider WM, Chevillotte MD, Rice CM. Interferon-stimulated genes: a complex web of host defenses. Annu Rev Immunol. 2014;32:513-45. doi: 10.1146/annurev-immunol-032713-120231. PubMed PMID: 24555472; PMCID: PMC4313732.

95. Schoggins JW. Interferon-Stimulated Genes: What Do They All Do? Annu Rev Virol. 2019. Epub 2019/07/10. doi: 10.1146/annurev-virology-092818-015756. PubMed PMID: 31283436.

96. Chan-Tack KM, Forrest G. Failure of interferon alpha-2b in a patient with West Nile virus meningoencephalitis and acute flaccid paralysis. Scand J Infect Dis. 2005;37(11-12):944-6. Epub 2005/11/26. doi: 10.1080/00365540500262690. PubMed PMID: 16308241.

97. Daffis S, Samuel MA, Suthar MS, Keller BC, Gale M, Jr., Diamond MS. Interferon regulatory factor IRF-7 induces the antiviral alpha interferon response and protects against lethal West Nile virus infection. J Virol. 2008;82(17):8465-75. Epub 2008/06/20. doi: 10.1128/JVI.00918-08. PubMed PMID: 18562536; PMCID: PMC2519659.

98. Diamond MS, Roberts TG, Edgil D, Lu B, Ernst J, Harris E. Modulation of Dengue virus infection in human cells by alpha, beta, and gamma interferons. J Virol. 2000;74(11):4957-66. Epub 2000/05/09. doi: 10.1128/jvi.74.11.4957-4966.2000. PubMed PMID: 10799569; PMCID: PMC110847.

99. Samuel MA, Diamond MS. Alpha/beta interferon protects against lethal West Nile virus infection by restricting cellular tropism and enhancing neuronal survival. J Virol. 2005;79(21):13350-61. Epub 2005/10/18. doi: 10.1128/JVI.79.21.13350-13361.2005. PubMed PMID: 16227257; PMCID: PMC1262587.

100. Shresta S, Kyle JL, Snider HM, Basavapatna M, Beatty PR, Harris E. Interferon-dependent immunity is essential for resistance to primary dengue virus infection in mice, whereas T- and B-cell-dependent immunity are less critical. J Virol. 2004;78(6):2701-10. Epub 2004/03/03. doi: 10.1128/jvi.78.6.2701-2710.2004. PubMed PMID: 14990690; PMCID: PMC353772.

101. Frumence E, Roche M, Krejbich-Trotot P, El-Kalamouni C, Nativel B, Rondeau P, Misse D, Gadea G, Viranaicken W, Despres P. The South Pacific epidemic strain of Zika virus replicates efficiently in human epithelial A549 cells leading to IFN-beta production and apoptosis induction. Virology. 2016;493:217-26. doi: 10.1016/j.virol.2016.03.006. PubMed PMID: 27060565.

102. Hamel R, Dejarnac O, Wichit S, Ekchariyawat P, Neyret A, Luplertlop N, Perera-Lecoin M, Surasombatpattana P, Talignani L, Thomas F, Cao-Lormeau VM, Choumet V, Briant L, Despres P, Amara A, Yssel H, Misse D. Biology of Zika Virus Infection in Human Skin Cells. J Virol. 2015;89(17):8880-96. doi: 10.1128/JVI.00354-15. PubMed PMID: 26085147; PMCID: PMC4524089.

103. Jiang D, Weidner JM, Qing M, Pan XB, Guo H, Xu C, Zhang X, Birk A, Chang J, Shi PY, Block TM, Guo JT. Identification of five interferon-induced cellular proteins that inhibit west nile virus and dengue virus infections. J Virol. 2010;84(16):8332-41. Epub 2010/06/11. doi: 10.1128/JVI.02199-09. PubMed PMID: 20534863; PMCID: PMC2916517.

104. Krishnan MN, Ng A, Sukumaran B, Gilfoy FD, Uchil PD, Sultana H, Brass AL, Adametz R, Tsui M, Qian F, Montgomery RR, Lev S, Mason PW, Koski RA, Elledge SJ, Xavier RJ, Agaisse H, Fikrig E. RNA interference screen for human genes associated with West Nile virus infection. Nature. 2008;455(7210):242-5. Epub 2008/08/12. doi: 10.1038/nature07207. PubMed PMID: 18690214; PMCID: PMC3136529.

105. Li J, Ding SC, Cho H, Chung BC, Gale M, Jr., Chanda SK, Diamond MS. A short hairpin RNA screen of interferon-stimulated genes identifies a novel negative regulator of the cellular antiviral response. MBio. 2013;4(3):e00385-13. Epub 2013/06/20. doi: 10.1128/mBio.00385-13. PubMed PMID: 23781071; PMCID: PMC3684836.

106. Schoggins JW, Wilson SJ, Panis M, Murphy MY, Jones CT, Bieniasz P, Rice CM. A diverse range of gene products are effectors of the type I interferon antiviral response. Nature. 2011;472(7344):481-5. Epub 2011/04/12. doi: 10.1038/nature09907. PubMed PMID: 21478870; PMCID: PMC3409588.

107. Dukhovny A, Lamkiewicz K, Chen Q, Fricke M, Jabrane-Ferrat N, Marz M, Jung JU, Sklan EH. A CRISPR Activation Screen Identifies Genes That Protect against Zika Virus Infection. J Virol. 2019;93(16). Epub 2019/05/31. doi: 10.1128/JVI.00211-19. PubMed PMID: 31142663; PMCID: PMC6675891.

108. Li Y, Muffat J, Omer Javed A, Keys HR, Lungjangwa T, Bosch I, Khan M, Virgilio MC, Gehrke L, Sabatini DM, Jaenisch R. Genome-wide CRISPR screen for Zika virus resistance in human neural cells. Proc Natl Acad Sci U S A. 2019;116(19):9527-32. Epub 2019/04/26. doi: 10.1073/pnas.1900867116. PubMed PMID: 31019072; PMCID: PMC6510995.

109. Marceau CD, Puschnik AS, Majzoub K, Ooi YS, Brewer SM, Fuchs G, Swaminathan K, Mata MA, Elias JE, Sarnow P, Carette JE. Genetic dissection of Flaviviridae host factors through genome-scale CRISPR screens. Nature. 2016;535(7610):159-63. Epub 2016/07/08. doi: 10.1038/nature18631. PubMed PMID: 27383987; PMCID: PMC4964798.

110. Savidis G, McDougall WM, Meraner P, Perreira JM, Portmann JM, Trincucci G, John SP, Aker AM, Renzette N, Robbins DR, Guo Z, Green S, Kowalik TF, Brass AL. Identification of Zika Virus and Dengue Virus Dependency Factors using Functional Genomics. Cell Rep. 2016;16(1):232-46. Epub 2016/06/28. doi: 10.1016/j.celrep.2016.06.028. PubMed PMID: 27342126.

111. Monel B, Compton AA, Bruel T, Amraoui S, Burlaud-Gaillard J, Roy N, Guivel-Benhassine F, Porrot F, Genin P, Meertens L, Sinigaglia L, Jouvenet N, Weil R, Casartelli N, Demangel C, Simon-Loriere E, Moris A, Roingeard P, Amara A, Schwartz O. Zika virus induces massive cytoplasmic vacuolization and paraptosis-like death in infected cells. EMBO J. 2017;36(12):1653-68. doi: 10.15252/embj.201695597. PubMed PMID: 28473450; PMCID: PMC5470047.

112. Savidis G, Perreira JM, Portmann JM, Meraner P, Guo Z, Green S, Brass AL. The IFITMs Inhibit Zika Virus Replication. Cell Rep. 2016;15(11):2323-30. doi: 10.1016/j.celrep.2016.05.074. PubMed PMID: 27268505.

113. Bailey CC, Zhong G, Huang IC, Farzan M. IFITM-Family Proteins: The Cell's First Line of Antiviral Defense. Annu Rev Virol. 2014;1:261-83. doi: 10.1146/annurev-virology-031413-085537. PubMed PMID: 25599080; PMCID: PMC4295558.

114. Li L, Zhao H, Liu P, Li C, Quanquin N, Ji X, Sun N, Du P, Qin CF, Lu N, Cheng G. PARP12 suppresses Zika virus infection through PARP-dependent degradation of NS1 and NS3 viral proteins. Sci Signal. 2018;11(535). doi: 10.1126/scisignal.aas9332. PubMed PMID: 29921658.

115. Van der Hoek KH, Eyre NS, Shue B, Khantisitthiporn O, Glab-Ampi K, Carr JM, Gartner MJ, Jolly LA, Thomas PQ, Adikusuma F, Jankovic-Karasoulos T, Roberts CT, Helbig KJ, Beard MR. Viperin is an important host restriction factor in control of Zika virus infection. Sci Rep. 2017;7(1):4475. doi: 10.1038/s41598-017-04138-1. PubMed PMID: 28667332; PMCID: PMC5493656.

116. Richardson RB, Ohlson MB, Eitson JL, Kumar A, McDougal MB, Boys IN, Mar KB, De La Cruz-Rivera PC, Douglas C, Konopka G, Xing C, Schoggins JW. A CRISPR screen identifies IFI6 as an ER-resident interferon effector that blocks flavivirus replication. Nat Microbiol. 2018;3(11):1214-23. Epub 2018/09/19. doi: 10.1038/s41564-018-0244-1. PubMed PMID: 30224801; PMCID: PMC6202210.

117. Puschnik AS, Majzoub K, Ooi YS, Carette JE. A CRISPR toolbox to study virus-host interactions. Nat Rev Microbiol. 2017;15(6):351-64. Epub 2017/04/20. doi: 10.1038/nrmicro.2017.29. PubMed PMID: 28420884; PMCID: PMC5800792.

118. Spence JS, He R, Hoffmann HH, Das T, Thinon E, Rice CM, Peng T, Chandran K, Hang HC. IFITM3 directly engages and shuttles incoming virus particles to lysosomes. Nat Chem Biol. 2019;15(3):259-68. Epub 2019/01/16. doi: 10.1038/s41589-018-0213-2. PubMed PMID: 30643282; PMCID: PMC6466627.

119. Hill SC, Vasconcelos J, Neto Z, Jandondo D, Zé-Zé L, Aguiar RS, Xavier J, Thézé J, Mirandela M, Micolo Cândido AL, Vaz F, Sebastião CdS, Wu C-H, Kraemer MUG, Melo A, Schamber-Reis BLF, de Azevedo GS, Tanuri A, Higa LM, Clemente C, da Silva SP, da Silva Candido D, Claro IM, Quibuco D, Domingos C, Pocongo B, Watts AG, Khan K, Alcantara LCJ, Sabino EC, Lackritz E, Pybus OG, Alves M-J, Afonso J, Faria NR. Emergence of the Asian lineage of Zika virus in Angola: an outbreak investigation. The Lancet Infectious Diseases. 2019;19(10):1138-47. doi: 10.1016/s1473-3099(19)30293-2.

120. Division of Public Health Surveillance and Response and Centre for Emerging and Zoonotic Diseases NHLS, National Institute for Communicable Diseases. Emergence of the Asian strain of Zika virus in Cape Verde2016.

121. Williams KL, Stumpf M, Naiman NE, Ding S, Garrett M, Gobillot T, Vezina D, Dusenbury K, Ramadoss NS, Basom R, Kim PS, Finzi A, Overbaugh J. Identification of HIV gp41-specific antibodies that mediate killing of infected cells. PLoS Pathog. 2019;15(2):e1007572. Epub 2019/02/20. doi: 10.1371/journal.ppat.1007572. PubMed PMID: 30779811; PMCID: PMC6396944.

122. Doepker L. E. SCA, Ralph D., Gobillot T. A., Garrett M., Vigdorovich V., Sather D. N., Nduati R., Matsen IV F. A., Overbaugh J. Diversity and function of maternal HIV-1-specific antibodies at the time of vertical transmission. bioRxiv. 2019. Epub September 23, 2019. doi: https://doi.org/10.1101/776856.

123. Stettler K, Beltramello M, Espinosa DA, Graham V, Cassotta A, Bianchi S, Vanzetta F, Minola A, Jaconi S, Mele F, Foglierini M, Pedotti M, Simonelli L, Dowall S, Atkinson B, Percivalle E, Simmons CP, Varani L, Blum J, Baldanti F, Cameroni E, Hewson R, Harris E, Lanzavecchia A, Sallusto F, Corti D. Specificity, cross-reactivity, and function of antibodies elicited by Zika virus infection. Science. 2016;353(6301):823-6. doi: 10.1126/science.aaf8505. PubMed PMID: 27417494.

124. Bedin F, Boulet L, Voilin E, Theillet G, Rubens A, Rozand C. Paper-based point-of-care testing for cost-effective diagnosis of acute flavivirus infections. J Med Virol. 2017;89(9):1520-7. doi: 10.1002/jmv.24806. PubMed PMID: 28295400.

125. Lustig Y, Zelena H, Venturi G, Van Esbroeck M, Rothe C, Perret C, Koren R, Katz-Likvornik S, Mendelson E, Schwartz E. Sensitivity and Kinetics of an NS1-Based Zika Virus Enzyme-Linked Immunosorbent Assay in Zika Virus-Infected Travelers from Israel, the Czech Republic, Italy, Belgium, Germany, and Chile. J Clin Microbiol. 2017;55(6):1894-901. doi: 10.1128/JCM.00346-17. PubMed PMID: 28381608; PMCID: PMC5442546.

126. Zhang B, Pinsky BA, Ananta JS, Zhao S, Arulkumar S, Wan H, Sahoo MK, Abeynayake J, Waggoner JJ, Hopes C, Tang M, Dai H. Diagnosis of Zika virus infection on a nanotechnology platform. Nat Med. 2017;23(5):548-50. doi: 10.1038/nm.4302. PubMed PMID: 28263312.

127. Wong SJ, Furuya A, Zou J, Xie X, Dupuis AP, 2nd, Kramer LD, Shi PY. A Multiplex Microsphere Immunoassay for Zika Virus Diagnosis. EBioMedicine. 2017;16:136-40. doi: 10.1016/j.ebiom.2017.01.008. PubMed PMID: 28094237; PMCID: PMC5474433.

128. Bosch I, de Puig H, Hiley M, Carre-Camps M, Perdomo-Celis F, Narvaez CF, Salgado DM, Senthoor D, O'Grady M, Phillips E, Durbin A, Fandos D, Miyazaki H, Yen CW, Gelvez-Ramirez M, Warke RV, Ribeiro LS, Teixeira MM, Almeida RP, Munoz-Medina JE, Ludert JE, Nogueira ML, Colombo TE, Terzian ACB, Bozza PT, Calheiros AS, Vieira YR, Barbosa-Lima G, Vizzoni A, Cerbino-Neto J, Bozza FA, Souza TML, Trugilho MRO, de Filippis AMB, de Sequeira PC, Marques ETA, Magalhaes T, Diaz FJ, Restrepo BN, Marin K, Mattar S, Olson D, Asturias EJ, Lucera M, Singla M, Medigeshi GR, de Bosch N, Tam J, Gomez-Marquez J, Clavet C, Villar L, Hamad-Schifferli K, Gehrke L. Rapid antigen tests for dengue virus serotypes and Zika virus in patient serum. Sci Transl Med. 2017;9(409). doi: 10.1126/scitranslmed.aan1589. PubMed PMID: 28954927.

129. Mishra N, Caciula A, Price A, Thakkar R, Ng J, Chauhan LV, Jain K, Che X, Espinosa DA, Montoya Cruz M, Balmaseda A, Sullivan EH, Patel JJ, Jarman RG, Rakeman JL, Egan

CT, Reusken C, Koopmans MPG, Harris E, Tokarz R, Briese T, Lipkin WI. Diagnosis of Zika Virus Infection by Peptide Array and Enzyme-Linked Immunosorbent Assay. MBio. 2018;9(2). doi: 10.1128/mBio.00095-18. PubMed PMID: 29511073.

130. Larman HB, Laserson U, Querol L, Verhaeghen K, Solimini NL, Xu GJ, Klarenbeek PL, Church GM, Hafler DA, Plenge RM, Nigrovic PA, De Jager PL, Weets I, Martens GA, O'Connor KC, Elledge SJ. PhIP-Seq characterization of autoantibodies from patients with multiple sclerosis, type 1 diabetes and rheumatoid arthritis. J Autoimmun. 2013;43:1-9. doi: 10.1016/j.jaut.2013.01.013. PubMed PMID: 23497938; PMCID: PMC3677742.

131. Larman HB, Zhao Z, Laserson U, Li MZ, Ciccia A, Gakidis MA, Church GM, Kesari S, Leproust EM, Solimini NL, Elledge SJ. Autoantigen discovery with a synthetic human peptidome. Nat Biotechnol. 2011;29(6):535-41. doi: 10.1038/nbt.1856. PubMed PMID: 21602805; PMCID: PMC4169279.

132. Shah AA, Xu G, Rosen A, Hummers LK, Wigley FM, Elledge SJ, Casciola-Rosen L. Brief Report: Anti-RNPC-3 Antibodies As a Marker of Cancer-Associated Scleroderma. Arthritis Rheumatol. 2017;69(6):1306-12. doi: 10.1002/art.40065. PubMed PMID: 28217959; PMCID: PMC5449218.

133. Xu GJ, Kula T, Xu Q, Li MZ, Vernon SD, Ndung'u T, Ruxrungtham K, Sanchez J, Brander C, Chung RT, O'Connor KC, Walker B, Larman HB, Elledge SJ. Viral immunology. Comprehensive serological profiling of human populations using a synthetic human virome. Science. 2015;348(6239):aaa0698. doi: 10.1126/science.aaa0698. PubMed PMID: 26045439; PMCID: PMC4844011.

134. Xu GJ, Shah AA, Li MZ, Xu Q, Rosen A, Casciola-Rosen L, Elledge SJ. Systematic autoantigen analysis identifies a distinct subtype of scleroderma with coincident cancer. Proc Natl Acad Sci U S A. 2016;113(47):E7526-E34. doi: 10.1073/pnas.1615990113. PubMed PMID: 27821747; PMCID: PMC5127349.

135. Williams KL, Wang B, Arenz D, Williams JA, Dingens AS, Cortez V, Simonich CA, Rainwater S, Lehman DA, Lee KK, Overbaugh J. Superinfection Drives HIV Neutralizing Antibody Responses from Several B Cell Lineages that Contribute to a Polyclonal Repertoire. Cell Rep. 2018;23(3):682-91. Epub 2018/04/19. doi: 10.1016/j.celrep.2018.03.082. PubMed PMID: 29669274; PMCID: PMC5990032.

136. Williams KL, Cortez V, Dingens AS, Gach JS, Rainwater S, Weis JF, Chen X, Spearman P, Forthal DN, Overbaugh J. HIV-specific CD4-induced Antibodies Mediate Broad and Potent Antibody-dependent Cellular Cytotoxicity Activity and Are Commonly Detected in Plasma From HIV-infected humans. EBioMedicine. 2015;2(10):1464-77. Epub 2015/12/03. doi: 10.1016/j.ebiom.2015.09.001. PubMed PMID: 26629541; PMCID: PMC4634620.

137. Hirsch AJ, Roberts VHJ, Grigsby PL, Haese N, Schabel MC, Wang X, Lo JO, Liu Z, Kroenke CD, Smith JL, Kelleher M, Broeckel R, Kreklywich CN, Parkins CJ, Denton M, Smith P, DeFilippis V, Messer W, Nelson JA, Hennebold JD, Grafe M, Colgin L, Lewis A, Ducore R, Swanson T, Legasse AW, Axthelm MK, MacAllister R, Moses AV, Morgan TK, Frias AE, Streblow DN. Zika virus infection in pregnant rhesus macaques causes placental dysfunction and immunopathology. Nat Commun. 2018;9(1):263. doi: 10.1038/s41467-017-02499-9. PubMed PMID: 29343712; PMCID: PMC5772047.

138. Burke V, Williams C, Sukumaran M, Kim SS, Li H, Wang XH, Gorny MK, Zolla-Pazner S, Kong XP. Structural basis of the cross-reactivity of genetically related human anti-HIV-1 mAbs: implications for design of V3-based immunogens. Structure. 2009;17(11):1538-46.

Epub 2009/11/17. doi: 10.1016/j.str.2009.09.012. PubMed PMID: 19913488; PMCID: PMC3683248.

139. Gorny MK, VanCott TC, Hioe C, Israel ZR, Michael NL, Conley AJ, Williams C, Kessler JA, 2nd, Chigurupati P, Burda S, Zolla-Pazner S. Human monoclonal antibodies to the V3 loop of HIV-1 with intra- and interclade cross-reactivity. J Immunol. 1997;159(10):5114-22. Epub 1997/11/20. PubMed PMID: 9366441.

140. Stanfield RL, Gorny MK, Williams C, Zolla-Pazner S, Wilson IA. Structural rationale for the broad neutralization of HIV-1 by human monoclonal antibody 447-52D. Structure. 2004;12(2):193-204. Epub 2004/02/14. doi: 10.1016/j.str.2004.01.003. PubMed PMID: 14962380.

141. Mitchell WM, Ding L, Gabriel J. Inactivation of a common epitope responsible for the induction of antibody-dependent enhancement of HIV. AIDS. 1998;12(2):147-56. Epub 1998/02/19. doi: 10.1097/00002030-199802000-00004. PubMed PMID: 9468363.

142. Xu JY, Gorny MK, Palker T, Karwowska S, Zolla-Pazner S. Epitope mapping of two immunodominant domains of gp41, the transmembrane protein of human immunodeficiency virus type 1, using ten human monoclonal antibodies. J Virol. 1991;65(9):4832-8. Epub 1991/09/01. PubMed PMID: 1714520; PMCID: PMC248941.

143. Gnann JW, Jr., Nelson JA, Oldstone MB. Fine mapping of an immunodominant domain in the transmembrane glycoprotein of human immunodeficiency virus. J Virol. 1987;61(8):2639-41. PubMed PMID: 2439707; PMCID: PMC255715.

144. Gnann JW, Jr., Schwimmbeck PL, Nelson JA, Truax AB, Oldstone MB. Diagnosis of AIDS by using a 12-amino acid peptide representing an immunodominant epitope of the human immunodeficiency virus. J Infect Dis. 1987;156(2):261-7. PubMed PMID: 2439614.

145. Palker TJ, Matthews TJ, Clark ME, Cianciolo GJ, Randall RR, Langlois AJ, White GC, Safai B, Snyderman R, Bolognesi DP, et al. A conserved region at the COOH terminus of human immunodeficiency virus gp120 envelope protein contains an immunodominant epitope. Proc Natl Acad Sci U S A. 1987;84(8):2479-83. PubMed PMID: 2436231; PMCID: PMC304675.

146. Zolla-Pazner S, Cohen SS, Krachmarov C, Wang S, Pinter A, Lu S. Focusing the immune response on the V3 loop, a neutralizing epitope of the HIV-1 gp120 envelope. Virology. 2008;372(2):233-46. doi: 10.1016/j.virol.2007.09.024. PubMed PMID: 18061228.

147. Goo L, Chohan V, Nduati R, Overbaugh J. Early development of broadly neutralizing antibodies in HIV-1-infected infants. Nat Med. 2014;20(6):655-8. doi: 10.1038/nm.3565. PubMed PMID: 24859529; PMCID: PMC4060046.

148. Gach JS, Mara KJV, LaBranche CC, van Gils MJ, McCoy LE, Klasse PJ, Montefiori DC, Sanders RW, Moore JP, Forthal DN. Antibody Responses Elicited by Immunization with BG505 Trimer Immune Complexes. J Virol. 2019;93(20). Epub 2019/08/04. doi: 10.1128/JVI.01188-19. PubMed PMID: 31375582; PMCID: PMC6798112.

149. Sanders RW, van Gils MJ, Derking R, Sok D, Ketas TJ, Burger JA, Ozorowski G, Cupo A, Simonich C, Goo L, Arendt H, Kim HJ, Lee JH, Pugach P, Williams M, Debnath G, Moldt B, van Breemen MJ, Isik G, Medina-Ramirez M, Back JW, Koff WC, Julien JP, Rakasz EG, Seaman MS, Guttman M, Lee KK, Klasse PJ, LaBranche C, Schief WR, Wilson IA, Overbaugh J, Burton DR, Ward AB, Montefiori DC, Dean H, Moore JP. HIV-1 VACCINES. HIV-1 neutralizing antibodies induced by native-like envelope trimers. Science.

2015;349(6244):aac4223. Epub 2015/06/20. doi: 10.1126/science.aac4223. PubMed PMID: 26089353; PMCID: PMC4498988.

150. Emerson RO, DeWitt WS, Vignali M, Gravley J, Hu JK, Osborne EJ, Desmarais C, Klinger M, Carlson CS, Hansen JA, Rieder M, Robins HS. Immunosequencing identifies signatures of cytomegalovirus exposure history and HLA-mediated effects on the T cell repertoire. Nat Genet. 2017;49(5):659-65. Epub 2017/04/04. doi: 10.1038/ng.3822. PubMed PMID: 28369038.

151. Munoz LS, Parra B, Pardo CA, Neuroviruses Emerging in the Americas S. Neurological Implications of Zika Virus Infection in Adults. J Infect Dis. 2017;216(suppl_10):S897-S905. doi: 10.1093/infdis/jix511. PubMed PMID: 29267923; PMCID: PMC5853915.

152. Priyamvada L, Suthar MS, Ahmed R, Wrammert J. Humoral Immune Responses Against Zika Virus Infection and the Importance of Preexisting Flavivirus Immunity. J Infect Dis. 2017;216(suppl_10):S906-S11. doi: 10.1093/infdis/jix513. PubMed PMID: 29267924; PMCID: PMC5853377.

153. Schuler-Faccini L, Ribeiro EM, Feitosa IM, Horovitz DD, Cavalcanti DP, Pessoa A, Doriqui MJ, Neri JI, Neto JM, Wanderley HY, Cernach M, El-Husny AS, Pone MV, Serao CL, Sanseverino MT, Brazilian Medical Genetics Society-Zika Embryopathy Task F. Possible Association Between Zika Virus Infection and Microcephaly - Brazil, 2015. MMWR Morb Mortal Wkly Rep. 2016;65(3):59-62. doi: 10.15585/mmwr.mm6503e2. PubMed PMID: 26820244.

154. Zorrilla CD, Garcia Garcia I, Garcia Fragoso L, De La Vega A. Zika Virus Infection in Pregnancy: Maternal, Fetal, and Neonatal Considerations. J Infect Dis. 2017;216(suppl_10):S891-S6. doi: 10.1093/infdis/jix448. PubMed PMID: 29267916; PMCID: PMC5853951.

155. Musso D, Nilles EJ, Cao-Lormeau VM. Rapid spread of emerging Zika virus in the Pacific area. Clin Microbiol Infect. 2014;20(10):O595-6. Epub 2014/06/10. doi: 10.1111/1469-0691.12707. PubMed PMID: 24909208.

156. McNab F, Mayer-Barber K, Sher A, Wack A, O'Garra A. Type I interferons in infectious disease. Nat Rev Immunol. 2015;15(2):87-103. doi: 10.1038/nri3787. PubMed PMID: 25614319.

157. Contreras D, Arumugaswami V. Zika Virus Infectious Cell Culture System and the In Vitro Prophylactic Effect of Interferons. J Vis Exp. 2016(114). Epub 2016/09/02. doi: 10.3791/54767. PubMed PMID: 27584546; PMCID: PMC5091946.

158. Quick J, Grubaugh ND, Pullan ST, Claro IM, Smith AD, Gangavarapu K, Oliveira G, Robles-Sikisaka R, Rogers TF, Beutler NA, Burton DR, Lewis-Ximenez LL, de Jesus JG, Giovanetti M, Hill SC, Black A, Bedford T, Carroll MW, Nunes M, Alcantara LC, Jr., Sabino EC, Baylis SA, Faria NR, Loose M, Simpson JT, Pybus OG, Andersen KG, Loman NJ. Multiplex PCR method for MinION and Illumina sequencing of Zika and other virus genomes directly from clinical samples. Nat Protoc. 2017;12(6):1261-76. doi: 10.1038/nprot.2017.066. PubMed PMID: 28538739; PMCID: PMC5902022.

159. Guindon S, Dufayard JF, Lefort V, Anisimova M, Hordijk W, Gascuel O. New algorithms and methods to estimate maximum-likelihood phylogenies: assessing the performance of PhyML 3.0. Syst Biol. 2010;59(3):307-21. doi: 10.1093/sysbio/syq010. PubMed PMID: 20525638.

160. Nahabedian J, Sharma A, Kaczmarek ME, Wilkerson GK, Sawyer SL, Overbaugh J. Owl monkey CCR5 reveals synergism between CD4 and CCR5 in HIV-1 entry. Virology. 2017;512:180-6. doi: 10.1016/j.virol.2017.09.018. PubMed PMID: 28972927.

161. Welm BE, Dijkgraaf GJ, Bledau AS, Welm AL, Werb Z. Lentiviral transduction of mammary stem cells for analysis of gene function during development and cancer. Cell Stem Cell. 2008;2(1):90-102. doi: 10.1016/j.stem.2007.10.002. PubMed PMID: 18371425; PMCID: PMC2276651.

162. Shalem O, Sanjana NE, Hartenian E, Shi X, Scott DA, Mikkelson T, Heckl D, Ebert BL, Root DE, Doench JG, Zhang F. Genome-scale CRISPR-Cas9 knockout screening in human cells. Science. 2014;343(6166):84-7. Epub 2013/12/18. doi: 10.1126/science.1247005. PubMed PMID: 24336571; PMCID: PMC4089965.

163. Weintraub AS, Li CH, Zamudio AV, Sigova AA, Hannett NM, Day DS, Abraham BJ, Cohen MA, Nabet B, Buckley DL, Guo YE, Hnisz D, Jaenisch R, Bradner JE, Gray NS, Young RA. YY1 Is a Structural Regulator of Enhancer-Promoter Loops. Cell. 2017;171(7):1573-88 e28. doi: 10.1016/j.cell.2017.11.008. PubMed PMID: 29224777; PMCID: PMC5785279.

164. Brass AL, Huang IC, Benita Y, John SP, Krishnan MN, Feeley EM, Ryan BJ, Weyer JL, van der Weyden L, Fikrig E, Adams DJ, Xavier RJ, Farzan M, Elledge SJ. The IFITM proteins mediate cellular resistance to influenza A H1N1 virus, West Nile virus, and dengue virus. Cell. 2009;139(7):1243-54. doi: 10.1016/j.cell.2009.12.017. PubMed PMID: 20064371; PMCID: PMC2824905.

165. Bayer A, Lennemann NJ, Ouyang Y, Bramley JC, Morosky S, Marques ET, Jr., Cherry S, Sadovsky Y, Coyne CB. Type III Interferons Produced by Human Placental Trophoblasts Confer Protection against Zika Virus Infection. Cell Host Microbe. 2016;19(5):705-12. Epub 2016/04/14. doi: 10.1016/j.chom.2016.03.008. PubMed PMID: 27066743; PMCID: PMC4866896.

166. Chan JF, Yip CC, Tsang JO, Tee KM, Cai JP, Chik KK, Zhu Z, Chan CC, Choi GK, Sridhar S, Zhang AJ, Lu G, Chiu K, Lo AC, Tsao SW, Kok KH, Jin DY, Chan KH, Yuen KY. Differential cell line susceptibility to the emerging Zika virus: implications for disease pathogenesis, non-vector-borne human transmission and animal reservoirs. Emerg Microbes Infect. 2016;5:e93. Epub 2016/08/25. doi: 10.1038/emi.2016.99. PubMed PMID: 27553173; PMCID: PMC5034105.

167. Mlakar J, Korva M, Tul N, Popovic M, Poljsak-Prijatelj M, Mraz J, Kolenc M, Resman Rus K, Vesnaver Vipotnik T, Fabjan Vodusek V, Vizjak A, Pizem J, Petrovec M, Avsic Zupanc T. Zika Virus Associated with Microcephaly. N Engl J Med. 2016;374(10):951-8. Epub 2016/02/11. doi: 10.1056/NEJMoa1600651. PubMed PMID: 26862926.

168. Tang H, Hammack C, Ogden SC, Wen Z, Qian X, Li Y, Yao B, Shin J, Zhang F, Lee EM, Christian KM, Didier RA, Jin P, Song H, Ming GL. Zika Virus Infects Human Cortical Neural Progenitors and Attenuates Their Growth. Cell Stem Cell. 2016;18(5):587-90. Epub 2016/03/10. doi: 10.1016/j.stem.2016.02.016. PubMed PMID: 26952870; PMCID: PMC5299540.

169. de Weerd NA, Vivian JP, Nguyen TK, Mangan NE, Gould JA, Braniff SJ, Zaker-Tabrizi L, Fung KY, Forster SC, Beddoe T, Reid HH, Rossjohn J, Hertzog PJ. Structural basis of a unique interferon-beta signaling axis mediated via the receptor IFNAR1. Nat Immunol. 2013;14(9):901-7. doi: 10.1038/ni.2667. PubMed PMID: 23872679.

170. Jaks E, Gavutis M, Uze G, Martal J, Piehler J. Differential receptor subunit affinities of type I interferons govern differential signal activation. J Mol Biol. 2007;366(2):525-39. doi: 10.1016/j.jmb.2006.11.053. PubMed PMID: 17174979.

171. Iyer SS, Bibollet-Ruche F, Sherrill-Mix S, Learn GH, Plenderleith L, Smith AG, Barbian HJ, Russell RM, Gondim MV, Bahari CY, Shaw CM, Li Y, Decker T, Haynes BF, Shaw GM, Sharp PM, Borrow P, Hahn BH. Resistance to type 1 interferons is a major determinant of HIV-1 transmission fitness. Proc Natl Acad Sci U S A. 2017;114(4):E590-E9. Epub 2017/01/11. doi: 10.1073/pnas.1620144114. PubMed PMID: 28069935; PMCID: PMC5278458.

172. Lima MC, de Mendonca LR, Rezende AM, Carrera RM, Anibal-Silva CE, Demers M, D'Aiuto L, Wood J, Chowdari KV, Griffiths M, Lucena-Araujo AR, Barral-Netto M, Azevedo EAN, Alves RW, Farias PCS, Marques ETA, Castanha PMS, Donald CL, Kohl A, Nimgaonkar VL, Franca RFO. The Transcriptional and Protein Profile From Human Infected Neuroprogenitor Cells Is Strongly Correlated to Zika Virus Microcephaly Cytokines Phenotype Evidencing a Persistent Inflammation in the CNS. Front Immunol. 2019;10:1928. Epub 2019/09/03. doi: 10.3389/fimmu.2019.01928. PubMed PMID: 31474994; PMCID: PMC6707094.

173. Gibbert K, Schlaak JF, Yang D, Dittmer U. IFN-alpha subtypes: distinct biological activities in anti-viral therapy. Br J Pharmacol. 2013;168(5):1048-58. doi: 10.1111/bph.12010. PubMed PMID: 23072338; PMCID: PMC3594665.

174. Lavoie TB, Kalie E, Crisafulli-Cabatu S, Abramovich R, DiGioia G, Moolchan K, Pestka S, Schreiber G. Binding and activity of all human alpha interferon subtypes. Cytokine. 2011;56(2):282-9. doi: 10.1016/j.cyto.2011.07.019. PubMed PMID: 21856167.

175. Schreiber G, Piehler J. The molecular basis for functional plasticity in type I interferon signaling. Trends Immunol. 2015;36(3):139-49. doi: 10.1016/j.it.2015.01.002. PubMed PMID: 25687684.

176. Gorman MJ, Caine EA, Zaitsev K, Begley MC, Weger-Lucarelli J, Uccellini MB, Tripathi S, Morrison J, Yount BL, Dinnon KH, 3rd, Ruckert C, Young MC, Zhu Z, Robertson SJ, McNally KL, Ye J, Cao B, Mysorekar IU, Ebel GD, Baric RS, Best SM, Artyomov MN, Garcia-Sastre A, Diamond MS. An Immunocompetent Mouse Model of Zika Virus Infection. Cell Host Microbe. 2018;23(5):672-85 e6. doi: 10.1016/j.chom.2018.04.003. PubMed PMID: 29746837; PMCID: PMC5953559.

177. Wu X, Dao Thi VL, Huang Y, Billerbeck E, Saha D, Hoffmann HH, Wang Y, Silva LAV, Sarbanes S, Sun T, Andrus L, Yu Y, Quirk C, Li M, MacDonald MR, Schneider WM, An X, Rosenberg BR, Rice CM. Intrinsic Immunity Shapes Viral Resistance of Stem Cells. Cell. 2018;172(3):423-38 e25. Epub 2017/12/19. doi: 10.1016/j.cell.2017.11.018. PubMed PMID: 29249360; PMCID: PMC5786493.

178. Gizzi AS, Grove TL, Arnold JJ, Jose J, Jangra RK, Garforth SJ, Du Q, Cahill SM, Dulyaninova NG, Love JD, Chandran K, Bresnick AR, Cameron CE, Almo SC. A naturally occurring antiviral ribonucleotide encoded by the human genome. Nature. 2018;558(7711):610-4. doi: 10.1038/s41586-018-0238-4. PubMed PMID: 29925952; PMCID: PMC6026066.

179. OhAinle M, Helms L, Vermeire J, Roesch F, Humes D, Basom R, Delrow JJ, Overbaugh J, Emerman M. A virus-packageable CRISPR screen identifies host factors mediating interferon inhibition of HIV. Elife. 2018;7. Epub 2018/12/07. doi: 10.7554/eLife.39823. PubMed PMID: 30520725; PMCID: PMC6286125.

180. Boonyaratanakornkit JB, Bartlett EJ, Amaro-Carambot E, Collins PL, Murphy BR, Schmidt AC. The C proteins of human parainfluenza virus type 1 (HPIV1) control the transcription of a broad array of cellular genes that would otherwise respond to HPIV1 infection. J Virol. 2009;83(4):1892-910. Epub 2008/12/05. doi: 10.1128/JVI.01373-08. PubMed PMID: 19052086; PMCID: PMC2643784.

181. Doench JG, Fusi N, Sullender M, Hegde M, Vaimberg EW, Donovan KF, Smith I, Tothova Z, Wilen C, Orchard R, Virgin HW, Listgarten J, Root DE. Optimized sgRNA design to maximize activity and minimize off-target effects of CRISPR-Cas9. Nat Biotechnol. 2016;34(2):184-91. Epub 2016/01/19. doi: 10.1038/nbt.3437. PubMed PMID: 26780180; PMCID: PMC4744125.

182. Sanjana NE, Shalem O, Zhang F. Improved vectors and genome-wide libraries for CRISPR screening. Nat Methods. 2014;11(8):783-4. Epub 2014/07/31. doi: 10.1038/nmeth.3047. PubMed PMID: 25075903; PMCID: PMC4486245.

183. Hart T, Chandrashekhar M, Aregger M, Steinhart Z, Brown KR, MacLeod G, Mis M, Zimmermann M, Fradet-Turcotte A, Sun S, Mero P, Dirks P, Sidhu S, Roth FP, Rissland OS, Durocher D, Angers S, Moffat J. High-Resolution CRISPR Screens Reveal Fitness Genes and Genotype-Specific Cancer Liabilities. Cell. 2015;163(6):1515-26. Epub 2015/12/03. doi: 10.1016/j.cell.2015.11.015. PubMed PMID: 26627737.

184. Wang T, Birsoy K, Hughes NW, Krupczak KM, Post Y, Wei JJ, Lander ES, Sabatini DM. Identification and characterization of essential genes in the human genome. Science. 2015;350(6264):1096-101. Epub 2015/10/17. doi: 10.1126/science.aac7041. PubMed PMID: 26472758; PMCID: PMC4662922.

185. Wang T, Wei JJ, Sabatini DM, Lander ES. Genetic screens in human cells using the CRISPR-Cas9 system. Science. 2014;343(6166):80-4. Epub 2013/12/18. doi: 10.1126/science.1246981. PubMed PMID: 24336569; PMCID: PMC3972032.

186. Li W, Xu H, Xiao T, Cong L, Love MI, Zhang F, Irizarry RA, Liu JS, Brown M, Liu XS. MAGeCK enables robust identification of essential genes from genome-scale CRISPR/Cas9 knockout screens. Genome Biol. 2014;15(12):554. Epub 2014/12/06. doi: 10.1186/s13059-014-0554-4. PubMed PMID: 25476604; PMCID: PMC4290824.

187. Hsu YL, Shi SF, Wu WL, Ho LJ, Lai JH. Protective roles of interferon-induced protein with tetratricopeptide repeats 3 (IFIT3) in dengue virus infection of human lung epithelial cells. PLoS One. 2013;8(11):e79518. Epub 2013/11/14. doi: 10.1371/journal.pone.0079518. PubMed PMID: 24223959; PMCID: PMC3817122.

188. Souza BS, Sampaio GL, Pereira CS, Campos GS, Sardi SI, Freitas LA, Figueira CP, Paredes BD, Nonaka CK, Azevedo CM, Rocha VP, Bandeira AC, Mendez-Otero R, Dos Santos RR, Soares MB. Zika virus infection induces mitosis abnormalities and apoptotic cell death of human neural progenitor cells. Sci Rep. 2016;6:39775. Epub 2016/12/23. doi: 10.1038/srep39775. PubMed PMID: 28008958; PMCID: PMC5180086.

189. Samuel CE. Adenosine deaminases acting on RNA (ADARs) are both antiviral and proviral. Virology. 2011;411(2):180-93. Epub 2011/01/08. doi: 10.1016/j.virol.2010.12.004. PubMed PMID: 21211811; PMCID: PMC3057271.

190. Zhu J, Ghosh A, Sarkar SN. OASL-a new player in controlling antiviral innate immunity. Curr Opin Virol. 2015;12:15-9. Epub 2015/02/14. doi: 10.1016/j.coviro.2015.01.010. PubMed PMID: 25676874; PMCID: PMC4470762.

191. Li Y, Banerjee S, Goldstein SA, Dong B, Gaughan C, Rath S, Donovan J, Korennykh A, Silverman RH, Weiss SR. Ribonuclease L mediates the cell-lethal phenotype of double-stranded RNA editing enzyme ADAR1 deficiency in a human cell line. Elife. 2017;6. Epub 2017/04/01. doi: 10.7554/eLife.25687. PubMed PMID: 28362255; PMCID: PMC5404912.

192. Wang Y, Li Z, Xu P, Huang L, Tong J, Huang H, Meng A. Angiomotin-like2 gene (amotl2) is required for migration and proliferation of endothelial cells during angiogenesis. J Biol Chem. 2011;286(47):41095-104. Epub 2011/09/23. doi: 10.1074/jbc.M111.296806. PubMed PMID: 21937427; PMCID: PMC3220490.

193. Nordmann A, Wixler L, Boergeling Y, Wixler V, Ludwig S. A new splice variant of the human guanylate-binding protein 3 mediates anti-influenza activity through inhibition of viral transcription and replication. FASEB J. 2012;26(3):1290-300. Epub 2011/11/23. doi: 10.1096/fj.11-189886. PubMed PMID: 22106366.

194. Tretina K, Park ES, Maminska A, MacMicking JD. Interferon-induced guanylate-binding proteins: Guardians of host defense in health and disease. J Exp Med. 2019;216(3):482-500. Epub 2019/02/14. doi: 10.1084/jem.20182031. PubMed PMID: 30755454; PMCID: PMC6400534.

195. Meertens L, Hafirassou ML, Couderc T, Bonnet-Madin L, Kril V, Kummerer BM, Labeau A, Brugier A, Simon-Loriere E, Burlaud-Gaillard J, Doyen C, Pezzi L, Goupil T, Rafasse S, Vidalain PO, Bertrand-Legout A, Gueneau L, Juntas-Morales R, Ben Yaou R, Bonne G, de Lamballerie X, Benkirane M, Roingeard P, Delaugerre C, Lecuit M, Amara A. FHL1 is a major host factor for chikungunya virus infection. Nature. 2019;574(7777):259-63. Epub 2019/09/27. doi: 10.1038/s41586-019-1578-4. PubMed PMID: 31554973.

196. Wang B, Wang M, Zhang W, Xiao T, Chen CH, Wu A, Wu F, Traugh N, Wang X, Li Z, Mei S, Cui Y, Shi S, Lipp JJ, Hinterndorfer M, Zuber J, Brown M, Li W, Liu XS. Integrative analysis of pooled CRISPR genetic screens using MAGeCKFlute. Nat Protoc. 2019;14(3):756-80. Epub 2019/02/03. doi: 10.1038/s41596-018-0113-7. PubMed PMID: 30710114; PMCID: PMC6862721.

197. Waggoner JJ, Gresh L, Mohamed-Hadley A, Ballesteros G, Davila MJ, Tellez Y, Sahoo MK, Balmaseda A, Harris E, Pinsky BA. Single-Reaction Multiplex Reverse Transcription PCR for Detection of Zika, Chikungunya, and Dengue Viruses. Emerg Infect Dis. 2016;22(7):1295-7. Epub 2016/05/18. doi: 10.3201/eid2207.160326. PubMed PMID: 27184629; PMCID: PMC4918162.

198. Ren P, Ortiz DA, Terzian ACB, Colombo TE, Nogueira ML, Vasilakis N, Loeffelholz MJ. Evaluation of Aptima Zika Virus Assay. J Clin Microbiol. 2017;55(7):2198-203. doi: 10.1128/JCM.00603-17. PubMed PMID: 28468854; PMCID: PMC5483922.

199. (RePORT) NRPORT. Zika Virus in Pregnancy in Nigeria (5R21AI137840)2020.

200. Ooi YS, Majzoub K, Flynn RA, Mata MA, Diep J, Li JK, van Buuren N, Rumachik N, Johnson AG, Puschnik AS, Marceau CD, Mlera L, Grabowski JM, Kirkegaard K, Bloom ME, Sarnow P, Bertozzi CR, Carette JE. An RNA-centric dissection of host complexes controlling flavivirus infection. Nat Microbiol. 2019;4(12):2369-82. Epub 2019/08/07. doi: 10.1038/s41564-019-0518-2. PubMed PMID: 31384002; PMCID: PMC6879806.